NACA TN 3725

NATIONAL ADVISORY COMMITTEE FOR AERONAUTICS

TECHNICAL NOTE 3725

AERODYNAMIC INTERFERENCE OF SLENDER WING-TAIL COMBINATIONS

By Alvin H. Sacks

Ames Aeronautical Laboratory
Moffett Field, Calif.

Washington
January 1957

TABLE OF CONTENTS

	Page
SUMMARY	1
INTRODUCTION	1
SYMBOLS	2
SUBSCRIPTS	6
SPECIAL NOTATIONS	6
ANALYSIS	6
STEADY STRAIGHT FLIGHT	8
Plane Wing and Cruciform Tail	8
Longitudinal stability	11
Directional stability	21
Lateral stability	27
Cruciform Wing and Cruciform Tail	32
PITCHING AND PLUNGING FLIGHT	36
LIMITATIONS OF THE THEORY	45
WATER-TANK EXPERIMENT	48
CONCLUDING REMARKS	51
APPENDIX - EVALUATION OF THE IMAGINARY PART OF A COMPLEX SQUARE ROOT	53
REFERENCES	55
FIGURES	57

NATIONAL ADVISORY COMMITTEE FOR AERONAUTICS

TECHNICAL NOTE 3725

AERODYNAMIC INTERFERENCE OF SLENDER WING-TAIL COMBINATIONS

By Alvin H. Sacks

SUMMARY

Mathematical expressions are derived for the interference forces and moments acting on the tails of slender plane and cruciform wing-tail combinations of general plan form in steady straight flight at combined angles of attack and sideslip. The derivations are made within the limitations of slender-body theory under the assumption that the vortex sheet leaves the wing as a flat sheet and becomes fully rolled up ahead of the tail. The derived expressions are used to calculate the steady lifts, side forces, pitching moments, and rolling moments of a number of wing-tail combinations. The effects of changes in tail height, tail length, ratio of tail span to wing span, tail incidence, and tail thickness are calculated. The resulting curves, and particularly their nonlinearities, are discussed at some length in connection with static stability. In general, the most dramatic effects are noted when the vortices shed from the wing strike the tips of the tail trailing edge.

An expression is developed for the lift of a plane wing-tail combination which is pitching and plunging, and the associated stability derivatives are calculated as functions of the angle of attack. Discontinuities in lift-curve slope C_{L_α} and the stability derivative $C_{L_{\dot{\alpha}}}$ are noted for plane wing-tail combinations with high tails if the span of the tail is slightly greater than the span of the vortices shed by the wing.

Photographs of the wake of the wing in the presence of the tail, as observed in a water tank, are presented for a plane triangular wing-tail combination with a high tail. The measured variation of the lateral spacing of the wing vortices with distance in the presence of the tail is presented and discussed in connection with the assumptions of the analysis. The tail was found to cause an appreciable inboard shift of the wing vortices for the case investigated.

INTRODUCTION

It is now generally recognized that for wing-tail combinations involving low-aspect-ratio wings and moderate tail lengths it is not permissible to neglect the rolling up of the vortex sheet in calculating

wing-tail interference effects. Since such cases are often encountered in connection with high-speed airplane and missile designs, some effort has been devoted in recent years to the calculation of wing-tail interference, accounting in some manner for the rolling up of the vortex sheets.

Except for some numerical work in tracing the rolling-up process itself (e.g., refs. 1, 2, and 3), the distortion of the vortex sheet is usually accounted for simply by assuming the sheet to be fully rolled up, and the emphasis has generally been on obtaining expressions for the forces on the tail in terms of the positions of the vortices shed by the wing (e.g., refs. 4, 5, 6, and 7). In 1948, however, Graham (ref. 8) actually calculated the variation of tail lift with angle of attack for some planar wing-tail combinations. This was done by expressing the vortex positions as a function of the angle of attack under the two alternative assumptions of a flat vortex sheet and a fully rolled-up vortex sheet shed by the wing. Graham's results, which for the slender tail case were only approximate, showed some interesting departures from the usually assumed linear variations. In 1952 Morikawa (ref. 9) investigated the "maximum" wing-body-tail interference (which occurs when the rolled-up vortices lie in the plane of the tail) by restricting the analysis to angles of attack near zero and at the same time assuming that the vortex sheets are fully rolled up. This avoids any consideration of the nonlinear variation of tail lift with angle of attack.

In the present paper, the emphasis is placed on calculating the variations of total forces and moments with angles of attack and sideslip for a number of slender plane and cruciform wing-tail combinations and for some airplane-type arrangements of a plane wing and a horizontal and vertical tail. Significant nonlinearities are found, and these will be discussed in some detail with regard to their effects on the static stability of the various combinations. The lift of a plane wing-tail combination which is pitching and plunging will also be determined and the variation of pertinent stability derivatives with angle of attack will be calculated.

The primary assumption in the present analysis will be that the vortex sheet leaves the slender wing as a flat sheet and becomes fully rolled up ahead of the tail. It will also be assumed, as is customary, that the tail does not influence the positions of the vortices shed by the wing. The validity of both of these assumptions has been investigated experimentally by means of a water tank, and these results will also be presented and discussed.

SYMBOLS

A aspect ratio

b local semithickness of horizontal tail

C_L $\dfrac{L}{\frac{1}{2}\rho U_o^2 S_w}$

C_l $\dfrac{L'}{\frac{1}{2}\rho U_o^2 S_w (2s_o)}$

C_m $\dfrac{M}{\frac{1}{2}\rho U_o^2 S_w c}$

C_n $\dfrac{N}{\frac{1}{2}\rho U_o^2 S_w (2s_o)}$

C_{n_β} $\left.\dfrac{\partial C_n}{\partial \beta}\right]_{\beta=0}$

C_Y $\dfrac{Y}{\frac{1}{2}\rho U_o^2 S_w}$

C_{L_α} $\left.\dfrac{\partial C_L}{\partial \alpha}\right]_{\dot{\alpha}=q=0}$

$C_{L_{\dot{\alpha}}}$ $\left.\dfrac{\partial C_L}{\partial (\dot{\alpha}c/U_o)}\right]_{\dot{\alpha}=q=0}$

C_{L_q} $\left.\dfrac{\partial C_L}{\partial (qc/U_o)}\right]_{\dot{\alpha}=q=0}$

c maximum chord of wing

c_l distance from wing apex to pivot point

c' maximum chord of tail

d tail length, l-c

e distance behind wing trailing edge at which vortex sheet is essentially rolled up

h_T height of trailing edge of horizontal tail above wing chord plane

i_T incidence of horizontal tail relative to wing chord plane, radians

L	force in the z direction (approximately lift)
L'	rolling moment about x axis
l	over-all length of wing-tail combination
m	number of external (free) vortices
M	pitching moment about pivot point $x = c_1$
N	yawing moment about pivot point $x = c_1$
p	angular rolling velocity about the x axis, radians/sec
q	angular pitching velocity about the pivot point $x = c_1$, radians/sec
R	$V + iW$
r	angular yawing velocity about the pivot point $x = c_1$, radians/sec
r_o	radius of transformed circle corresponding to wing or tail cross section
s	local semispan of wing or tail
S	airplane cross-sectional area
S_w	plan-form area of wing (area of one wing of cruciform)
s_o	maximum semispan of wing (at $x = c$)
s_1	maximum semispan of tail (at $x = l$)
t	time, sec
t_o	maximum span of vertical tail panel
t_1	local span of upper vertical tail panel
t_2	local span of lower vertical tail panel
U_o	component of flight velocity along the negative x axis
V_o	component of flight velocity along the positive y axis ($V_o = U_o\beta$ if $p = 0$)
V	$V_o - r(x - c_1)$
W_o	component of flight velocity along the positive z axis ($W_o = -U_o\alpha$ if $p = 0$)

W $W_o - q(x - c_1)$

x_{TE+} distance from wing apex to position immediately behind wing trailing edge

xyz Cartesian coordinates fixed in the tail as illustrated in figure 1(a)

x_1 distance behind the wing trailing edge

x' distance behind apex of the tail, $x_1 - d + c'$

Y force in the y direction (side force)

y_1, z_1 y and z coordinates of starboard rolled-up vortex

α angle of attack, radians

α_{cr} angle of attack at which the rolled-up wing vortices intersect the line containing the trailing edge of the horizontal tail

$\dot{\alpha}$ time rate of change of angle of attack, radians/sec

β angle of sideslip, radians

Γ strength of one rolled-up vortex shed from the wing

Γ_k circulation of kth external (free) vortex, positive counterclockwise

ζ $y + iz$

ζ_k position of kth external (free) vortex, $y_k + iz_k$

ξ $\frac{x'}{s_o}$

ρ fluid mass density

σ complex coordinate in transformed circle plane

σ_k position of kth external vortex in transformed circle plane

σ_{k_r} position of kth external vortex relative to its image in the transformed circle, $\sigma_k - \frac{r_o^2}{\bar{\sigma}_k}$

$\frac{b}{s}$ horizontal-tail thickness ratio (constant for conical tails treated herein)

SUBSCRIPTS

I	due to vortex interference
l	tail trailing edge
T	tail (when used on forces and moments indicates isolated tail)
TE	wing trailing edge
w	wing

SPECIAL NOTATIONS

$\oint$	contour integral taken once round the cross section in the positive (counterclockwise) sense
R	real part
I	imaginary part
$(\bar{\ })$	complex conjugate of ( )

ANALYSIS

The present report is concerned with the calculation of the total aerodynamic forces and moments exerted on some plane and cruciform slender wing-tail combinations in steady and maneuvering flight. The calculations will be made within the limitations of slender-body theory and will employ the techniques developed in references 10 and 11. Inasmuch as it was shown in the former reference that the forces and moments are linear in the potential (although not in the motions), it is permissible to calculate the forces and moments due to vortex interference alone and add them to those of the isolated wing and tail. Consequently, the major portion of this report will be concerned with the calculation of the forces and moments due to wing-tail interference.

It was shown in reference 11 that the components of force and moment due to vortex interference can be expressed as

$$Y_I - iL_I = -i\rho U_o \left[\left(\sum_{k=1}^{m} \Gamma_k \bar{\sigma}_{k_r} \right)_{x=l} - \left(\sum_{k=1}^{m} \Gamma_k \bar{\sigma}_{k_r} \right)_{x=x_{TE+}} \right] -$$

$$i\rho \int_{TE}^{l} \frac{\partial}{\partial t} \left(\sum_{k=1}^{m} \Gamma_k \bar{\sigma}_{k_r} \right) dx + \rho p \int_{TE}^{l} \sum_{k=1}^{m} \Gamma_k \bar{\sigma}_{k_r} dx \qquad (1)$$

$$N_I - iM_I = i\rho U_o \int_{TE}^{l} (x - c_1) \frac{\partial}{\partial x}\left(\sum_{k=1}^{m} \Gamma_k \bar{\sigma}_{k_r}\right) dx +$$

$$i\rho \int_{TE}^{l} (x - c_1) \frac{\partial}{\partial t}\left(\sum_{k=1}^{m} \Gamma_k \bar{\sigma}_{k_r}\right) dx - \rho p \int_{TE}^{l} (x - c_1) \sum_{k=1}^{m} \Gamma_k \bar{\sigma}_{k_r} dx \qquad (2)$$

$$L_I' = \frac{1}{2} \rho U_o \mathbf{R} \oint_{x=l} F' d(\zeta\bar{\zeta}) - \frac{1}{2} \rho U_o \mathbf{R} \oint_{x=x_{TE+}} F' d(\zeta\bar{\zeta}) +$$

$$\frac{1}{2} \rho \mathbf{R} \int_{TE}^{l} dx \frac{\partial}{\partial t} \oint F' d(\zeta\bar{\zeta}) - \rho \mathbf{R} \int_{TE}^{l} \bar{R} \sum_{k=1}^{m} \Gamma_k \sigma_{k_r} dx \qquad (3)$$

where $\mathbf{R}$ denotes the real part, p is the rate of roll about the x axis, F' is the complex potential due to the wing vortices and their images in the tail, and σ_{k_r} represents the (complex) distance between the kth shed vortex and its image in the transformed circle plane.

Evidently, the two essential quantities to be determined before equations (1) to (3) can be applied are the additional complex potential F' and the sum $\sum_{k=1}^{m} \Gamma_k \sigma_{k_r}$ representing the impulse of the shed vortices and their images.

Although the analyses of references 10 and 11 employed a coordinate system whose x axis passes through the airplane nose, it can be shown that the results of those analyses are unaffected by a normal translation of the x axis provided that the cross-sectional area satisfies the condition $S = (dS/dx) = 0$ at the airplane nose. This condition is satisfied by all the wings of the wing-tail combinations to be treated in the present analysis, and it is convenient for our purpose here to use a coordinate system fixed in the tail as illustrated in figure 1(a).

It can be seen from equation (1) that for steady straight flight $[p = (\partial/\partial t) = 0]$ the interference lift and side force are independent of the plan forms of the wing and tail. Consequently, the calculated curves of steady lift and side force presented in this report are for slender wings and tails of arbitrary plan form except that their trailing edges

must lie in planes normal to the x axis. On the other hand, equations (1), (2), and (3) show that the lift and side force in unsteady flight and the moments in steady flight require integrations over specified plan forms. The calculations of steady moments and of unsteady lift presented in this report have been carried out for triangular plan forms only.

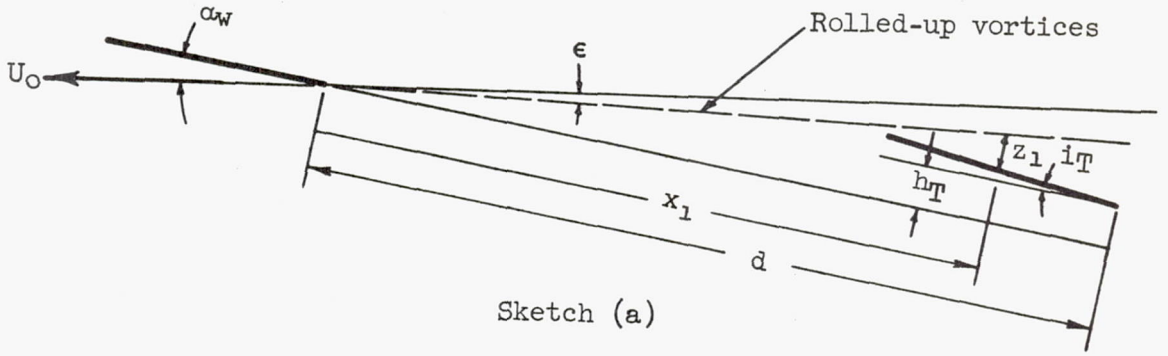
STEADY STRAIGHT FLIGHT

In this portion of the analysis we shall specialize equations (1) and (2) to steady straight flight by setting $p = (\partial/\partial t) = 0$. The last two terms of each of these equations are thus eliminated.

Plane Wing and Cruciform Tail

For most of the wing-tail combinations to be treated here, the wing is taken as a planar, slender, pointed thin wing having its maximum span at the trailing edge which is assumed straight. In all cases, the tail is considered rigidly attached to the wing. It is also assumed that the vortex sheet leaves the wing as a flat sheet at the trailing edge and becomes fully rolled up into two discrete line vortices somewhere ahead of the tail.

It is further assumed that the tail does not influence the vortex positions. The validity of this assumption has been investigated experimentally and will be discussed in a later section of this report. For



Sketch (a)

such cases, then it can be seen from sketch (a) that the vertical position z_1 of both vortices relative to the horizontal tail is given by

$$z_1 = (\alpha_w - \epsilon)x_1 - h_T - (d - x_1)i_T \qquad (4)$$

where the angle ϵ is easily computed by calculating the velocity of a two-dimensional vortex pair placed at the centroids of vorticity of the

wing. Since this procedure places the vortices $(\pi/2)s_o$ apart, due to the elliptic circulation distribution (which is unaffected by sideslip) the angle ϵ is found to be equal to $(2/\pi^2)\alpha_w$. It should be mentioned that the positions calculated in this way are in good agreement with those observed experimentally behind a wing alone, as pointed out in reference 12, even though the details of the rolling up have been ignored. The lateral positions (in body axes) are evidently

$$y_1 = \frac{\pi}{4} s_o - \beta x_1 \; ; \qquad y_2 = -\frac{\pi}{4} s_o - \beta x_1 \tag{5}$$

where the subscripts 1 and 2 on y refer to the starboard and port vortices, respectively. Thus the positions of the two rolled-up vortices at a distance x_1 behind the wing are completely defined by

$$\left.\begin{aligned} \zeta_1 = y_1 + iz_1 &= \frac{\pi}{4} s_o - i(h_T + di_T) - x_1\left\{\beta - i\left[\alpha_w\left(1 - \frac{2}{\pi^2}\right) + i_T\right]\right\} \\ \zeta_2 = y_2 + iz_1 &= -\frac{\pi}{4} s_o - i(h_T + di_T) - x_1\left\{\beta - i\left[\alpha_w\left(1 - \frac{2}{\pi^2}\right) + i_T\right]\right\} \end{aligned}\right\} \tag{6}$$

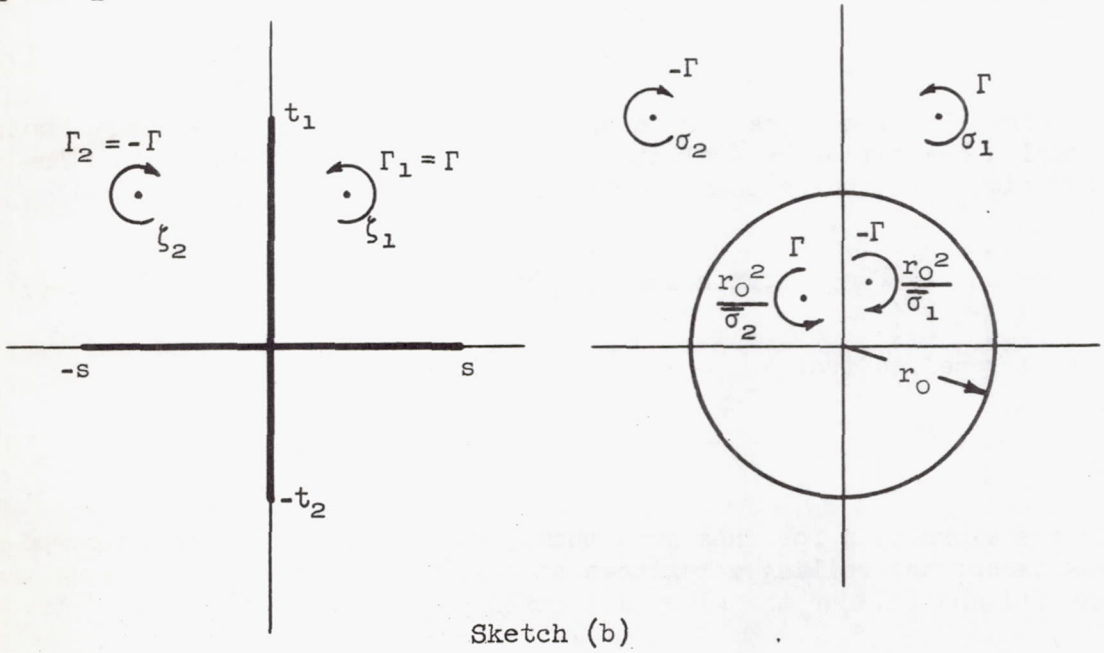
The magnitude of the strength Γ of each of the rolled-up vortices is obtained by equating the impulse of the vortex pair to the lift of the wing, that is,

$$\rho U_o \Gamma \frac{\pi}{2} s_o = L_w = \pi \rho U_o^2 \alpha_w s_o^2$$

or

$$\Gamma = 2U_o \alpha_w s_o \tag{7}$$

It is noted that for the fully rolled-up vortex pair $m = 2$ and $\Gamma_2 = -\Gamma_1 = -\Gamma$ (see sketch (b)). Finally, in order to calculate the



Sketch (b)

sum $\sum_{k=1}^{m} \Gamma_k \sigma_{k_r}$, the transformation of the tail cross section to a circle (leaving the flow field at infinity unchanged) is required. Such a transformation for the class of cross sections shown in sketch (b) is given in reference 10 as

$$\zeta^2 - s^2 = \left[\frac{i}{2}(h - f) + \sigma - \frac{(h+f)^2}{16\sigma}\right]^2 \tag{8}$$

and

$$r_o = \frac{h + f}{4}$$

where

$$h = \sqrt{s^2 + t_1^2} \; ; \qquad f = \sqrt{s^2 + t_2^2}$$

so that the inverse transformation relating the vortex positions in the two planes is

$$\sigma_k = -\frac{1}{4}\left\{ i\left(\sqrt{s^2 + t_1^2} - \sqrt{s^2 + t_2^2}\right) - 2\sqrt{\zeta_k^2 - s^2} + \sqrt{\left[i\left(\sqrt{s^2+t_1^2} - \sqrt{s^2+t_2^2}\right) - 2\sqrt{\zeta_k^2 - s^2}\right]^2 + \left[\sqrt{s^2+t_1^2} + \sqrt{s^2+t_2^2}\right]^2} \right\} \tag{9}$$

In writing the transformation in this form, we require that square roots of complex quantities be evaluated in the manner of the appendix. The proper signs are thus automatically taken care of.

The sum $\sum_{k=1}^{m} \Gamma_k \sigma_{k_r}$ can now be determined from equations (7) and (9) if it is recalled that

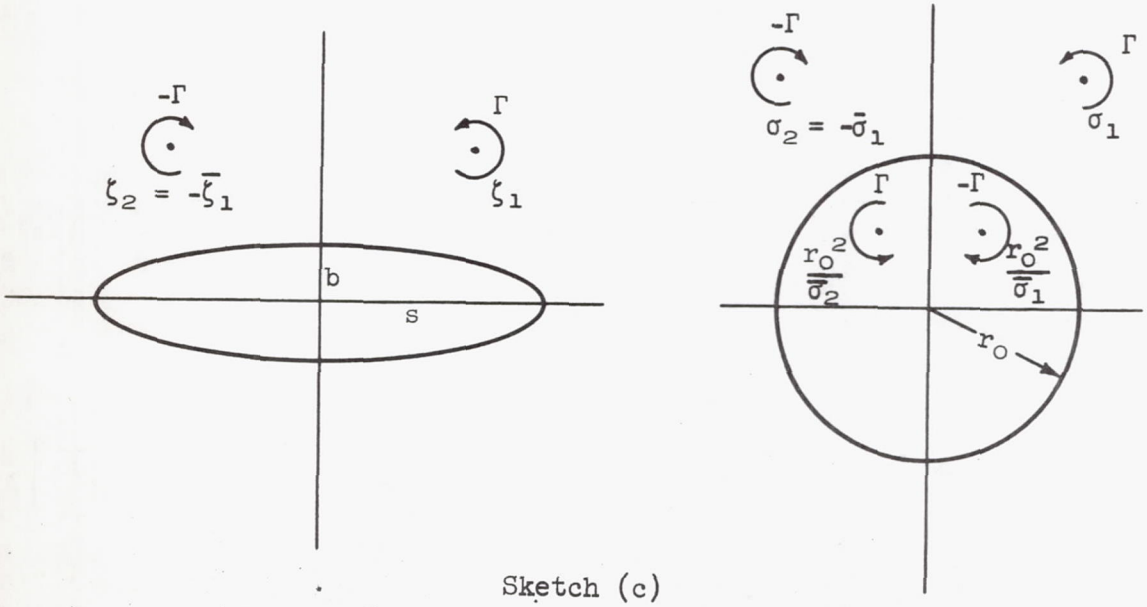
$$\sigma_{k_r} \equiv \sigma_k - \frac{r_o^2}{\bar{\sigma}_k} \tag{10}$$

With the expression for this sum, then, all the force and moment components except the rolling moment can be calculated directly from equations (1) and (2) for the wing-tail combinations discussed above. It

will be noted that the above expressions for the sum $\sum_{k=1}^{m} \Gamma_k \sigma_{k_r}$ have been developed only for the fully rolled-up vortices. However, between the wing and tail, since there is no body, the impulse $\rho U_o \sum_{k=1}^{m} \Gamma_k \sigma_{k_r}$ is independent of the wake shape, being always equal to the lift of the wing. Therefore, it has only been assumed that the vortices become fully rolled up somewhere ahead of the tail.

The following paragraphs will be concerned with the actual calculations relating to the longitudinal, directional, and lateral stability of several wing-tail combinations falling into the category discussed in the foregoing analysis. The determination of the integral $\oint F'd(\zeta\bar{\zeta})$ will be carried out in the discussion of lateral stability since it arises only in the calculation of the rolling moments.

Longitudinal stability.- Since the vertical tail has no effect on the purely longitudinal ($\beta = 0$) aerodynamic characteristics of the wing-tail combination, we can for this discussion set $t_1 = t_2 = 0$, thereby simplifying the calculations. In fact, since equation (8) then reduces to the Joukowsky transformation, the addition of elliptical thickness to the horizontal tail offers no difficulty and will be incorporated. Thus the expression for σ_k to be used for calculating the longitudinal characteristics will be (see sketch (c))



Sketch (c)

$$\sigma_k = \frac{1}{2}\left[\zeta_k + \sqrt{\zeta_k{}^2 - (s^2 - b^2)}\right] \tag{11}$$

and

$$r_o = \frac{s + b}{2}$$

The thickness of the tail will be kept small in the calculations, in view of the assumption that the tail does not affect the vortex positions. The wing-tail combinations treated in this section will have the general appearance shown in figure 1(b). The wing is shown as a triangular flat plate and the horizontal tail is shown as a thin elliptic cone since these assumptions will be made in the calculation of the pitching moments. However, they will not be made for the calculation of the steady lift since equation (1) shows that the interference lift and side force in steady straight flight are independent of plan form.

If it is noted that, due to symmetry (see sketch (c)) $\sigma_2 = -\bar{\sigma}_1$, the sum $\sum_{k=1}^{2} \Gamma_k \sigma_{k_r}$ over the tail can be written directly as

$$\sum_{k=1}^{2} \Gamma_k \sigma_{k_r} = \Gamma_1 \sigma_{1r} + \Gamma_2 \sigma_{2_r} = \Gamma\left(\sigma_{1r} + \bar{\sigma}_{1r}\right) = 2\Gamma \mathbf{R}\left(\sigma_{1r}\right) \tag{12}$$

But from equations (10) and (11) we have

$$\sigma_{1r} = \sigma_1 - \frac{r_o{}^2}{\bar{\sigma}_1}$$

$$= \frac{1}{2}\left\{\zeta_1 + \sqrt{\zeta_1{}^2 - (s^2 - b^2)} - \left(\frac{s + b}{s - b}\right)\left[\bar{\zeta}_1 - \sqrt{\bar{\zeta}_1{}^2 - (s^2 - b^2)}\right]\right\} \tag{13}$$

so equation (12) becomes

$$\sum_{k=1}^{2} \Gamma_k \sigma_{k_r} = \Gamma \mathbf{R}\left\{\zeta_1 + \sqrt{\zeta_1{}^2 - (s^2 - b^2)} - \left(\frac{s + b}{s - b}\right)\left[\zeta_1 - \sqrt{\zeta_1{}^2 - (s^2 - b^2)}\right]\right\} \tag{14}$$

Returning now to equation (1) we have for steady straight flight

$$Y_I - iL_I = -i\rho U_o \left[\left(\sum_{k=1}^{m} \Gamma_k \bar{\sigma}_{k_r} \right)_{x=l} - \left(\sum_{k=1}^{m} \Gamma_k \bar{\sigma}_{k_r} \right)_{x=x_{TE+}} \right] \tag{15}$$

and, by virtue of symmetry for $\beta = 0$, the interference side force Y_I vanishes. (This also follows from eq. (14) which shows that the above sums are real.) The interference lift L_I is given by the negative of the imaginary part of equation (15).

$$L_I = \rho U_o \mathbf{R} \left[\left(\sum_{k=1}^{m} \Gamma_k \sigma_{k_r} \right)_{x=l} - \left(\sum_{k=1}^{m} \Gamma_k \sigma_{k_r} \right)_{x=x_{TE+}} \right] \tag{16}$$

which can now be evaluated from equations (6), (7), and (14). That is, from equation (6), $\mathbf{R}(\zeta_1) = (\pi/4)s_o$ for all x and we note that immediately behind the wing $s = b = 0$. Thus it follows from equations (7), (14), and (16) that

$$L_I = \frac{4}{1 - (b/s)_l} \rho U_o{}^2 \alpha_w s_o \left[\mathbf{R} \sqrt{\zeta_{1_l}{}^2 - s_1{}^2 \left(1 - \frac{b^2}{s^2} \right)_l} - \frac{\pi}{4} s_o \right] \tag{17}$$

where s_1 is the semispan of the tail at its trailing edge. The quantity ζ_{1_l} gives the position of the starboard vortex at $x = l$ and is evaluated from equation (6) by setting $\beta = 0$ and $x_1 = d$. The total lift of the wing-tail combination is obtained by adding to equation (17) the lifts of the wing and tail alone as given by slender-body theory (see eq. (7)). The resulting expression for the lift coefficient, based on the area of the wing, is

$$C_L = \frac{\pi}{2} A_w \left(\alpha_w + \alpha_T \frac{s_1{}^2}{s_o{}^2} \right) + \frac{2A_w \alpha_w}{1 - (b/s)_l} \left[\mathbf{R} \sqrt{\frac{\zeta_{1_l}{}^2}{s_o{}^2} - \frac{s_1{}^2}{s_o{}^2} \left(1 - \frac{b^2}{s^2} \right)_l} - \frac{\pi}{4} \right] \tag{18}$$

and it can be seen that, to the order of the present analysis, tail thickness affects the lift only if the tail has a blunt trailing edge. The procedure for calculating the real part of the square root without ambiguity has been discussed in Appendix B of reference 11.

By making use of the same substitutions in equation (2) as were used in equation (1) for the interference side force and lift, one finds similarly that the interference yawing moment vanishes (for $\beta = 0$) and that, after integration by parts, the interference pitching moment about the pivot point $x = c_1$ can be expressed as

$$M_I = -\frac{4}{1-(b/s)}\rho U_o^2 \alpha_w s_o \left[\left(l - c_1\right) \mathbf{R} \sqrt{\zeta_{1l}^2 - s_1^2 \left(1 - \frac{b^2}{s^2}\right)_l} - \right.$$

$$\left. \frac{\pi}{4} s_o \left(l - c_1 - c'\right) - \int_o^{c'} \mathbf{R} \sqrt{\zeta_1^2 - s^2 \left(1 - \frac{b^2}{s^2}\right)} \, dx' \right] \tag{19}$$

provided that b/s is constant over the tail.[1] In this expression c' is the chord of the tail and x' is distance along the x axis measured from the apex of the tail. Now let us choose the pivot point to be $c_1 = 2/3\ c$ and the plan forms of wing and tail to be triangular. Then the triangular wing contributes no pitching moment, and if we add the known pitching moment of the conical tail alone as given by

$$M_T = -L_T \left(d + \frac{c}{3} - \frac{c'}{3}\right) = -\pi\rho U_o^2 \alpha_T s_1^2 \left(d + \frac{c}{3} - \frac{c'}{3}\right) \tag{20}$$

the resulting expression for the total pitching-moment coefficient, based on the wing area $s_o c$ and the wing chord c is

$$C_m = -\frac{\pi}{2} A_w \alpha_T \frac{s_1^2}{s_o^2} \left(\frac{d}{c} + \frac{1}{3} - \frac{1}{3}\frac{c'}{c}\right) -$$

$$\frac{2A_w\alpha_w}{1-(b/s)} \left[\left(\frac{d}{c} + \frac{1}{3}\right) \mathbf{R} \sqrt{\frac{\zeta_{1l}^2}{s_o^2} - \frac{s_1^2}{s_o^2}\left(1 - \frac{b^2}{s^2}\right)} - \frac{\pi}{4}\left(\frac{d}{c} + \frac{1}{3} - \frac{c'}{c}\right) - \right.$$

$$\left. \frac{A_w}{4} \int_o^{\frac{c'}{s_o}} \mathbf{R} \sqrt{\frac{\zeta_1^2}{s_o^2} - \frac{s^2}{s_o^2}\left(1 - \frac{b^2}{s^2}\right)} d\left(\frac{x'}{s_o}\right) \right] \tag{21}$$

The integration indicated in equation (21) is most easily carried out if the real part is taken after the integration. With this in mind, then, we observe that the variable x' is related to x_1 by (see fig. 1(b))

[1]The corresponding expression for arbitrary chordwise thickness distribution ($b/s \neq$ const.) can just as easily be obtained in the same way, but the calculated results will depend on the particular shape chosen and the integrals will in general have to be evaluated by numerical or graphical methods for each case.

$$x_1 = x' + d - c' \tag{22}$$

and that for the conical tail $s/s_o = (A_T/4)(x'/s_o)$ and b/s is constant. Hence, by means of equation (6), the complex square root in the integrand can be expressed as

$$\sqrt{\frac{\zeta_1^2}{s_o^2} - \frac{s^2}{s_o^2}\left(1 - \frac{b^2}{s^2}\right)} = \sqrt{B + C\left(\frac{x'}{s_o}\right) + D\left(\frac{x'}{s_o}\right)^2} = \sqrt{X} \tag{23}$$

where

$$\left.\begin{aligned} B &= \left\{\frac{\pi}{4} + i\left[\alpha_w\left(1 - \frac{2}{\pi^2}\right)\left(\frac{d - c'}{s_o}\right) - \left(\frac{h_T + i_T c'}{s_o}\right)\right]\right\}^2 \\ C &= \left[\alpha_w\left(1 - \frac{2}{\pi^2}\right) + i_T\right]\left[i\,\frac{\pi}{2} - 2\alpha_w\left(1 - \frac{2}{\pi^2}\right)\left(\frac{d - c'}{s_o}\right) + 2\left(\frac{h_T + i_T c'}{s_o}\right)\right] \\ D &= -\left[\alpha_w\left(1 - \frac{2}{\pi^2}\right) + i_T\right]^2 - \frac{A_T^2}{16}\left(1 - \frac{b^2}{s^2}\right) \end{aligned}\right\} \tag{24}$$

and the integral in equation (21) can be expressed in the form

$$\int_0^{\frac{c'}{s_o}} \mathbf{R}\sqrt{X}\,d\xi = \frac{1}{4D}\mathbf{R}\left[(2D\xi + C)\sqrt{X} + \frac{4BD - C^2}{2\sqrt{D}}\ln\left(\sqrt{X} + \xi\sqrt{D} + \frac{C}{2\sqrt{D}}\right)\right]_0^{\frac{c'}{s_o}}$$

$$= \frac{1}{4D}\Bigg[\mathbf{R}(2D\xi + C)\,\mathbf{R}\sqrt{X} - \mathbf{I}(2D\xi + C)\,\mathbf{I}\sqrt{X} +$$

$$\frac{1}{2}\mathbf{R}\left(\frac{4BD - C^2}{\sqrt{D}}\right)\mathbf{R}\ln\left(\sqrt{X} + \xi\sqrt{D} + \frac{C}{2\sqrt{D}}\right) -$$

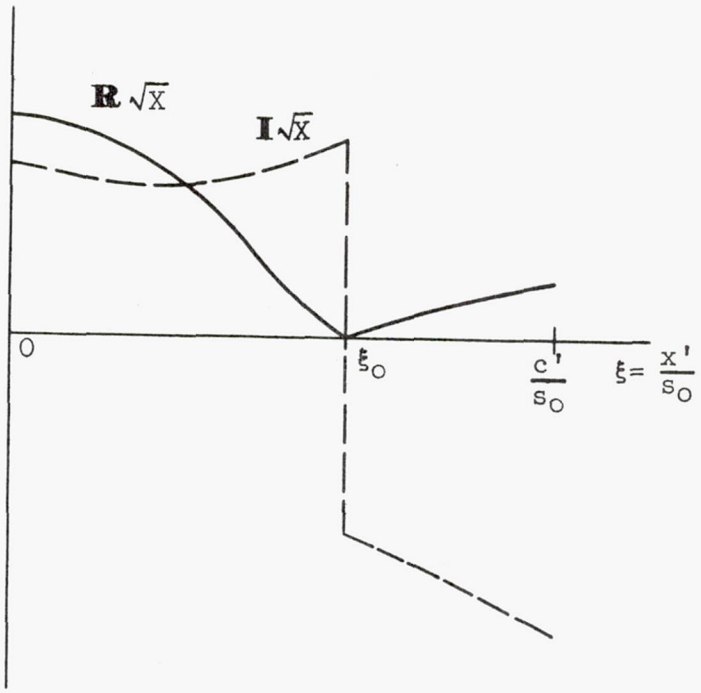
$$\frac{1}{2}\,\mathbf{I}\left(\frac{4BD - C^2}{\sqrt{D}}\right)\mathbf{I}\ln\left(\sqrt{X} + \xi\sqrt{D} + \frac{C}{2\sqrt{D}}\right)\Bigg]_0^{\frac{c'}{s_o}} \tag{25}$$

where $\xi = (x'/s_o)$. Now if any of the terms in this expression has a discontinuity within the interval of integration the integral must be divided at that point. Such discontinuities will in fact occur if the rolled-up vortex passes through the horizontal tail. This occurrence

will be discussed later from the physical point of view, but for the moment we need only to recognize that the mathematical expression of this situation is (for a triangular tail)

$$z_1 = 0 \quad \text{for} \quad \frac{\pi}{A_T} \leq \frac{x'}{s_o} \leq \frac{c'}{s_o} \tag{26}$$

where z_1 is given by the imaginary part of equation (6). The variations of $\mathbf{R}\sqrt{X}$ and $\mathbf{I}\sqrt{X}$ for a typical case in which equation (26) is satisfied are shown in sketch (d) and it can be seen that at $\xi = \xi_o$ (the value of x'/s_o at which z_1 is zero) the real part of the square root vanishes and the imaginary part has a discontinuity.



Sketch (d)

Thus, making use of the continuity of the real part of the square root at $\xi = \xi_o$, and writing out the real and imaginary parts of the

logarithm, we can finally write equation (25) in the form

$$\int_0^{\frac{c'}{s_0}} \mathbf{R}\sqrt{X}\,d\xi = \int_0^{\xi_0} \mathbf{R}\sqrt{X}\,d\xi + \int_{\xi_0}^{\frac{c'}{s_0}} \mathbf{R}\sqrt{X}\,d\xi$$

$$= \frac{1}{4D}[G]_{\xi=\frac{c'}{s_0}} - \frac{1}{4D}[G]_{\xi=0} + \frac{1}{4D}\left(\mathbf{R}\left(\frac{4BD - C^2}{2\sqrt{D}}\right)\left(\ln\left|\sqrt{X} + \xi\sqrt{D} + \frac{C}{2\sqrt{D}}\right|_{\xi_0-} - \right.\right.$$

$$\left.\ln\left|\sqrt{X} + \xi\sqrt{D} + \frac{C}{2\sqrt{D}}\right|_{\xi_0+}\right) - \mathbf{I}(2D\xi + C)\left(\mathbf{I}\sqrt{X}_{\xi_0-} - \mathbf{I}\sqrt{X}_{\xi_0+}\right) -$$

$$\left.\mathbf{I}\left(\frac{4BD - C^2}{2\sqrt{D}}\right)\left\{\tan^{-1}\left[\frac{\mathbf{I}\left(\sqrt{X} + \xi\sqrt{D} + \frac{C}{2\sqrt{D}}\right)}{\mathbf{R}\left(\sqrt{X} + \xi\sqrt{D} + \frac{C}{2\sqrt{D}}\right)}\right]_{\xi_0-} - \tan^{-1}\left[\frac{\mathbf{I}\left(\sqrt{X} + \xi\sqrt{D} + \frac{C}{2\sqrt{D}}\right)}{\mathbf{R}\left(\sqrt{X} + \xi\sqrt{D} + \frac{C}{2\sqrt{D}}\right)}\right]_{\xi_0+} + 2n\pi\right\}\right) \tag{26a}$$

where G is identical with the quantity in the brackets of equation (25) and the subscripts ξ_0- and ξ_0+ refer, respectively, to values immediately before and after the discontinuity. The value of n (an integer or zero) is determined by the fact that the resulting expression for the integral must be a continuous function of α_w since B, C, and D are continuous functions of α_w.

Calculations have been carried out by means of equation (18) and equations (21) through (26a) to determine the total lift and pitching-moment coefficients of a number of wing-tail combinations of the

type shown in figure 1(b). It can be seen from equations (18) and (21) (recalling eq. (6)) that the theoretical lift and pitching moment are nonlinear functions of the angle of attack α_w. In view of this fact, it seems appropriate to postpone temporarily the calculation of stability derivatives and to calculate instead the actual variations of forces and moments with angle of attack. For the present calculations, the aspect ratio of both wing and tail was chosen as 2 in all cases, and the effects of horizontal tail height h_T, tail-span-to-wing-span ratio s_1/s_0, tail incidence i_T, horizontal-tail thickness ratio b/s, and tail length d have been investigated. The calculated results are presented in figures 2 to 6 and the lift coefficients are divided by $(\pi/2)A_w$ since equation (18) shows the lift coefficient to be linear[2] with respect to the wing aspect ratio A_w. The pitching moments are nonlinear in A_w since equation (21) contains products of A_w with d/c and c'/c which are themselves proportional to A_w since all quantities are specified in terms of the wing semispan s_0.

The effect of horizontal-tail height on the lift and pitching moments is illustrated in figure 2 for zero tail incidence and zero tail thickness. It can be seen from equation (17) that for $b/s = 0$, the interference lift becomes equal and opposite to the lift of the wing if $\mathbf{R}\sqrt{\zeta_{1l}^2 - s_1^2} = 0$. This condition is satisfied if ζ_{1l} is real and less than s_1, that is, if the rolled-up vortices from the wing just intersect the trailing edge of the tail. In figure 2, the tail heights have been chosen so that this situation occurs at simple values of α_w, and it can be seen that, in each case, at that angle of attack the total lift is equal to the lift of the tail alone which is equal to the lift of the wing since the tail span is equal to the wing span. It would appear from figure 2 that unless the horizontal tail is placed either low ($h_T \leq 0$) or very high, the lift and pitching-moment curves are apt to be highly nonlinear, even in the relatively low positive angle-of-attack range. Severe static instability precedes the "critical" angle of attack (the angle of attack at which the wing vortices intersect the tail trailing edge) and abrupt changes in both lift-curve slope and static stability are observed at the critical angle.

While the sharp breaks in the lift and pitching-moment curves indicated by the theory will no doubt be smoothed out somewhat in actual flight through a real fluid, it might be well to consider the significance of the critical angle of attack described above. First, the existence of such a well-defined critical angle is predicated on the assumption that the vortices shed from the wing lie in a horizontal line when viewed in planes $x = \text{const.}$, that is, that the vortex sheet either remains flat or is fully rolled up ahead of the tail. In such a case, the tail experiences a maximum download when the line containing its

[2]It must be noted that the equations also show the lift and pitching moment to be nonlinear with respect to all of the parameters investigated in the calculations. The calculated effects of the separate parameters are therefore not additive.

trailing edge intersects the vortices, as the tail is then in a maximum downwash field. Such a critical angle might be thought of as a local stall angle for the airplane and will be predicted by the theory for all slender plane wing-tail combinations whose wing and tail do not lie in the same plane. It might be said that if the wing and tail lie in the same plane, the critical angle is zero, but since the downwash is then also zero, the angle has little significance.

The critical angle of attack can be calculated directly from equation (6) by setting z_1 (i.e., the imaginary part of ζ_1 or ζ_2) to zero at $x_1 = d$. Thus one finds

$$\alpha_{cr} = \frac{h_T/s_o}{(d/s_o)[1 - (2/\pi^2)]} \tag{27}$$

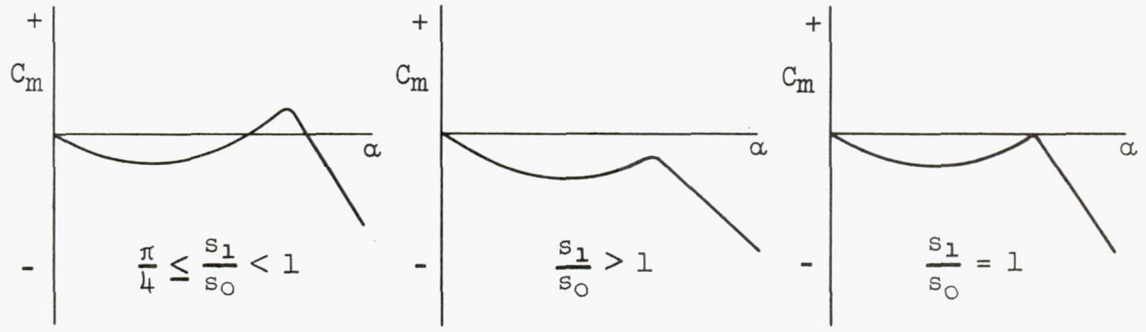
for the combinations treated in this section. Evidently, then, α_{cr} depends on the ratio of tail height to tail length and will be positive if the tail is above the plane of the wing and negative if the tail lies below the plane of the wing. For the former case (high tail), the tail will experience a maximum download, causing a peak positive pitching moment, while for the latter case (low tail), the tail will experience a maximum upload, causing a peak negative pitching moment. These two types of cases are clearly seen in figure 2. The critical angle of attack can of course be made larger than the stall angle of the wing itself by placing the tail very high. In figure 2 for $h_T/s_o = 1.9137$, for example, the lift and pitching-moment curves remain fairly linear up to an angle of attack of about 10°. It should be mentioned with regard to the above discussion that, if the vortex sheet is only partially rolled up at the tail location, the vortices do not lie in a horizontal line there, the critical angle of attack loses definition, and the lift and moment curves, although nonlinear, will not exhibit the sharp breaks discussed above.

In figure 3, the ratio of tail span to wing span is varied for a given tail height. It can be seen that the lift and pitching-moment curves exhibit sharp peaks when the ratio of tail span to wing span becomes equal to or slightly greater than $\pi/4$ (the ratio of vortex span to wing span). That is, once again, the curves have sudden changes in slope if the wing vortices strike the tail trailing edge near the tips. Thus, it might be said that there is a critical ratio of tail span to wing span as well as a critical angle of attack. However, it should be pointed out that the specific value of $\pi/4$ is a consequence of several assumptions; namely, (1) that the vortices are fully rolled up ahead of the tail, (2) that the tail has no influence on the vortex positions, and (3) that the trailing-edge cross section of the tail is fully effective in destroying the downwash field of the wing, even though the chord of the tail vanishes at the tips. This last assumption is associated with the slender-body assumption that the flow in planes $x = \text{const.}$ is essentially two-dimensional.

The sign of the pitching moment at the critical angle of attack can be determined from the ratio of tail span to wing span, provided this

ratio is equal to or greater than the critical ratio. It has already been pointed out that the lift of the plane wing-tail combination at the critical angle of attack is equal to the lift of the tail alone at its geometric angle of attack, if the tail span is at least as great as the vortex span. Therefore, the lift on the tail of the combination is equal to the difference between the lifts of the isolated tail and wing at their geometric angles of attack. But, according to slender-wing theory, these lifts depend only on the maximum spans of the wing and tail. Hence, it can be concluded that if the span of the tail is less than the span of the wing, the lift on the tail at the critical angle of attack is negative and the pitching moment of the combination is therefore positive. Since it was stipulated above that the ratio of tail span to wing span was greater than the critical value, the conclusion is that for $\frac{\pi}{4} \leq \frac{s_1}{s_o} < 1$, the pitching moment at the critical angle of attack is positive. On the other hand, if the tail span is greater than the wing span, the lift on the tail is positive at $\alpha = \alpha_{cr}$, so the pitching moment of the combination is negative. Finally, if $s_1/s_o = 1$, the lift on the tail, and hence the pitching moment of the combination, vanishes at the critical angle of attack.

The above conclusions may be summarized schematically as shown in sketch (e). It can be seen that in the first case there are three trim



Sketch (e)

points, two stable, and one unstable; in the second case there is only one trim point, which is stable; and in the third case there are two trim points, one stable and one neutrally stable. In the above discussion, the tail incidence has been assumed to be zero. It has also been assumed that the pitching moment of the wing alone is zero, which is the case for all the combinations treated in this paper.

The effect of changes in tail length on the lift and pitching-moment curves is shown in figure 4 for two tail heights with the tail at zero incidence and the tail span equal to the wing span. For zero tail height (fig. 4(a)), the predominant effect of increasing the tail length is apparently the larger pitching moments due to the increased lever arm. However, the lift on the tail at a given angle of attack is also seen to increase with the tail length. This is due to the greater vertical distance between the tail and the wing vortices, which results in a reduction of wing-tail interference.

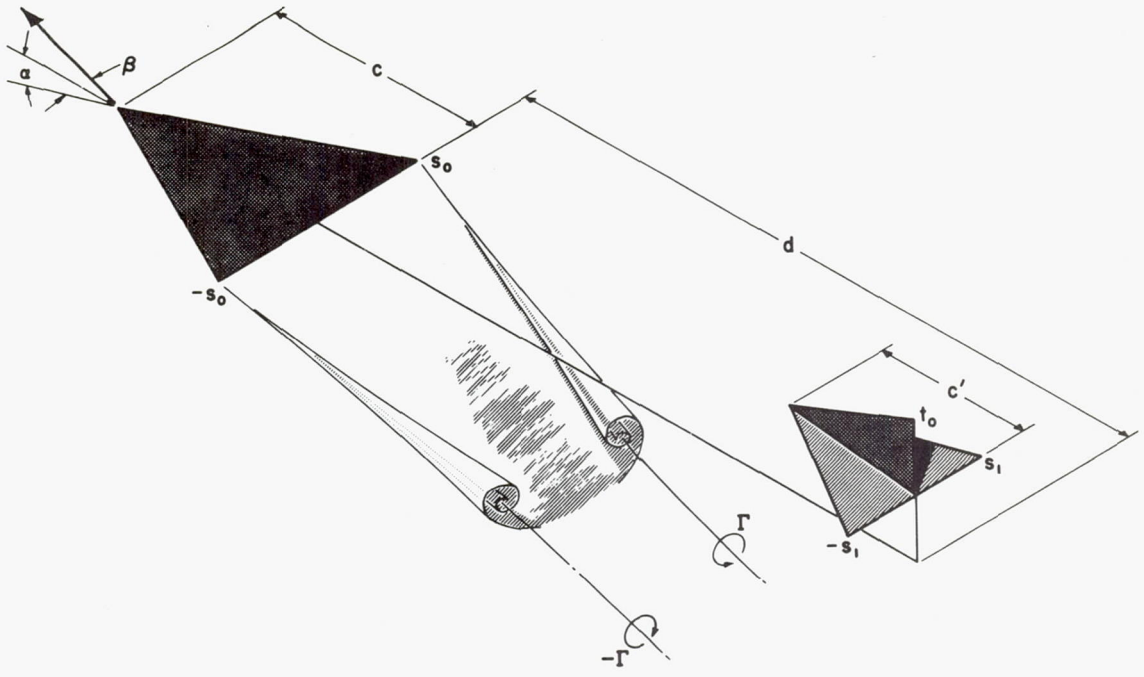
For the case of a given nonzero tail height (fig. 4(b), h_T/s_o=0.9568), the most obvious effect of a change in tail length is a corresponding change in the critical angle of attack. It can be seen that reducing the tail length ratio d/s_o from 6 to 4 increases α_{cr} from 0.20 to 0.30, as predicted by equation (27). Now it is interesting to compare figure 4(b) with figure 2 in which α_{cr} was changed by a change in tail height with a fixed tail length. Let us say, for example, that we start with a wing-tail combination having $d/s_o = 6$ and $\alpha_{cr} = 0.2$, and we wish to shift α_{cr} to 0.15. A comparison of figures 4(b) and 2 shows that, if this shift is accomplished by increasing the tail length ratio to 8, the resulting pitching moments are about 50 percent larger than if it is accomplished by lowering the horizontal tail.

In figure 5, the tail incidence is varied at two different tail heights for a fixed tail length ($d/s_o = 6$) and a fixed span ratio ($s_1/s_o = 1$). It can be seen that for $h_T = 0$ (fig. 5(a)), the lift and pitching-moment curves are shifted linearly up and down with tail incidence. Since the curves are slightly nonlinear in the angle of attack, however, the result is a slightly nonlinear variation of trim lift coefficient with control setting (for an all-movable tail). Now if the tail does not lie in the plane of the wing, ($h_T/s_o = 0.9568$, fig. 5(b)), the nonlinearities in the lift and pitching-moment curves, and hence in control effectiveness, become more pronounced. It can be seen in figure 5(b) that the change in trim angle of attack from $i_T = 0$ to $i_T = -0.1$ is more than twice that from $i_T = +0.1$ to $i_T = 0$. Also, there are evidently incidence settings between 0 and -0.1 for which there will be three trim angles of attack, as in the preceding discussion.

The effect of tail thickness is shown in figure 6 and the effect on the lift and pitching moment for zero tail height (fig. 6(a)) is seen to be small for the configuration chosen. However, there is a consistent decrease in tail lift associated with the increase of tail thickness. For the high-tail case (fig. 6(b)), this effect is magnified at positive angles of attack, with the result that the nonlinearities due to tail height increase with tail thickness. It should be recalled that the tail thickness introduced here is of a very special type (elliptic cone tail) and incorporates a blunt trailing edge. The present theory would predict no effect of thickness on the lift and only a small effect on the pitching moment if the tail trailing edge were sharp. On the other hand, ordinary slender-body theory (i.e., with no wing-tail interference) would predict no effect of elliptic thickness on either the lift or the pitching moment, regardless of whether the trailing edge is blunt or sharp (see ref. 10).

Directional stability.- In this portion of the analysis, the emphasis will be on the effectiveness of the vertical tail, and we turn to a

somewhat more special class of wing-tail combinations as shown in sketch (f) although the plan forms need not be triangular. Thus we let



Sketch (f)

$t_2 = b/s = 0$. The inverse transformation of equation (9) then gives the vortex positions in the σ plane as

$$\sigma_k = -\frac{1}{4}\left\{ i\left(\sqrt{s^2 + t_1^2} - s\right) - 2\sqrt{\zeta_k^2 - s^2} + \sqrt{\left[i\left(\sqrt{s^2 + t_1^2} - s\right) - 2\sqrt{\zeta_k^2 - s^2}\right]^2 + \left[\sqrt{s^2 + t_1^2} + s\right]^2}\right\} \quad (28)$$

and ζ_k is again given by equations (6). Now, by direct substitution into equation (10) with the auxiliary formulas of equation (8), it can be shown that[3]

[3]The actual evaluation of the imaginary part of the square root indicated in equation (29) is not entirely straightforward if ambiguities are to be avoided. Consequently the procedure is given in the appendix. Taking the real part of the simpler square root has been discussed in Appendix B of reference 11.

$$\left.\begin{aligned} \mathbf{R}\left(\sigma_{k_r}\right) &= \mathbf{R}\sqrt{\zeta_k^2 - s^2} \\ \mathbf{I}\left(\sigma_{k_r}\right) &= -\frac{1}{2}\,\mathbf{I}\sqrt{\left[i\left(\sqrt{s^2 + t_1^2} - s\right) - 2\sqrt{\zeta_k^2 - s^2}\right]^2 + \left[\sqrt{s^2 + t_1^2} + s\right]^2} \end{aligned}\right\} \tag{29}$$

and with these expressions one can easily write the real and imaginary parts of the sum $\sum_{k=1}^{2} \Gamma_k \sigma_{k_r}$ from which the interference lift and side force can be obtained directly by means of equation (15). It can be seen from equation (29) that the real part of the above sum is independent of t_1, so it follows from equation (15) that the interference lift is independent of the size of the vertical tail, even for $\beta \neq 0$.

The lift of the wing alone is given by equation (7) and the side force and lift of the tail alone are given by (see ref. 10)

$$Y_T - iL_T = \pi\rho U_o^2\left[\frac{\beta}{2}\left(s_1^2 - \frac{t_o^2}{2} - s_1\sqrt{s_1^2 + t_o^2}\right) - i\alpha_T s_1^2\right] \tag{30}$$

This side force and lift when added to equation (7) and to the interference forces calculated by means of equations (15) and (29) yield the total side force and lift on wing-tail combinations of arbitrary plan form of the type shown in sketch (f) at combined angles of attack and sideslip.

Calculations have been carried out in this manner to obtain the variations of side force and lift coefficients, based on wing area, with angle of attack and sideslip for several vertical tail sizes with zero tail height and tail incidence ($h_T = i_T = 0$). These calculations were made only for one ratio of tail span to wing span ($s_1/s_o = 1$) and one tail length ratio ($d/s_o = 6$) inasmuch as the effects of these parameters may be surmised from the previous discussion on longitudinal stability. The results are presented in figures 7 and 8 in the form of force coefficients against sideslip angle for various angles of attack. It can be seen from figure 7 that at the very small angles of attack, the side force is linear with respect to the angle of sideslip. In fact the values of the slopes there are given by ordinary slender-body theory for the tail alone. At somewhat larger angles of attack, however, the curves are quite nonlinear and it will be noticed that the angle of attack at which the curve is most nonlinear increases with the tail size. It can in fact be shown that the most severe nonlinearities occur at such an angle of attack and sideslip that one of the rolled-up vortices from the wing

strikes the tip of the vertical tail, since in that situation the vertical fin experiences a maximum side force due to the vortex. The angles of attack and sideslip corresponding to this condition are given, according to the present theory, by equations (6) if we set ζ_1 or ζ_2 equal to it_o at $x_1 = d$. Thus we find

$$\beta = \pm \frac{\pi/4}{d/s_o}; \qquad \alpha = \frac{(t_o/s_o) + (h_T/s_o)}{(d/s_o)(1 - 2/\pi^2)} \tag{31}$$

In order to facilitate the fairing of the curves in figure 7, the angle of sideslip given by equation (31) was calculated for the cases shown in the figure, and the corresponding side forces were computed. It will be noted that if the angle of attack is less than that of equation (31), then one vortex strikes the trailing edge of the vertical tail at the angle of sideslip indicated in equation (31), thus causing a sharp peak in the variation of C_Y with β. On the other hand, at angles of attack higher than that of equation (31), the vortex passes above the vertical tail and the variation of side force with angle of sideslip is smooth although nonlinear. In figure 7(b) we see a very sharp peak in the curve for $\alpha = 0.20$ which corresponds almost exactly to the angle of attack indicated by equation (31) for the vertical tail size $t_o/s_1 = 1.0$.

Another important point regarding figure 7 can be seen by observing the variation of the slope $(\partial C_Y/\partial\beta)_{\beta=0}$ with angle of attack, since this quantity gives a measure of the directional stability; that is, since the vertical tail lies behind the probable center of gravity of the airplane, a positive C_{Y_β} corresponds to a negative C_{n_β} which is unstable. Thus it can be seen from the slopes through the origin in figure 7 that increasing the angle of attack has a destabilizing effect for angles of attack below the value given in equation (31). It should be mentioned here that, according to slender-body theory (no interference), the stability derivative $(\partial C_Y/\partial\beta)_{\beta=0}$ is independent of the angle of attack.

The variation of lift coefficient with angle of sideslip is given in figure 8 for various angles of attack. As was mentioned earlier, the lift is independent of the size of the vertical tail. It is observed that the lift is a minimum at $\beta = 0$ due to the fact that the horizontal tail is then in a maximum downwash field. Again, the effect of sideslip is felt only at the tail, so it can be concluded that at $\beta = 0$ the pitching moment has a positive maximum; hence sideslipping produces a nose-down pitching moment.

In order to see a little more clearly the effect of angle of attack on directional stability, approximate calculations have been made of the derivative $(\partial C_n/\partial\beta)_{\beta=0}$ at various angles of attack. It can be seen from equation (2) that a detailed calculation of the yawing-moment variation and subsequent differentiation with respect to β would be virtually

impossible by analytical means in view of the complicated expression of equation (29). Consequently, rather than performing laborious numerical calculations and measuring slopes graphically, we shall simply assume that the center of pressure of the tail is unaffected by the wing vortices and lies always at the 2/3-root chord of the tail.[4] Hence, since the flat-plate wing experiences no side force, the derivative C_{n_β} is given approximately (for $c'/c = 1$ and $d/s_o = 6$) by

$$C_{n_\beta} = (\partial C_n/\partial\beta)_{\beta=0} \approx -(d/2s_o)(\partial C_Y/\partial\beta)_{\beta=0} \approx -3(\partial C_Y/\partial\beta)_{\beta=0} \qquad (32)$$

where the yawing-moment coefficient is based on the wing span $2s_o$ and the slopes $(\partial C_Y/\partial\beta)_{\beta=0}$ are measured on figure 7. The resulting variations of C_{n_β} with angle of attack are shown in figure 9 and it can be seen that an increase in vertical tail size provides substantial increases in directional stability but that the directional stability diminishes considerably with increasing angle of attack. For the cases calculated ($s_1/s_o = 1$), it is observed that at about 10° angle of attack the stability contributed by a vertical tail the same size as one panel of the horizontal tail ($t_o/s_1 = 1.0$) is equal to the stability contributed by a vertical tail only half that size at $\alpha = 0$.

As was mentioned earlier, a negative value of C_{n_β} indicates directional instability, but in no case has a negative value been shown in the above figures. It might be well to consider now the likelihood of such an instability. First it will be recalled that the strengths and positions of the rolled-up vortices were calculated under the assumption that the circulation distribution at the wing trailing edge is elliptic, as predicted by slender-body theory for low angles of attack. In order to gain some idea of the effect of changes in circulation distribution, it was assumed that the circulation distribution tends toward a triangle at the higher angles of attack, as does the span loading at $\beta = 0$ according to low-speed experiments on triangular wings. Thus, keeping the same lift on the wing as before (eq. (7)), with a triangular circulation distribution, the lateral spacing of the vortices becomes equal to s_o and the strengths then become in the same manner as equation (7),

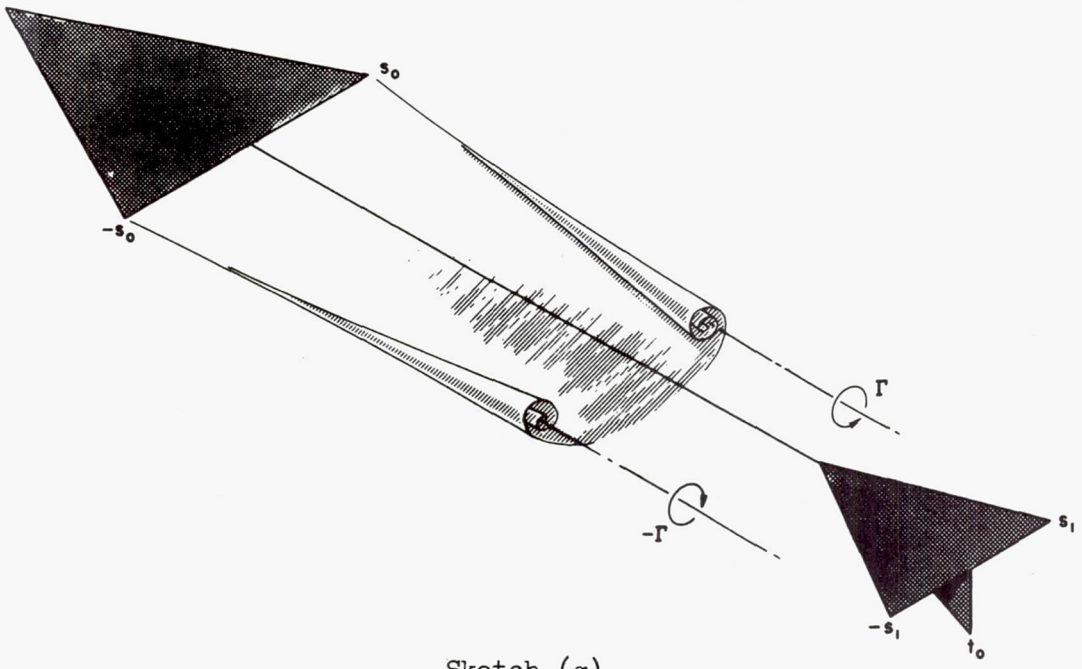
$$\Gamma = \pi U_o \alpha s_o \qquad (33)$$

[4]As a rough check on this approximation, the pitching moments were calculated in this manner for several span ratios with $h_T/s_o = 0.9568$, $d/s_o = 6$ and were compared with those shown in figure 3. The average error for these cases was of the order of 10 percent for the angle range calculated. For shorter tail lengths, the error will of course be larger. It should be noted that with this approximation the dependence of the moments upon plan form is contained in the choice of the center of pressure of the tail. The choice of the 2/3-root chord implies a triangular tail.

Using this strength and spacing, then, the variations of C_Y and C_L with β for $t_o/s_1 = 1$ were recalculated at $\alpha = 0.24$ and the results are given in figures 7(b) and 8. It can be seen that this change in circulation distribution has magnified the effects of sideslip and has produced a decidedly unstable side force slope at $\beta = 0$. The effect on the variation of lift, however, is small.

On an actual airplane or missile, a long fuselage whose nose is well ahead of the wing would further reduce the directional stability, although no calculations of this effect can be made here because of the complicated influence of the fuselage on the positions of the vortices at the tail. Thus it can be seen that the curves presented in figures 7, 8, and 9 are probably not unduly pessimistic.

As was mentioned previously, the greatest loss of directional stability due to wing-tail interference is suffered when the angle of attack is such that at some angle of sideslip one vortex strikes the tip of the vertical tail. The sign of this angle of attack can be reversed simply by inverting the tail assembly as shown in sketch (g). With this arrangement, the loss of directional stability can more easily be moved out of



Sketch (g)

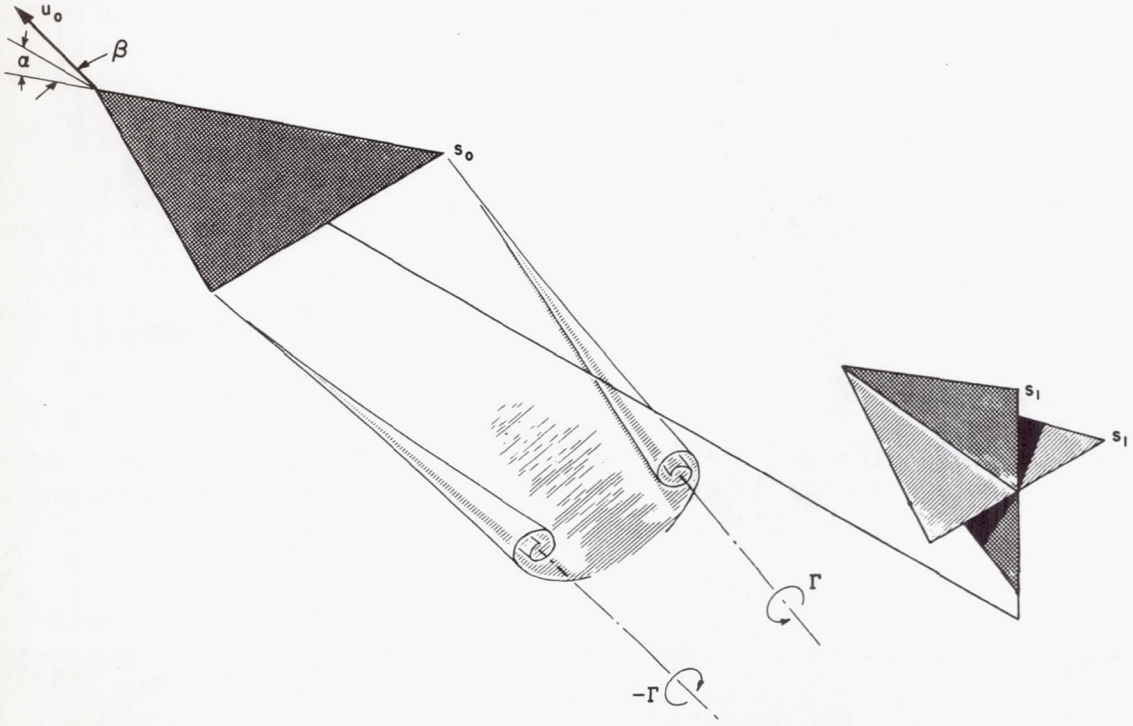
the flight range of angle of attack. The calculated curves of C_{n_β} against angle of attack are shown in figure 9 and are seen to be reflections about the $\alpha = 0$ axis of the curves obtained with the vertical tail above the horizontal. The arrangement shown in sketch (g) has obvious disadvantages in other respects, of course, as for example a negative dihedral effect and complications of the practical landing gear problem.

Lateral stability.- In this portion of the analysis we shall be concerned with the variation of rolling moment with sideslip angle at various angles of attack. According to equation (3), the interference rolling moment in steady straight flight is

$$L_I' = \frac{1}{2}\rho U_o \mathbf{R} \oint_{x=l} F'd(\zeta\bar{\zeta}) - \frac{1}{2}\rho U_o \mathbf{R} \oint_{x=x_{TE+}} F'd(\zeta\bar{\zeta}) - \rho \mathbf{R} \int_{TE}^{l} \bar{R} \sum_{k=1}^{m} \Gamma_k \sigma_{k_r}\, dx \tag{34}$$

and it is seen that the real part of the integral $\oint F'd(\zeta\bar{\zeta})$ is to be evaluated at $x = l$ and at $x = x_{TE+}$. It must be noted here, however, that the contour integral is to be performed round a contour enclosing not only the airplane cross section but also the stream surfaces forming the vortex sheets. This is because of the development in references 10 and 11 where (a) the boundary condition required that the contour of integration be composed of stream surfaces and (b) it was decided to enclose all the external vortices within the contour in order to simplify the treatment of the analytic integrals. Here, since the nonanalytic integrand contains logarithmic singularities outside the body, there will be a contribution to the integral along the branch cuts representing the vortex sheets.

To illustrate the application of equation (34), we shall confine our attention to flat-plate wings and symmetric cruciform tails, as shown in sketch (h). The plan forms, however, need not be triangular. In the



Sketch (h)

present case, since the external vortices arise from a separate wing, there is a vortex sheet common to both vortices and across which the potential differs by a constant, namely the circulation Γ. Therefore, since the sign of $d(\zeta\bar{\zeta})$ is opposite on the two sides, the contribution to the nonanalytic integral along this cut, regardless of its shape, is found to be

$$\mathbf{R}\oint_{\substack{\text{vortex}\\ \text{sheet}}} F'd(\zeta\bar{\zeta}) = \mathbf{R}\int_{\zeta=\zeta_2}^{\zeta=\zeta_1} -\Gamma d(y^2 + z^2)$$

$$= -\Gamma(y_1^2 + z_1^2 - y_2^2 - z_2^2) = -\Gamma(y_1^2 - y_2^2) \tag{35}$$

since from equations (4) and (6) $z_1 = z_2$.

As for the remaining contour integration round the airplane cross section, it will be convenient to perform that in the transformed σ plane where on the circle $\sigma\bar{\sigma} = r_o^2$. The transformation for the symmetric cruciform tail of sketch (h) is obtained from equation (8) by setting $t_1 = t_2 = s$ so that

$$\zeta^2 = \sigma^2 + \frac{r_o^4}{\sigma^2} \tag{36}$$

and $r_o = s/\sqrt{2}$. It follows, then, that on the circle where $\sigma = r_o e^{i\theta}$

$$d(\zeta\bar{\zeta}) = \zeta\frac{d\bar{\zeta}}{d\bar{\sigma}}d\bar{\sigma} + \bar{\zeta}\frac{d\zeta}{d\sigma}d\sigma$$

$$= \pm 4r_o^2 \sin 2\theta\, d\theta \tag{37}$$

Now, recalling that F' is the additional complex potential due to the shed vortices and their images, we can write F' in the σ plane as (see sketch (b), page 9)

$$F' = -\frac{i\Gamma}{2\pi}\left[\ln(\sigma - \sigma_1) - \ln\left(\sigma - \frac{r_o^2}{\bar{\sigma}_1}\right) - \ln(\sigma - \sigma_2) + \ln\left(\sigma - \frac{r_o^2}{\bar{\sigma}_2}\right)\right] \tag{38}$$

and it is seen from equations (37) and (38) that the contribution of the starboard vortex and its image to the real part of the contour integral round the tail cross section is made up of integrals of the type

$$\mathbf{R}\int_{\text{tail}} F'd(\zeta\bar{\zeta}) \equiv I_1 = \pm\frac{2\Gamma r_o^2}{\pi}\int \mathbf{I}\left[\ln\left(\sigma - \sigma_1\right) - \ln\left(\sigma - \frac{r_o^2}{\bar{\sigma}_1}\right)\right]\sin 2\theta\, d\theta \tag{39}$$

or, since the real and imaginary parts of σ on the circle are given by $\tau = r_o\cos\theta$ and $\eta = r_o\sin\theta$, it is found that

$$I_1 = \pm \frac{2\Gamma r_0^2}{\pi} \int \left[\tan^{-1}\left(\frac{\sin\theta - \frac{\eta_1}{r_0}}{\cos\theta - \frac{\tau_1}{r_0}} \right) - \tan^{-1}\left(\frac{\sin\theta - \frac{r_0\eta_1}{r_1^2}}{\cos\theta - \frac{r_0\tau_1}{r_1^2}} \right) \right] \sin 2\theta \, d\theta \quad (40)$$

where $\tau_1 = r_1\cos\theta_1$ and $\eta_1 = r_1\sin\theta_1$ are the coordinates of the starboard vortex in the σ plane. The entire integral round the circle is made up by choosing the proper sign of equation (37) and therefore of I_1 appropriate to each half-quadrant and combining the resulting definite integrals. Since each half-quadrant of the circle corresponds to a particular surface of the cruciform tail, the signs are easily chosen by observing that $d(\zeta\bar{\zeta}) = d(y^2 + z^2)$ and deciding whether this quantity is positive or negative in each half-quadrant as the contour of the cruciform tail is circumscribed in the counterclockwise sense in the physical plane. The resulting expression for the real part of the integral round the tail due to both vortices is found in this manner, after integration by parts, to be

$$\mathbf{R}\oint_{\text{tail}} F'd(\zeta\bar{\zeta}) = \frac{2\Gamma r_0^2}{\pi}\left(\frac{r_0^4}{r_1^4}\right)\left(\frac{1}{2}\left(\frac{\eta_1^2-\tau_1^2}{r_0^2}\right)\left(1+\frac{r_1^4}{r_0^4}\right)\left\{2\tan^{-1}\left[\frac{1-\frac{r_1^4}{r_0^4}}{2\left(\frac{\eta_1^2-\tau_1^2}{r_0^2}\right)}\right]-3\pi\right\}-\right.$$

$$\left.\frac{\tau_1\eta_1}{r_0^2}\left(1-\frac{r_1^4}{r_0^4}\right)\ln\left|\frac{1+\frac{r_1^4}{r_0^4}+4\frac{\tau_1\eta_1}{r_0^2}}{1+\frac{r_1^4}{r_0^4}-4\frac{\tau_1\eta_1}{r_0^2}}\right|\right)-$$

$$\frac{2\Gamma r_0^2}{\pi}\left(\frac{r_0^4}{r_2^4}\right)\left(\frac{1}{2}\left(\frac{\eta_2^2-\tau_2^2}{r_0^2}\right)\left(1+\frac{r_2^4}{r_0^4}\right)\left\{2\tan^{-1}\left[\frac{1-\frac{r_2^4}{r_0^4}}{2\left(\frac{\eta_2^2-\tau_2^2}{r_0^2}\right)}\right]-3\pi\right\}-\right.$$

$$\left.\frac{\tau_2\eta_2}{r_0^2}\left(1-\frac{r_2^4}{r_0^4}\right)\ln\left|\frac{1+\frac{r_2^4}{r_0^4}+4\frac{\tau_2\eta_2}{r_0^2}}{1+\frac{r_2^4}{r_0^4}-4\frac{\tau_2\eta_2}{r_0^2}}\right|\right) \quad (41)$$

where

$$\tau_1 = \mathbf{R}(\sigma_1);\ \eta_1 = \mathbf{I}(\sigma_1);\ \tau_2 = \mathbf{R}(\sigma_2);\ \eta_2 = \mathbf{I}(\sigma_2)$$

$$r_1^2 = [\mathbf{R}(\sigma_1)]^2 + [\mathbf{I}(\sigma_1)]^2;\ r_2^2 = [\mathbf{R}(\sigma_2)]^2 + [\mathbf{I}(\sigma_2)]^2$$

and the arctangents are taken to lie between 0 and 2π. Note that the expressions of equations (35) and (41) both vanish at $x=x_{TE+}$ so that $\mathbf{R}\oint_{x=x_{TE+}} F'd(\zeta\bar{\zeta}) = 0$; also, at $x = l$, $y_1^2 - y_2^2 = -\pi s_0\beta d$ from equation (5).

Turning now to the last term of equation (34), if we rewrite the transformation of equation (36) in the form

$$\zeta^2 - s^2 = \left(\sigma - \frac{r_o^2}{\sigma}\right)^2 \tag{42}$$

since $r_o^2 = s^2/2$, it follows directly that the vortex positions in the σ plane are given by

$$\sigma_k = \frac{1}{2}\left(\sqrt{\zeta_k^2 - s^2} + \sqrt{\zeta_k^2 + s^2}\right) \tag{43}$$

Hence the quantity σ_{k_r} appearing in the summation of equation (34) is

$$\sigma_{k_r} = \sigma_k - \frac{r_o^2}{\bar{\sigma}_k} = \frac{1}{2}\left(\sqrt{\zeta_k^2 - s^2} + \sqrt{\zeta_k^2 + s^2} + \sqrt{\bar{\zeta}_k^2 - s^2} - \sqrt{\bar{\zeta}_k^2 + s^2}\right)$$

$$= \mathbf{R}\sqrt{\zeta_k^2 - s^2} + i\mathbf{I}\sqrt{\zeta_k^2 + s^2} \tag{44}$$

so that the sum is given by

$$\sum_{k=1}^{2} \Gamma_k \sigma_{k_r} = \Gamma_1 \sigma_{1r} + \Gamma_2 \sigma_{2r} = \Gamma\left(\sigma_{1r} - \sigma_{2r}\right)$$

$$= \Gamma\left(\mathbf{R}\sqrt{\zeta_1^2 - s^2} + i\mathbf{I}\sqrt{\zeta_1^2 + s^2} - \mathbf{R}\sqrt{\zeta_2^2 - s^2} - i\mathbf{I}\sqrt{\zeta_2^2 + s^2}\right) \tag{45}$$

Thus if we consider only zero tail incidence i_T so that $\alpha_W = \alpha_T = \alpha$, and recall that for steady straight flight $\bar{R} = U_o\beta + iU_o\alpha$, the last integral of equation (34) can be written in the form

$$\mathbf{R}\int_{TE}^{l} \bar{R} \sum_{k=1}^{m} \Gamma_k \sigma_{k_r} dx = U_o\beta s_o^2 \Gamma\, \mathbf{R} \int_0^{\frac{c'}{s_o}} \left(\sqrt{\frac{\zeta_1^2}{s_o^2} - \frac{s^2}{s_o^2}} - \sqrt{\frac{\zeta_2^2}{s_o^2} - \frac{s^2}{s_o^2}}\right) d\left(\frac{x'}{s_o}\right) -$$

$$U_o\alpha s_o^2 \Gamma\, \mathbf{I} \int_0^{\frac{c'}{s_o}} \left(\sqrt{\frac{\zeta_1^2}{s_o^2} + \frac{s^2}{s_o^2}} - \sqrt{\frac{\zeta_2^2}{s_o^2} + \frac{s^2}{s_o^2}}\right) d\left(\frac{x'}{s_o}\right) +$$

$$U_o\beta s_o^2 \Gamma \frac{\pi}{2}\left(\frac{d - c'}{s_o}\right) \tag{46}$$

The last term of this expression is the contribution of the integral between the trailing edge of the wing and the apex of the tail; that is, where $s = 0$. The vortex positions ζ_1 and ζ_2 and the circulation Γ are given by equations (6) and (7), respectively.

The integrals appearing in equation (46), which is valid for any plan form with straight trailing edge, are of precisely the same form as those encountered in equation (21) for the pitching moment and may be treated in an analogous manner (for triangular plan forms) by making use of the Appendix. In the present case the second integral of equation (46) has a discontinuity of the real part of the square root, and the imaginary part vanishes, when the vortex passes through the vertical tail. Thus sketch (d), page 16, is applicable to such cases if we interchange the labels on the two curves. The condition for the vortex passing through the vertical tail is $y_1 = 0$ for $z_1 \leq s_T \leq s_1$ where y_1 and z_1 are given by equation (6). Thus if $h_T = i_T = 0$, this condition becomes (for triangular plan forms)

$$y_1 = 0 \text{ for } \frac{\frac{4}{A_T}\alpha\left(1-\frac{2}{\pi^2}\right)\left(\frac{d-c'}{s_o}\right)}{1-\frac{4}{A_T}\alpha\left(1-\frac{2}{\pi^2}\right)} \leq \frac{x'}{s_o} \leq \frac{c'}{s_o} \tag{47}$$

If equation (47) is satisfied, then the second integral of equation (46) must be divided in a manner exactly analogous to that shown in equations (23) to (26a).

Finally, the interference rolling moment for the wing-tail combination of sketch (h) is obtained by substituting equations (35), (41), and (46) into equation (34). The coefficient C_{l_I} based on the wing span $2s_o$ is given by this result divided by $\rho U_o^2 S_w s_o$. Now, since the rolling moment of the symmetric cruciform tail alone is zero (see ref. 3), and the rolling-moment coefficient of the isolated triangular wing is (see ref. 10)

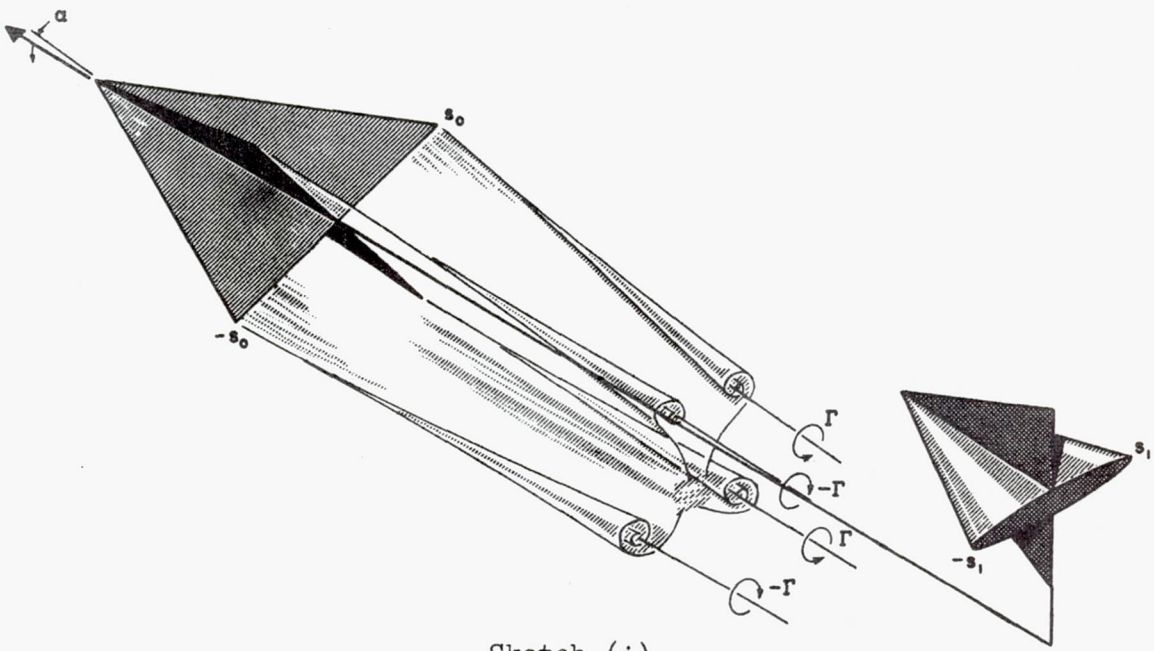
$$C_{l_W} = -\frac{\pi}{3}\alpha\beta \tag{48}$$

the total rolling-moment coefficient for the combination of sketch (h) is found by adding this to the above result for C_{l_I}.

Calculations have been carried out to determine the rolling moments for a wing-tail combination of triangular plan form having zero tail height, a tail-length ratio d/s_o of 6, and a span ratio s_1/s_o of 1. The variation of C_l with β was calculated at two angles of attack and the resulting curves are presented in figure 10. It can be seen that at both angles of attack the variation of rolling moment with angle of sideslip is quite nonlinear and has a sharp peak at the angle of sideslip at which the starboard wing vortex strikes the vertical tail according to equation (31). However, the peaks are in opposite directions so that the curves cross one another. The reason for this behavior lies in the vertical location of the impinging vortex relative to the axis of the tail. At $\alpha = 0.1$, the vortex striking the tail lies close to the tail axis and therefore, due to its direction of rotation, induces a large negative rolling moment at the critical sideslip angle. On the other hand, at $\alpha = 0.2$, the vortex strikes the vertical tail near its upper tip and therefore induces a positive rolling moment because of the velocity gradient associated with the vortex. For purposes of comparison, the rolling moments of the wing alone from equation (48) are also shown on figure 10 and it can be seen that the rolling moments are heavily influenced by wing-tail interference.

Cruciform Wing and Cruciform Tail

The method used in the foregoing analysis of wing-tail combinations having plane wings could equally well be applied to those having cruciform wings if one had analytical expressions for the positions of the rolled-up vortices behind such wings. For the special case of an equal-span cruciform wing in steady straight flight at 45° angle of bank, these vortex positions have been determined analytically in reference 13. Consequently, the longitudinal characteristics of a wing-tail combination of the type shown in sketch (i) (the so-called "interdigitated" arrangement) can be studied in exactly the same way as was the arrangement shown in figure 1(b), if equations (6) are replaced by the expressions of reference 13 or reference 3 for the positions of the four rolled-up vortices.



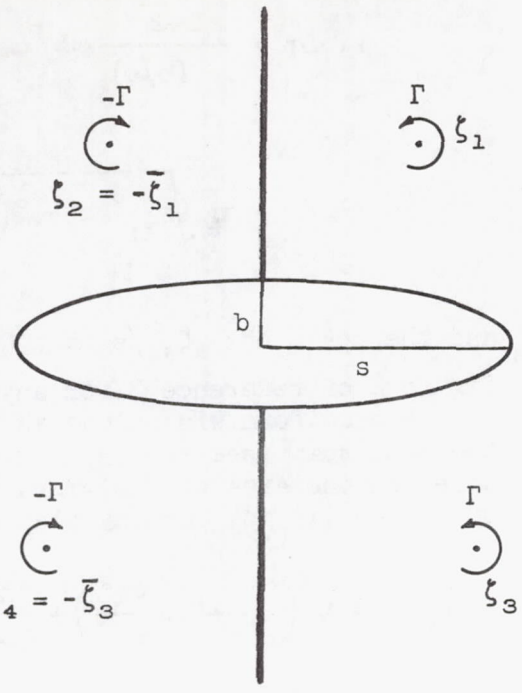
Sketch (i)

(Note, however, that ref. 13 uses wind axes.) It has been shown in reference 3 that the four vortices are of equal strength given by

$$\Gamma = \sqrt{2}\, U_o s_o \alpha_w \tag{49}$$

Now, if we recognize once again that the vertical tail has no influence on the purely longitudinal characteristics, a comparison of the base

cross section shown in sketch (j) with that of sketch (c), page 11, will show that equations (11) to (14) are directly applicable to the present case. Thus by simply extending the summation of equation (12) over four rather than two symmetrically placed vortices, we find, since $\sigma_2 = -\bar{\sigma}_1$ and $\sigma_4 = -\bar{\sigma}_3$ that



Sketch (j)

$$\sum_{k=1}^{4} \Gamma_k \sigma_{k_r} = \Gamma\left(\sigma_{1_r} + \bar{\sigma}_{1_r} + \sigma_{3_r} + \bar{\sigma}_{3_r}\right)$$

$$= 2\Gamma \mathbf{R}\left(\sigma_{1_r} + \sigma_{3_r}\right) \qquad (50)$$

Hence the counterpart of equation (14) is found to be, after simplification

$$\sum_{k=1}^{4} \Gamma_k \sigma_{k_r} = -\frac{2\Gamma}{1 - (b/s)} \mathbf{R}\left[\frac{b}{s}(\zeta_1 + \zeta_3) - \sqrt{\zeta_1^2 - s^2\left(1 - \frac{b^2}{s^2}\right)} - \sqrt{\zeta_3^2 - s^2\left(1 - \frac{b^2}{s^2}\right)}\right] \qquad (51)$$

The interference lift and side force can now be obtained directly from equation (15) from which it follows that the interference side force vanishes since the above sum is real. At this point it should be noted that the quantity $\mathbf{R}(\zeta_1 + \zeta_3)$ is a constant behind the wing, being equal to the lateral distance between the centroids of vorticity of the two halves of the wake. In fact, since the circulation distributions on the two component wings of a cruciform wing banked 45° are identical ellipses (see ref. 3), it follows that

$$\mathbf{R}(\zeta_1 + \zeta_3) = \frac{\pi s_o}{2\sqrt{2}} \qquad (52)$$

With this relation, if we note that immediately behind the wing $s = b = 0$, we can substitute directly into equation (16) for the interference lift.

Thus, making use of equation (51), we find

$$L_I = \frac{2\sqrt{2}}{1-(b/s)_l}\rho U_o^2 \alpha_w s_o \left[\mathbf{R}\sqrt{\zeta_{1_l}^2 - s_1^2\left(1-\frac{b^2}{s^2}\right)_l} + \right.$$

$$\left. \mathbf{R}\sqrt{\zeta_{3_l}^2 - s_1^2\left(1-\frac{b^2}{s^2}\right)_l} - \frac{\pi}{2\sqrt{2}} s_o \right] \tag{53}$$

and the positions ζ_{1_l}/s_o and ζ_{3_l}/s_o can be obtained directly from figure 2 of reference 3 for any given tail length. Now since the lift of the cruciform wing alone is the same as the lift of a plane wing of the same span (see ref. 3), it follows that the total lift coefficient, based on the area of the wing, for the cruciform wing-tail combination of sketch (i) is, for any plan form with straight trailing edge,

$$C_L = \frac{\pi}{2} A_w\left(\alpha_w + \alpha_T \frac{s_1^2}{s_o^2}\right) + \frac{\sqrt{2}A_w\alpha_w}{1-(b/s)_l}\left[\mathbf{R}\sqrt{\frac{\zeta_{1_l}^2}{s_o^2} - \frac{s_1^2}{s_o^2}\left(1-\frac{b^2}{s^2}\right)_l} + \right.$$

$$\left. \mathbf{R}\sqrt{\frac{\zeta_{3_l}^2}{s_o^2} - \frac{s_1^2}{s_o^2}\left(1-\frac{b^2}{s^2}\right)_l} - \frac{\pi}{2\sqrt{2}} \right] \tag{54}$$

Calculations have been carried out to determine the lift curves for several combinations having zero tail height, zero tail incidence, and zero tail thickness using equation (54). Furthermore, the aspect ratio of the wing was taken as 2, so that the only parameters investigated here are the tail-span-to-wing-span ratio s_1/s_o and the tail-length ratio d/s_o. The resulting lift curves are presented in figure 11 for a fixed tail length with several values of s_1/s_o and in figure 12 for a fixed ratio s_1/s_o with several tail lengths. It can be seen that the general character of the lift curves is very similar to that of the plane wing-tail combinations with tail heights different from zero. Here again there is a critical angle of attack at which the vortices strike the tail trailing edge, as can be seen by examining sketch (i), page 32. There are several important differences in this respect, however, between the characteristics of the plane and cruciform combinations. Due to the orientation of the vortices at the wing trailing edge with respect to the tail of the cruciform combination, α_{cr} depends on s_1/s_o as well as on h_T/s_o and d/s_o and no tail height is required for the existence of a critical angle of attack. On the other hand, the change in lift-curve slope at the critical angle is not so great for the cruciform since only half of the wing vortices strike the tail there. Also, in figure 11 since $h_T = 0$, there is complete symmetry with respect to angle of attack

and we find a negative critical angle equal to the positive one. At the negative critical angle, the upper two vortices strike the horizontal tail whereas at the positive critical angle it is the lower two vortices.

A final point that seems worthy of mention in this discussion concerns the existence of a so-called "leapfrog" distance for the cruciform wing at 45° bank. This is the distance behind the wing at which the upper two vortices pass between the lower two due to their mutual induced effects. It is clear that if the tail location and span are such that the vortices strike the tail trailing edge at the leapfrog distance $d=d_L$, a maximum effect may be expected. According to equation (60) of reference 3, the tail length for this condition is

$$\frac{d_L}{s_o} = 4.664 \frac{A_w}{C_{L_w}} = \frac{9.328}{\pi \alpha_w} \tag{55}$$

Hence the critical angle of attack for this maximum effect is given by

$$\alpha_{cr} = \frac{9.328}{\pi(d/s_o)} \tag{56}$$

Also from figure 2 of reference 3 it is found that if all four vortices are to strike the tail, the ratio of tail span to wing span s_1/s_o would have to be not less than 0.9 and the tail height ratio h_T/s_o would be equal to about 1.9. It should be pointed out that for the cruciform wing-tail combinations for which most of the calculations were made here ($d/s_o = 6$) the value of α_{cr} predicted by equation (56) is probably well beyond the range of validity of the present theory ($\alpha_{cr} \approx 28^o$). However, for the case $d/s_o = 12$ (see fig. 12) if the tail were raised so that $h_T/s_o = 1.9$, we should expect that the gentle dip in the lift curve shown at $\alpha = 0.06$ would be replaced by an abrupt dip at $\alpha = 0.247 = 14.2^o$.

Due to the complexity of the expressions given in reference 3 for the vortex positions ζ_1 and ζ_3, a direct application of equation (2) to obtain analytical expressions for the pitching moment appears to be virtually impossible. Consequently, rather than to embark on a program of numerical calculations, it was decided to approximate the pitching-moment variations by assuming that the center of pressure of the tail remains at its 2/3-chord position in spite of the vortices. Hence, since the pitching moment of the wing alone about its 2/3-chord point is zero, the total pitching-moment coefficient of the wing-tail combination about that point is given approximately by (see footnote 4, page 25)

$$C_m \approx -C_{L_T}'\left(\frac{d}{c} + \frac{1}{3} - \frac{1}{3}\frac{c'}{c}\right) \tag{57}$$

where the pitching-moment coefficient is based on the wing area and wing chord and the coefficient C_{L_T}' refers to the lift on the tail in the

presence of the wing wake. The resulting pitching-moment variations are presented in figures 13 and 14 and it is seen that they are comparable with the variations for the plane wing-tail combinations having varying tail span. The above discussion of the lift curves can in fact be extended to the pitching-moment curves in comparing the characteristics of the cruciform interdigitated wing-tail combinations with those of the plane wing-tail arrangements with high tails.

The influence of tail length on the value of the critical angle of attack and on the values of the pitching moment at that angle are clearly shown in figure 13. It can be seen that doubling the tail length reduces the critical angle of attack by one half, but does not change the value of the pitching moment at the critical angle. As a matter of fact, it can be shown that, for given values of s_1/s_o, h_T/s_o, and i_T, the pitching moment of equation (57) is a function of the parameter $\alpha(d/s_o)$ only. Hence, if we plot C_m vs. $\alpha(d/s_o)$, all the points calculated for figure 13 will fall on a single curve; therefore, figure 14 is plotted in this manner. Figure 14 shows the effect of span ratio s_1/s_o and it is noted that the maximum effect at the critical angle is experienced for $s_1/s_o = 0.6$. However, due to the change in relative vortex positions with distance behind the wing, the value of the critical span ratio will depend on the tail length for cruciform wing-tail combinations. It can be seen from figure 14 that if the ratio of tail span to wing span is sufficiently large (see $s_1/s_o = 2$), the nonlinearity associated with the critical angle of attack is diminished substantially and the pitching-moment curve becomes practically linear with angle of attack. The same statement can of course be made in regard to the plane wing-tail combinations treated earlier since the lift of a large tail surface overshadows the interference effects.

PITCHING AND PLUNGING FLIGHT

So far the cases considered in the present report have been confined entirely to steady straight flight. However, the expressions of equations (1), (2), and (3) are directly applicable to quasi-stationary motions (i.e., to unsteady motions whose frequencies are small compared with the flight velocity divided by the length of the body). In this section, we shall consider longitudinal motions of this type with the purpose of calculating the forces and moments acting on a plane triangular wing-tail combination which is pitching and plunging at an angle of attack α_w. The term pitching refers to an angular pitching velocity ($q \neq 0$); the term plunging refers to a time rate of change of angle of attack ($\dot{\alpha} \neq 0$).

It can be seen from equations (1) and (2) that the time derivative $\frac{\partial}{\partial t}\left(\sum_{k=1}^{m} \Gamma_k \sigma_{k_r}\right)$ is required for the calculation of the desired forces and

moments, so we must now express the positions and strengths of the wing vortices as functions of both x and t for the motions just described. In order to do this, we will first assume that the strength Γ of each rolled-up vortex at a distance x_1 behind the wing is equal to the value of Γ that existed at the trailing edge when the trailing edge occupied that position in space. That is to say,

$$\Gamma = \Gamma_{TE} - \frac{\partial \Gamma_{TE}}{\partial t} t_1$$

where t_1 is the time required for the wing to advance a distance x_1. Hence $t_1 = x_1/U_o$ and we have

$$\Gamma = \Gamma_{TE} - \frac{\partial \Gamma_{TE}}{\partial t}\left(\frac{x_1}{U_o}\right) \tag{58}$$

Now Γ_{TE} is given by the jump in potential $\Delta\varphi$ at the wing trailing edge which depends only on the angle of attack at the trailing edge. Thus for the pitching and plunging case, since φ does not depend on $\dot{\alpha}$,

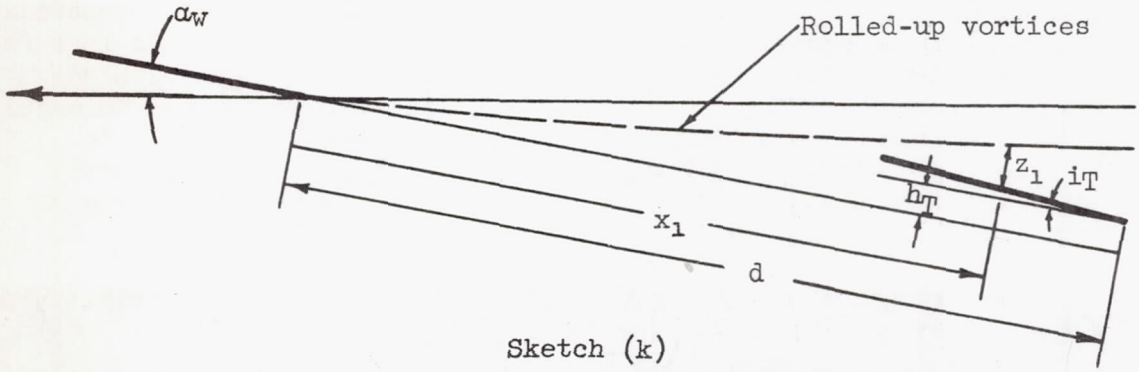
$$\Gamma_{TE} = 2s_o[U_o\alpha_w + q(c - c_1)] \tag{59}$$

where c_1 is the distance from the wing apex to the pivot point of the pitching motion. Note that this expression reduces to equation (7) if $q = 0$. Now, substituting equation (59) into equation (58) we find that the strength of the rolled-up wing vortex is given by

$$\Gamma(x,t) = 2s_o[U_o\alpha_w + q(c - c_1) - \dot{\alpha}x_1] \tag{60}$$

It has been assumed here that $\dot{q} = 0$.

The vortex position remains to be expressed as a function of x and t, but this can be done in a manner parallel to that for the steady case. Thus the slope $\partial z_1/\partial x$ is given by the velocity of a two-dimensional vortex pair of strength $\Gamma(x,t)$ spaced $(\pi/2)s_o$ apart. The vertical position z_1 of both rolled-up vortices relative to the tail is therefore (see sketch (k))



Sketch (k)

$$z_1 = \alpha_w x_1 - h_T - i_T(d - x_1) - \int_0^{x_1} \frac{\Gamma(x,t)}{2\pi(\pi/2)s_o U_o}\,dx$$

$$= \alpha_w x_1 - h_T - i_T(d - x_1) - \frac{1}{\pi^2}\left\{2\left[\alpha_w + \frac{q}{U_o}(c - c_1)\right]x_1 - \frac{\dot{\alpha}x_1^2}{U_o}\right\} \qquad (61)$$

which reduces to equation (4) if $q = \dot{\alpha} = 0$. Now for zero sideslip the lateral positions of the wing vortices are again independent of x_1 and we have corresponding to the expressions of equation (6)

$$\left.\begin{aligned}
\zeta_1 &= \frac{\pi}{4}s_o - i\left(h_T + di_T\right) + ix_1\left[\alpha_w\left(1 - \frac{2}{\pi^2}\right) + i_T - \frac{2}{\pi^2}\frac{q}{U_o}\left(c - c_1\right)\right] + \frac{i}{\pi}\frac{\dot{\alpha}x_1^2}{U_o} \\
\zeta_2 &= -\frac{\pi}{4}s_o - i\left(h_T + di_T\right) + ix_1\left[\alpha_w\left(1 - \frac{2}{\pi^2}\right) + i_T - \frac{2}{\pi^2}\frac{q}{U_o}\left(c - c_1\right)\right] + \frac{i}{\pi}\frac{\dot{\alpha}x_1^2}{U_o}
\end{aligned}\right\} \qquad (62)$$

Note that the plunging motion $\dot{\alpha}$ introduces a quadratic dependence of the vortex positions upon the distance x_1 as shown in sketch (k), while the pitching motion q causes no additional complication over the steady angle-of-attack problem. It should also be pointed out for the purpose of taking derivatives with respect to time that the only time-dependent quantity in equations (60) and (62) is the angle of attack α_w, assuming that $\ddot{\alpha} = 0$.

For the purely longitudinal motions being considered here, the inverse transformation for a thin elliptic-cone tail is given by equation (11) and the summation $\sum_{k=1}^{2}\Gamma_k\sigma_{k_r}$ is the same as was given in equation (14). The difference in the two cases, of course, (i.e., the steady and the unsteady) lies in the more complicated expressions of equations (60) and (62) for the strengths and positions of the vortices. Now, according to equation (1), the interference side force and lift for the present case are given by

$$Y_I - iL_I = -i\rho U_o\left[\left(\sum_{k=1}^{m}\Gamma_k\bar{\sigma}_{k_r}\right)_{x=l} - \left(\sum_{k=1}^{m}\Gamma_k\bar{\sigma}_{k_r}\right)_{x=x_{TE+}}\right] - i\rho\int_{TE}^{l}\frac{\partial}{\partial t}\left(\sum_{k=1}^{m}\Gamma_k\bar{\sigma}_{k_r}\right)dx \qquad (63)$$

and once more the interference side force vanishes due to symmetry. The derivative $\frac{\partial}{\partial t}\left(\sum_{k=1}^{m}\Gamma_k\bar{\sigma}_{k_r}\right)$ over the tail is obtained by differentiating equation (14) with respect to time t using equations (60) and (62) for Γ and ζ_1 and noting that

$$\left.\begin{aligned}\frac{\partial\Gamma}{\partial t} &= 2U_o s_o \dot{\alpha}\\ \frac{\partial\zeta_1}{\partial t} &= ix_1\dot{\alpha}\left(1-\frac{2}{\pi^2}\right)\end{aligned}\right\} \quad (64)$$

and

In this manner, one finds, after some manipulation, that the interference lift of the plane triangular wing-tail combination is, according to equation (63)

$$L_I = \frac{4\rho U_o{}^2 s_o{}^2}{1-(b/s)}\left[\alpha_w + \frac{q}{U_o}(c-c_1) - \frac{\dot{\alpha}d}{U_o}\right]\left[\mathbf{R}\sqrt{\frac{\zeta_{1_l}{}^2}{s_o{}^2} - \frac{s_1{}^2}{s_o{}^2}\left(1-\frac{b^2}{s^2}\right)} - \frac{\pi}{4}\frac{b}{s}\right] - \pi\rho U_o{}^2 s_o{}^2\left[\alpha_w + \frac{q}{U_o}(c-c_1)\right] -$$

$$\frac{4\rho\dot{\alpha}U_o s_o}{1-(b/s)}\left(1-\frac{2}{\pi^2}\right)\int_{d-c'}^{d} x_1\left[\alpha_w + \frac{q}{U_o}(c-c_1) - \frac{\dot{\alpha}x_1}{U_o}\right]\mathbf{I}\left\{\frac{\zeta_1}{\sqrt{\zeta_1{}^2 - s^2[1-(b^2/s^2)]}}\right\}dx_1 - \frac{b/s}{1-(b/s)}\pi\rho U_o\dot{\alpha}s_o{}^2c' +$$

$$\pi\rho U_o\dot{\alpha}s_o{}^2(d-c') + \frac{4\rho U_o\dot{\alpha}s_o}{1-(b/s)}\int_{d-c'}^{d}\mathbf{R}\sqrt{\zeta_1{}^2 - s^2[1-(b^2/s^2)]}\,dx_1 \quad (65)$$

where the thickness ratio b/s is again constant over the tail. Now for the isolated wing and tail, the lifts due to the pitching and plunging motions are additive, and the lift coefficients, based on

the wing area are given according to slender-body theory by (see, e.g., ref. 10)

$$C_{L_W} = \frac{\pi}{2} A_W \left[\alpha_W + \frac{q}{U_O} (c - c_1) \right] + \frac{2\pi}{3} \frac{\dot{\alpha} s_O}{U_O} \tag{66}$$

$$C_{L_T} = \frac{\pi}{2} A_W \frac{s_1^2}{s_O^2} \left[\alpha_T + \frac{q}{U_O} (l - c_1) \right] + \frac{2\pi}{3} \frac{\dot{\alpha} s_O}{U_O} \frac{s_1^2}{s_O^2} \frac{c'}{c} \tag{67}$$

Consequently, the total lift coefficient, based on the area of the wing, for the pitching and plunging wing-tail combination of figure 1(b) is, from equations (65), (66), and (67)

$$C_L = \frac{\pi}{2} A_W \frac{s_1^2}{s_O^2} \left[\alpha_T + \frac{q}{U_O} (l - c_1) \right] + \frac{2\pi}{3} \frac{\dot{\alpha} s_O}{U_O} \left(1 + \frac{s_1^2}{s_O^2} \frac{c'}{c} \right) +$$

$$\frac{2A_W}{1 - (b/s)} \left[\alpha_W + \frac{q}{U_O} (c - c_1) - \frac{\dot{\alpha} d}{U_O} \right] \left[\mathbf{R} \sqrt{\frac{\zeta_1 l^2}{s_O^2} - \frac{s_1^2}{s_O^2} \left(1 - \frac{b^2}{s^2} \right)} - \frac{\pi}{4} \frac{b}{s} \right] -$$

$$\frac{1}{1 - (b/s)} \frac{2A_W \dot{\alpha} s_O}{U_O} \left(1 - \frac{2}{\pi^2} \right) \int_{\frac{d - c'}{s_O}}^{\frac{d}{s_O}} \frac{x_1}{s_O} \left[\alpha_W + \frac{q}{U_O} (c - c_1) - \frac{\dot{\alpha} x_1}{U_O} \right] \mathbf{I} \left[\frac{\zeta_1 / s_O}{\sqrt{\frac{\zeta_1^2}{s_O^2} - \frac{s^2}{s_O^2} \left(1 - \frac{b^2}{s^2} \right)}} \right] d \left(\frac{x_1}{s_O} \right) -$$

$$\frac{b/s}{1 - (b/s)} \frac{\pi}{2} A_W \frac{\dot{\alpha} c'}{U_O} + \frac{\pi}{2} A_W \frac{\dot{\alpha} (d - c')}{U_O} + \frac{1}{1 - (b/s)} \frac{2A_W \dot{\alpha} s_O}{U_O} \int_{\frac{d - c'}{s_O}}^{\frac{d}{s_O}} \mathbf{R} \sqrt{\frac{\zeta_1^2}{s_O^2} - \frac{s^2}{s_O^2} \left(1 - \frac{b^2}{s^2} \right)} d \left(\frac{x_1}{s_O} \right) \tag{68}$$

where the expression for ζ_1 is given by equation (62). It can be seen that the lift is a nonlinear function of all three independent variables α_W, $\dot{\alpha}$, and q. Furthermore, the lift cannot be correctly

calculated by adding the lifts due to each of the three motions since equation (68) contains products of the independent variables. That is, the lift due to pitching and plunging for the wing-tail combination is not equal to the sum of the lift due to pitching and the lift due to plunging.

In reference 10 formulas were given for the stability derivatives of first and second order for slender wing-body combinations. In that analysis, as in the present one, it was found that the forces and moments were nonlinear with respect to some of the motions considered. However, in the analysis of reference 10, the forces and moments depended only on the first and second powers of the independent variables so that it was convenient to define stability derivatives with all of the independent variables (including the angle of attack) set to zero. In this way the conventional stability derivatives could be obtained by a combination of a small number of the derivatives of reference 10 and the latter had the advantage of bringing out a number of useful relationships among the various stability derivatives.

In the present analysis, on the other hand, the nonlinearities of the forces and moments including wing-tail interference are of a more complicated nature. The appearance of the square root involving a quadratic function of all the independent variables in the expressions for the lift and pitching moment indicates that an infinite number of stability derivatives of the type used in reference 10 would be required to obtain the commonly used stability derivatives. In other words, the forces and moments in the present analysis contain all orders of the independent variables, as can be seen by expanding the square root. Consequently, the stability derivatives in the present analysis (including C_{L_α}) will be defined as the appropriate partial derivatives evaluated with all the independent variables except the angle of attack set to zero. Thus the stability derivatives will all be functions of the angle of attack α_w and one must use the derivatives corresponding to the equilibrium angle of attack about which small oscillations are to be executed if the motion is to be calculated by means of the stability equations. This presumes, of course, that the equilibrium condition is steady straight flight at an angle of attack α_w at zero sideslip.

With the above definitions, it is easily found from equations (68) and (62) that

$$C_{L_\alpha}(\alpha) = \left.\frac{\partial C_L}{\partial \alpha}\right]_{\dot{\alpha}=q=0} = \frac{\pi}{2} A_W \frac{s_1^2}{s_o^2} - \frac{2A_W\alpha_W}{1-(b/s)} \frac{d}{s_o}\left(1-\frac{2}{\pi^2}\right) \mathbf{I}\left\{ \frac{\frac{\pi}{4} - i\frac{h_T}{s_o} + i\frac{d}{s_o}\alpha_W\left(1-\frac{2}{\pi^2}\right)}{\sqrt{\left[\frac{\pi}{4} - i\frac{h_T}{s_o} + i\frac{d}{s_o}\alpha_W\left(1-\frac{2}{\pi^2}\right)\right]^2 - \frac{s_1^2}{s_o^2}\left(1-\frac{b^2}{s^2}\right)}} \right\} +$$

$$\frac{2A_W}{1-(b/s)}\left\{ \mathbf{R}\sqrt{\left[\frac{\pi}{4} - i\frac{h_T}{s_o} + i\frac{d}{s_o}\alpha_W\left(1-\frac{2}{\pi^2}\right)\right]^2 - \frac{s_1^2}{s_o^2}\left(1-\frac{b^2}{s^2}\right)} - \frac{\pi}{4}\frac{b}{s} \right\} \tag{69}$$

$$C_{L_q}(\alpha) = \left.\frac{\partial C_L}{\partial\left(\frac{qc}{U_o}\right)}\right]_{\dot{\alpha}=q=0}$$

$$= \frac{\pi}{2} A_W \frac{s_1^2}{s_o^2}\left(\frac{1-c_1}{c}\right) + \frac{2A_W}{1-\frac{b}{s}}\left(\frac{c-c_1}{c}\right)\left\{ \mathbf{R}\sqrt{\left[\frac{\pi}{4} - i\frac{h_T}{s_o} + i\frac{d}{s_o}\alpha_W\left(1-\frac{2}{\pi^2}\right)\right]^2 - \frac{s_1^2}{s_o^2}\left(1-\frac{b^2}{s^2}\right)} - \frac{\pi}{4}\frac{b}{s} \right\} \tag{70}$$

$$C_{L_{\dot{\alpha}}}(\alpha) = \left.\frac{\partial C_L}{\partial\left(\frac{\dot{\alpha}c}{U_o}\right)}\right]_{\dot{\alpha}=q=0}$$

$$= \frac{2\pi}{3}\frac{s_o}{c}\left(1 + \frac{s_1^2}{s_o^2}\frac{c'}{c}\right) - \frac{2A_w}{1-\frac{b}{s}}\frac{d}{c}\left\{\mathbf{R}\sqrt{\left[\frac{\pi}{4} - i\frac{h_T}{s_o} + i\frac{d}{s_o}\alpha_w\left(1 - \frac{2}{\pi^2}\right)\right]^2 - \frac{s_1^2}{s_o^2}\left(1 - \frac{b^2}{s^2}\right)} - \frac{\pi}{4}\frac{b}{s}\right\} -$$

$$\frac{2A_w\alpha_w}{1-\frac{b}{s}}\frac{d^2}{cs_o}\mathbf{I}\left\{\frac{\frac{\pi}{4} - i\frac{h_T}{s_o} + i\alpha_w\frac{d}{s_o}\left(1 - \frac{2}{\pi^2}\right)}{\sqrt{\left[\frac{\pi}{4} - i\frac{h_T}{s_o} + i\frac{d}{s_o}\alpha_w\left(1 - \frac{2}{\pi^2}\right)\right]^2 - \frac{s_1^2}{s_o^2}\left(1 - \frac{b^2}{s^2}\right)}}\right\} -$$

$$2A_w\alpha_w\frac{s_o}{c}\left(1 - \frac{2}{\pi^2}\right)\frac{1}{1-\frac{b}{s}}\int_{\frac{d-c'}{s_o}}^{\frac{d}{s_o}}\frac{x_1}{s_o}\mathbf{I}\left\{\frac{\frac{\pi}{4} - i\left(\frac{h_T + di_T}{s_o}\right) + i\frac{x_1}{s_o}\left[i_T + \alpha_w\left(1 - \frac{2}{\pi^2}\right)\right]}{\sqrt{\left\{\frac{\pi}{4} - i\left(\frac{h_T + di_T}{s_o}\right) + i\frac{x_1}{s_o}\left[i_T + \alpha_w\left(1 - \frac{2}{\pi^2}\right)\right]\right\}^2 - \frac{s^2}{s_o^2}\left(1 - \frac{b^2}{s^2}\right)}}\right\} d\left(\frac{x_1}{s_o}\right) -$$

$$\frac{\frac{b}{s}}{1-\frac{b}{s}}\frac{\pi}{2}A_w\frac{c'}{c} + \frac{\pi}{2}A_w\left(\frac{d-c'}{c}\right) +$$

$$2A_w\frac{s_o}{c}\frac{1}{1-\frac{b}{s}}\int_{\frac{d-c'}{s_o}}^{\frac{d}{s_o}}\mathbf{R}\sqrt{\left\{\frac{\pi}{4} - i\left(\frac{h_T + di_T}{s_o}\right) + i\frac{x_1}{s_o}\left[i_T + \alpha_w\left(1 - \frac{2}{\pi^2}\right)\right]\right\}^2 - \frac{s^2}{s_o^2}\left(1 - \frac{b^2}{s^2}\right)}\, d\left(\frac{x_1}{s_o}\right) \quad (71)$$

The evaluation of the quantities appearing in the expression for $C_{L_{\dot{\alpha}}}$ is actually no more complicated than the evaluation of the integral already treated in finding the steady pitching moment (see eq. (21)), since the imaginary part can be taken after the integration. That is, the integral containing the imaginary part can be separated into integrals of the type

$$\int \frac{\xi \, d\xi}{\sqrt{X}} \quad \text{and} \quad \int \frac{\xi^2 d\xi}{\sqrt{X}}$$

where $X = B + C\xi + D\xi^2$ as before. Both of these integrals are reducible to that of equation (25) and can be handled in the same way.

It should be noted that, although the above expressions were derived for triangular wing and tail, equations (69) and (70) for C_{L_α} and C_{L_q} are actually independent of plan form and are valid for arbitrary slender plan forms so long as the trailing edge is normal to the x axis. The quantity b/s then refers to the value at the trailing edge of the tail.

Calculations have been made to determine the first-order stability derivatives C_{L_α}, C_{L_q}, and $C_{L_{\dot{\alpha}}}$ for two tail heights and for two ratios of tail span to wing span. The aspect ratio of both wing and tail was taken as 2, the tail length ratio $d/s_o = 6$, and the tail incidence and tail thickness were set to zero ($i_T = b/s = 0$). The results are presented in figure 15 and it is seen that the variations with angle of attack may be appreciable, even for the tail lying in the plane of the wing.

The two span ratios were chosen for the calculations so that one falls on either side of the critical span ratio ($s_1/s_o = \pi/4$). The variations of the stability derivatives shown in figure 15 are clearly more severe for the larger span ratio ($s_1/s_o = 1$) since, for span ratios greater than the critical, the trailing vortices strike the tail trailing edge at the critical angle of attack. It can be seen that for $s_1/s_o = 1$ and $\alpha_{cr} = 0.2$ both C_{L_α} and $C_{L_{\dot{\alpha}}}$ jump from a negative value to a large positive value as the critical angle is exceeded. For the lift-curve slope C_{L_α}, this was already noticeable in figures 2 and 3 showing the steady lift curves for the same configurations. It will also be noted in figure 15 that for $s_1/s_o = 1$ the derivatives C_{L_α} and C_{L_q} have their minimum values at the critical angle of attack, even for $\alpha_{cr} = 0$ (i.e., wing and tail in the same plane). This is not the case with the derivative $C_{L_{\dot{\alpha}}}$. The discontinuities in C_{L_α} and $C_{L_{\dot{\alpha}}}$ at the critical angle of attack for $\alpha_{cr} \neq 0$ are evidently removed and the variations with angle of attack considerably reduced if the ratio of tail span to wing span is reduced below the critical value.

For the case of wing and tail of equal span in the same plane, C_{L_α} is doubled as the angle of attack increases from 0° to 12°. On the other hand, if the tail span is half the wing span, the increase is only

about 25 percent. The variation of C_{L_q} is about 6 percent for the equal-span wing-tail combination and about 5 percent for $s_1/s_o = 0.5$ over the same angle range.

It has already been mentioned that in reference 10 a number of relationships were obtained among the stability derivatives for wing-body combinations by evaluating the derivatives at $\alpha = 0$. Although, as already discussed, there seems to be little point in defining stability derivatives for wing-tail combinations in the same manner, it is nevertheless of interest to see whether a similar type of relationship can be found at $\alpha_w = 0$. In fact if we set $\alpha_w = 0$, it becomes apparent that equations (69) and (70) are then related according to

$$\left(C_{L_q}\right)_{\alpha_w=0} = \left(\frac{l - c_1}{c}\right) C_{L_{\alpha_T}} + \left(\frac{c - c_1}{c}\right)\left[\left(C_{L_\alpha}\right)_{\alpha_w=0} - C_{L_{\alpha_T}}\right]$$

or

$$\left(C_{L_q}\right)_{\alpha_w=0} = \left(\frac{c - c_1}{c}\right)\left(C_{L_\alpha}\right)_{\alpha_w=0} + \left(\frac{\bar{d}}{c}\right) C_{L_{\alpha_T}} \tag{72}$$

so that C_{L_q} at $\alpha_w = 0$ for the wing-tail combination can be calculated from the lift-curve slope of the combination at $\alpha_w = 0$ and the lift-curve slope of the isolated tail. If there is no tail $C_{L_{\alpha_T}} = 0$ and equation (72) reduces to the relationship given in reference 10 between C_{L_q} and C_{L_α} for wing-body combinations, with the chord c as the reference length.

LIMITATIONS OF THE THEORY

It has been assumed in the foregoing analysis that the vortex sheet leaves the wing trailing edge as a flat sheet and that it becomes fully rolled up ahead of the tail. The former assumption does not admit separation of the flow from the wing surface and therefore implies small angles of attack. The latter assumption, on the other hand, seems to imply a high angle of attack. Actually, it requires that the tail length be greater than the distance in which the wing vortex sheet becomes fully rolled up, that is (see, e.g., ref. 3 or 12),

$$\frac{e}{2s_o} = k_1 \frac{A_w}{C_{L_w}} < \frac{d}{2s_o} \tag{73}$$

where k_1 depends on the circulation distribution. According to Kaden (ref. 14) the value $k_1 = 0.28$ gives the distance required for the vortex sheet behind a plane wing with elliptic circulation distribution to become "essentially rolled up." It can be seen from equation (73) that the restriction imposed on the configurations which can be treated becomes more severe as the angle of attack approaches zero. Hence the present calculations might be considered as a "moderate angle-of-attack" analysis for slender wing-tail combinations.

In view of equation (73), it is interesting to consider other analyses in which wing-tail combinations have been treated under the assumption of a flat vortex sheet lying in the plane of the wing and tail. The requirement for such results to be applicable is clearly

$$\frac{e}{2s_o} = k_1 \frac{A_w}{C_{L_w}} \gg \frac{d}{2s_o} \tag{74}$$

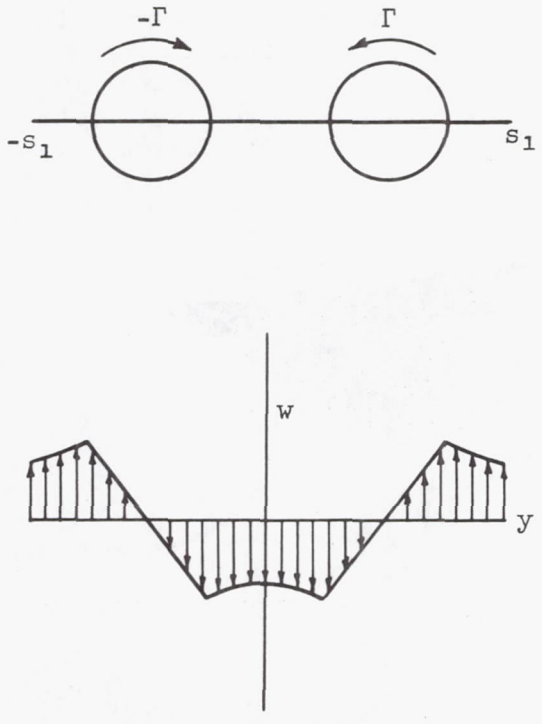
The "much greater" sign is introduced because the assumption of such analyses is not simply that the vortex sheet is not fully rolled up at the tail but rather that it remains completely flat - hence the more stringent requirement. It is evident then that if a wing-tail combination with a low-aspect-ratio wing is treated under the above assumption, the results are applicable only for vanishingly low lift coefficients or for extremely short tail lengths. There have recently been some such analyses (e.g., refs. 15 and 16) in which wing-tail combinations are treated with no apparent restrictions on aspect ratio or tail length. The results of such investigations when applied to low-aspect-ratio wings or sizable tail lengths should be viewed with caution. It should also be mentioned that the analyses of references 15 and 16 can lead only to stability derivatives which are independent of the angle of attack. Furthermore, the vortex sheet is assumed to lie in the plane of the tail at all (small) angles of attack. Although the vortex sheet does indeed lie in the plane of the tail at $\alpha = 0$ (for $h_T = 0$), the derivatives calculated at $\alpha = 0$ may nevertheless be in error since no account has been taken of the change of position of the vortex sheet with angle of attack.

In reference 15 the conclusion is drawn that the lift induced on the tail by an angle of attack of the wing in forward flight is equal to the lift induced on the wing by an angle of attack of the tail in reverse flight. That this conclusion is not in agreement with the present analysis can be seen by examining equation (17) for the interference lift in steady straight flight. For the slender case, as is treated in the present paper, reversal of the flight direction has no influence on the given expression other than to interchange s_1 and s_o. It is clear then that the above conclusion agrees with the present analysis only for the obvious case of $s_1/s_o = 1$. The difference, of course, stems from the

different assumptions regarding the vortex sheet shed by the wing. The appropriateness of the different assumptions can only be checked by experiment.

A further assumption of the present analysis is that the positions of the vortices shed from the wing are not influenced by the presence of the tail. Thus the vortex lines coincide not with the actual streamlines but with the streamlines in the absence of the tail. Hence, while the condition of no flow through the tail has been satisfied in the analysis, the vortices have nevertheless been permitted to penetrate the tail surface. In fact the most dramatic effects on stability are predicted for conditions under which the wing vortices either touch or pass through the tail. Although the present assumption that the tail does not influence the vortex positions is commonly made in calculations of wing-tail interference, the implications mentioned above seem to warrant investigation of this point. Therefore an experiment was conducted to investigate the influence of the tail on the vortices shed by the wing. This experiment will be discussed in the next section.

The rolled-up vortices were assumed in the analysis to be idealized line vortices having no viscous cores. This assumption will have no effect on the calculated results so long as the cores do not touch the tail. However, when the distance from the tail to the center of the vortex is smaller than the radius of the core, the viscous core will change the downwash distribution at the tail location and affect the calculated lift on the tail. In order to get some idea of the order of magnitude of this effect, a calculation was made by the method of reverse flow (see ref. 7) to determine the lift on a plane tail in the presence of two viscous vortices whose centers intersect the trailing edge of the tail as shown in sketch (l). For this calculation, it was assumed that the cores rotate as solid bodies, giving the downwash distribution shown in the absence of the tail. It was further assumed that the cores lay entirely within the span of the tail as shown, and that the span loading of the tail in reverse flow is elliptic. With these assumptions, it was found that if the vortex centers are located at $y = \pm s_1/2$ and the core radius is $s_1/4$ (as shown), then the negative lift on the tail due to the vortices is reduced by 12 percent from that calculated with no cores. Now, since the centers of the vortices were assumed to intersect the tail trailing edge, the above calculation corresponds to $\alpha = \alpha_{cr}$. Furthermore,



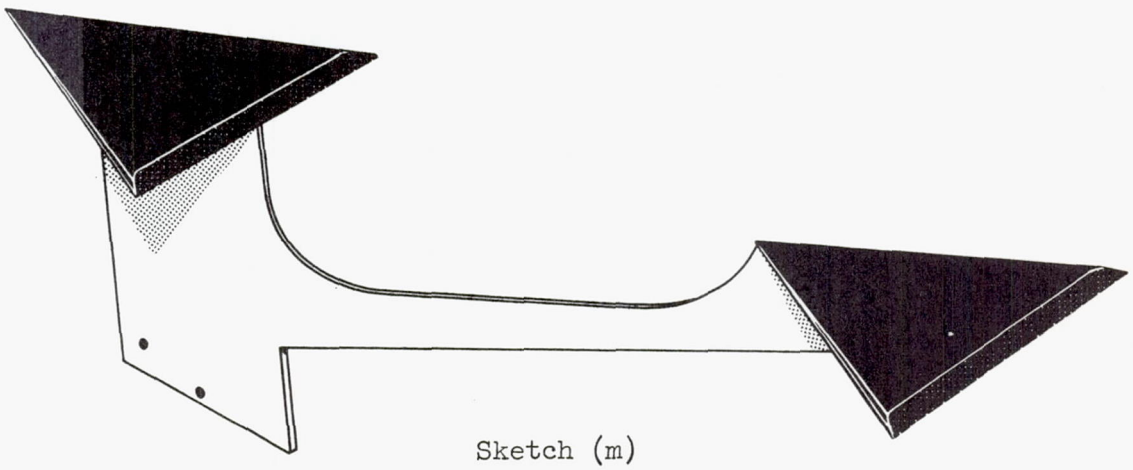
Sketch (l)

since the viscous cores can have no effect on the tail lift if they do not touch the tail, it can be concluded that the over-all effect of the viscous cores on the calculated lift and pitching-moment curves of figures 2 to 6 will be simply to round off the sharp peaks at $\alpha = \alpha_{cr}$.

Although the present analysis has been restricted to slender wing-tail combinations for which the vortex sheet leaves the wing as a flat sheet, it is important to note that the origin of the trailing vortices is immaterial to the method of calculation of wing-tail interference. If, for example, the wing is a delta wing with sharp leading edges, there may be separation vortices above the wing. These can be handled by the present method, provided that their positions and strengths over the wing are known. Similarly, if the wing is a sweptback wing (not necessarily slender), the vortices from the wing may be caused to roll up quickly because of tip-stalling or other viscous phenomena. Nevertheless, if the tail is slender and the vortices are rolled up ahead of the tail, the techniques used in the present analysis are still applicable for the calculation of the interference forces and moments. As a matter of fact, pitching-moment curves having the same general nonlinear character as those of figures 2 and 3 have been measured on swept-wing airplane models having high tails (see, e.g., refs. 17 and 18). Some of the trends in directional stability which have been calculated in the present report are also evident in the data of reference 18.

WATER-TANK EXPERIMENT

In order to investigate the influence of the tail on the paths of the vortices shed by the wing, a simple model was constructed consisting of an identical triangular wing and tail mounted on a thin plate, as shown in sketch (m). The plate acted as a model support and was attached to a rack which was driven vertically into a water tank by a gear mounted on an electric motor. The wake of the wing was made visible on the surface of the water by means of white poster paint applied to the beveled



Sketch (m)

trailing edge of the wing. As the wing passed through the water surface, the paint remained on the surface and the resulting wake patterns were photographed from above by a motion picture camera. The wing and tail were flat plates with rounded leading edges and beveled trailing edges, and the central plate was cut down to minimize its influence on the wing wake (see sketch (m)). The tail was mounted at zero incidence ($i_T = 0$) in a tail-high position ($h_T/s_o = 0.96$) so that at a critical angle of attack ($\alpha_{cr} = 0.2$) the analysis will predict that the wing vortices intersect the tail at its trailing edge.

The model was driven into the tank at three angles of attack, one below, one above, and one at the calculated critical angle of attack, and selected frames of the motion pictures obtained are presented in figure 16. The vertical and horizontal lines on either side of the frame are reference markers which are fixed relative to the tank (i.e., relative to the flight direction). The first picture in each case shows the vortex sheet leaving the wing trailing edge as a flat sheet.[5] At this point, the wing trailing edge has just penetrated the water surface, and the strut connecting the wing and tail can be seen above the water surface. For $\alpha = 12^\circ$ and 16° the tail is also visible but is out of focus, being closer to the camera. The second picture in each series shows the tail entering the water surface, and the remaining pictures show the development of the wing wake at various positions over the tail until the last frame shows the wing wake at the trailing edge of the tail.

In figure 16(a) there seem to be no obvious effects attributable to the tail, but the mounting strut has a marked effect on the shape of the center of the vortex sheet. It can be seen that the upward sweep of the center of the sheet follows the retreating edge of the strut.

Figure 16(b) shows the development of the wing wake over the tail at the calculated critical angle of attack. According to the analysis in the foregoing sections of this report, the wing vortices should intersect the tail at its trailing edge at this angle of attack. It was in fact largely this prediction that prompted the present experiment, in view of the discussion of the previous section. It is apparent from figure 16(b) that, although the vortices are quite distorted at the trailing edge of the tail, the centers of the vortices do very nearly coincide with the tail trailing edge. The tail seems to split the viscous cores of the vortices at the critical angle of attack. The asymmetry of the center portion of the vortex sheet seen in the photographs is probably due to an asymmetric disturbance produced by the strut.

In figure 16(c) a higher angle of attack is shown and the tail appears to sever the vortex sheet and produce considerable distortions above the surface of the tail.

---

[5]Subsequent detailed investigation has shown the existence of a relatively weak pair of separation vortices above the wing surface at all of the angles of attack studied here.

The distances behind the wing as shown on the above-mentioned pictures were measured by means of a tape which moved with the model and recorded on the film the distance between the wing trailing edge and the water surface. Thus it was a simple matter to obtain quantitative measurements of the vortex paths, provided the centroids of vorticity of the vortex sheet could be defined. Actually it is not possible to define these positions accurately from photographs, but it was assumed that the lateral position of the centroid of vorticity of each half of the wake could be taken as halfway between the outermost winds of the rolled-up portion of the sheet. The results of such measurements are shown in figure 17 as the variation of vortex span with distance behind the wing. The position occupied by the tail is indicated in the figure and it can be seen that the influence of the tail at all three angles of attack is such as to decrease the vortex span at the trailing edge of the tail.

The theoretical asymptotic vortex span of $(\pi/4)s_o$ for the wing alone is in close agreement with the experimentally observed positions at the lower angles of attack until the influence of the tail is felt at the station containing the apex of the tail. The sizable inward shift ahead of the tail at the largest angle of attack is associated with the change in circulation distribution on the wing as the angle of attack is increased. Inasmuch as the interference lift calculated in the analysis depends on the positions of the wing vortices at the trailing edge of the tail, it would be of interest to calculate the effect on the interference lift of the observed inward movement due to the tail. However, the interference lift is a function of the vertical positions as well as the lateral positions of the vortices, and it was felt that the vertical positions of the centroids of vorticity could not be defined with any degree of accuracy because of the unrolled-up portion of the vortex sheet. It is interesting to note that at the critical angle of attack $z_1 = 0$ and the interference lift does not depend on the lateral spacing of the vortices so long as they lie within the span of the tail. (This point has been discussed in the section titled "Longitudinal Stability.") Consequently, at the critical angle of attack the influence of the tail on the vortex positions has no effect on the interference lift for the span ratio tested. For other angles of attack or for sufficiently smaller tail spans this will not be the case.

The systematic tendency of the tail to draw the vortices together as observed in figure 17 suggested the possibility that the water-tank observations have been influenced by surface tension effects. Therefore, observations were made of the three-dimensional wake patterns below the surface of the water to see whether any significant changes were occurring at the water surface due to surface tension. This was done by thinning the poster paint so that some of it would adhere to the wing after the latter was submerged, thus extending the visible wake patterns below the water surface. Observations were made at various angles of attack, and it was found that no surface tension effects were discernible as long as the angle of attack was greater than 6°. Below that angle of attack, the difference between the patterns on the surface and below it became

visible. Apparently, the criterion of a low Weber number (ratio of surface tension forces to dynamic forces) was satisfied for angles of attack above 6°.

The assumption made in the analysis that the vortex sheet becomes fully rolled up ahead of the tail appears to be substantiated in the case of the model tested here.

CONCLUDING REMARKS

A theoretical investigation has been made of some of the aerodynamic characteristics and stability problems associated with slender wing-tail combinations. The vortex sheets shed by the wing have been assumed to be fully rolled up at the tail and to follow the same paths as calculated in the absence of the tail.

Mathematical expressions have been derived for the interference forces and moments acting on the tail. From these, calculations have been made of the effect of changes in tail height, tail length, tail incidence, tail thickness, and ratio of tail span to wing span. The calculated variations of forces and moments with angles of attack and sideslip were found in some cases to be highly nonlinear. Changes in the height of the horizontal tail and in the ratio of tail span to wing span were found to have a pronounced effect on static stability as well as on the stability derivative $C_{L_{\alpha}}$. The calculated results indicated a definite critical angle of attack for a given wing-tail combination and a critical ratio of tail span to wing span at which abrupt changes in the aerodynamic characteristics occurred in certain cases. In general, the most drastic effects are predicted when the vortices shed from the wing strike or pass near the tips of the tail trailing edge.

A water-tank experiment was conducted in order to observe the behavior of the wing wake in the presence of the tail. A plane-wing-tail combination with a high tail was tested and photographs indicated that the tail caused the wing vortices to be shifted inboard appreciably for the case tested (wing and tail of equal span). The vertical positions, however, were apparently relatively unaffected, and the tail was observed to sever the vortex cores at the calculated critical angle of attack (within the experimental accuracy).

The influence on the calculated results of the assumptions made regarding the vortex wake have been considered, and a conclusion drawn on the basis of a flat vortex sheet in the plane of the tail was compared with the results of the present analysis. The choice of such assumptions

must in the last analysis be made on the basis of experiment, and for the cases treated in the present paper the assumption of the fully rolled-up vortex sheets seems justified, provided that the tail length is not extremely short.

Ames Aeronautical Laboratory
National Advisory Committee for Aeronautics
Moffett Field, Calif., May 21, 1956

APPENDIX

EVALUATION OF THE IMAGINARY PART OF A COMPLEX SQUARE ROOT

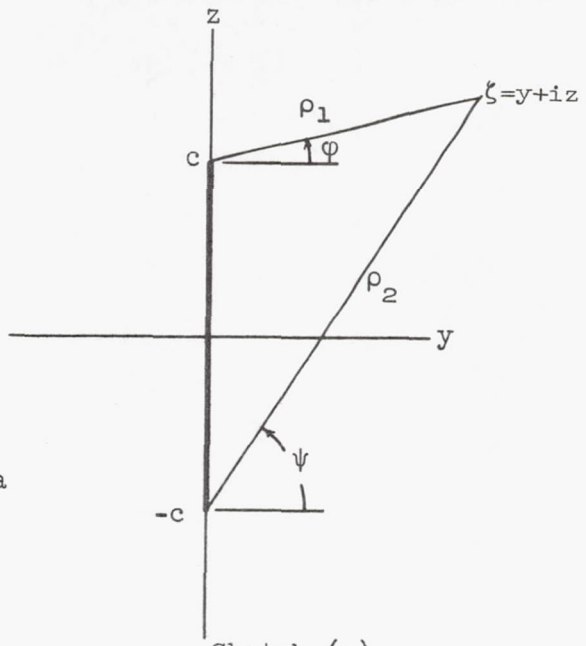
A complex square root of the type $\sqrt{\zeta^2 + c^2}$ where $\zeta = y + iz$ and c is real has branch points $\zeta = \pm ic$ and can be written in its factored form

$$\sqrt{\zeta^2 + c^2} = \sqrt{(\zeta - ic)(\zeta + ic)}$$

Now each factor can be written in polar coordinates referred to one of the branch points. Thus (see sketch (n)) let

$$\zeta - ic = \rho_1 e^{i\varphi} \; ; \; \zeta + ic = \rho_2 e^{i\psi}$$

where φ and ψ are both limited to a range of, say, $-(\pi/2)$ to $+(3\pi/2)$ (to give the proper sign changes through the line segment shown). This enables one to write



Sketch (n)

$$\sqrt{\zeta^2 + c^2} = \sqrt{\rho_1\rho_2}\, e^{i\left(\frac{\varphi+\psi}{2}\right)} = \sqrt{\rho_1\rho_2}\left[\cos\left(\frac{\varphi+\psi}{2}\right) + i \sin\left(\frac{\varphi+\psi}{2}\right)\right]$$

so that the imaginary part is

$$\mathbf{I}\sqrt{\zeta^2 + c^2} = \sqrt{\rho_1\rho_2}\, \sin\left(\frac{\varphi + \psi}{2}\right)$$

where

$$\rho_1 = \left|\sqrt{y^2 + (z - c)^2}\right|$$

$$\rho_2 = \left|\sqrt{y^2 + (z + c)^2}\right|$$

$$\varphi = \tan^{-1}\left(\frac{z - c}{y}\right)$$

$$\psi = \tan^{-1}\left(\frac{z + c}{y}\right)$$

The sign of the imaginary part of the square root is therefore determined by the quadrants of φ and ψ which depend on the position of the point ζ relative to the branch points $\zeta = \pm ic$ and also on the range of φ and ψ specified above.

REFERENCES

1. Westwater, F. L.: Rolling Up of the Surface of Discontinuity Behind an Aerofoil of Finite Span. R. and M. No. 1692, British A.R.C., Aug. 1935.

2. Rogers, Arthur Wm.: Application of Two-Dimensional Vortex Theory to the Prediction of Flow Fields Behind Wings of Wing-Body Combinations at Subsonic and Supersonic Speeds. NACA TN 3227, 1954.

3. Spreiter, John R., and Sacks, Alvin H.: A Theoretical Study of the Aerodynamics of Slender Cruciform-Wing Arrangements and Their Wakes. NACA TN 3528, 1956.

4. Landahl, M. T., and Skogstad, P. H.: Theoretical Investigation of Three-Dimensional Nonsymmetric Transonic Flow Patterns in Lift and Yaw. M.I.T. TACP Rep. 2, Sept. 1953.

5. Lomax, Harvard, and Byrd, Paul F.: Theoretical Aerodynamic Characteristics of a Family of Slender Wing-Body-Tail Combinations. NACA TN 2554, 1951.

6. Lagerstrom, P. A., and Graham, M. E.: Aerodynamic Interference in Supersonic Missiles. Rep. SM-13743, Douglas Aircraft Co., Inc., July 1950.

7. Heaslet, Max. A., and Spreiter, John R.: Reciprocity Relations in Aerodynamics. NACA Rep. 1119, 1953. (Formerly NACA TN 2700)

8. Graham, Martha E.: Some Linearized Computations of Supersonic Wing-Tail Interference. Rep. SM-13430, Douglas Aircraft Co., Inc. Dec. 1948.

9. Morikawa, George: Supersonic Wing-Body-Tail Interference. Jour. Aero. Sci., vol. 19, no. 5, May 1952, pp. 333-340.

10. Sacks, Alvin H.: Aerodynamic Forces, Moments, and Stability Derivatives for Slender Bodies of General Cross Section. NACA TN 3283, 1954.

11. Sacks, Alvin H.: Vortex Interference on Slender Airplanes. NACA TN 3525, 1955.

12. Spreiter, John R., and Sacks, Alvin H.: The Rolling Up of the Trailing Vortex Sheet and Its Effect on the Downwash Behind Wings. Jour. Aero. Sci., vol. 18, no. 1, Jan. 1951, pp. 21-32.

13. Sacks, Alvin H.: Behavior of Vortex System Behind Cruciform Wings - Motions of Fully Rolled-Up Vortices. NACA TN 2605, 1952.

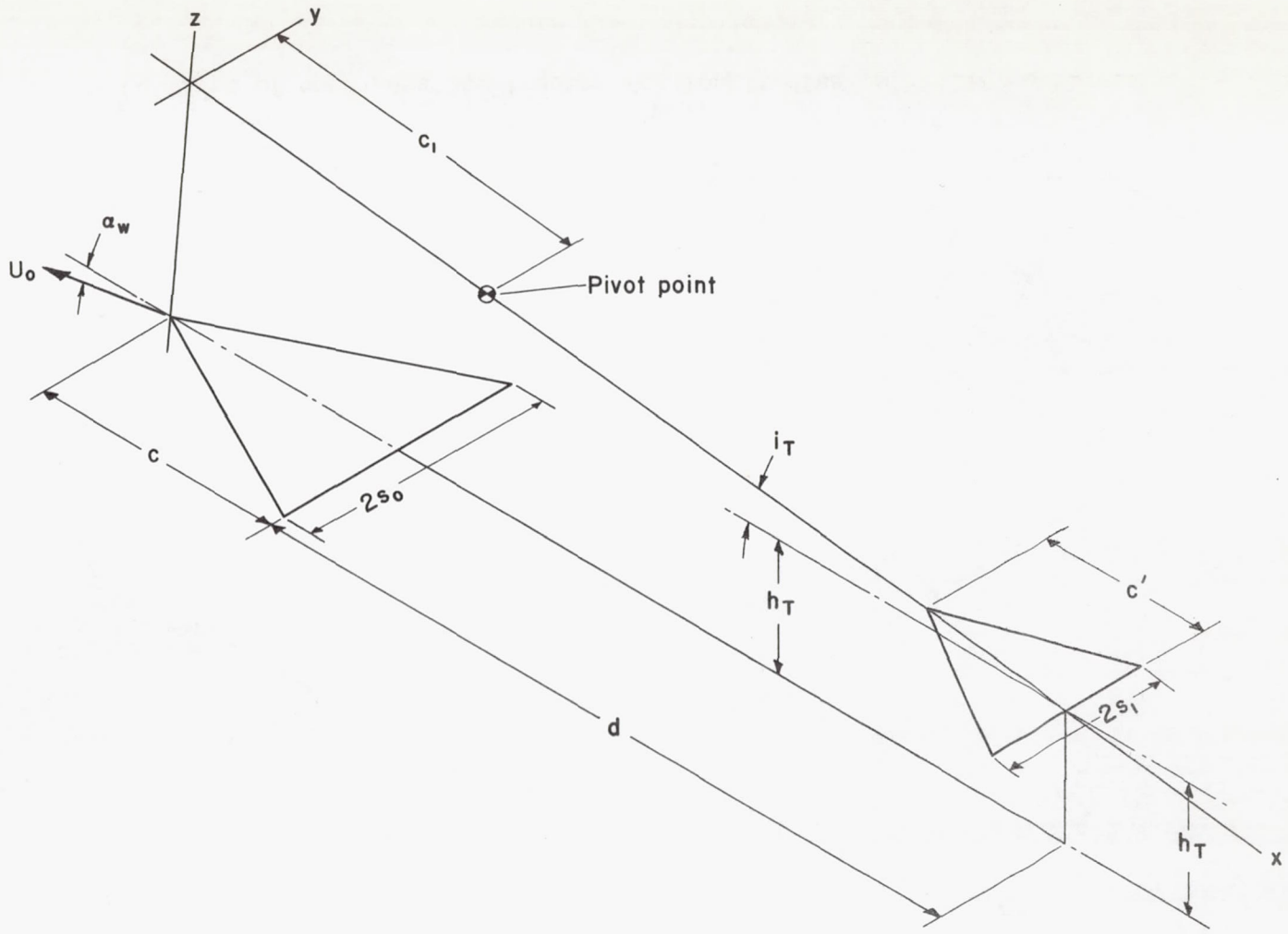
14. Kaden, H.: Aufwicklung einer unstabiln Unstetigkeitsfläche. Ing. Arch., vol. 2, 1931, pp. 140-168.

15. Tobak, Murray: On the Use of the Indicial Function Concept in the Analysis of Unsteady Motions of Wings and Wing-Tail Combinations. NACA Rep. 1188, 1954.

16. Martin, John C., Diederich, Margaret S., and Bobbitt, Percy J.: A Theoretical Investigation of the Aerodynamics of Wing-Tail Combinations Performing Time-Dependent Motions at Supersonic Speeds. NACA TN 3072, 1954.

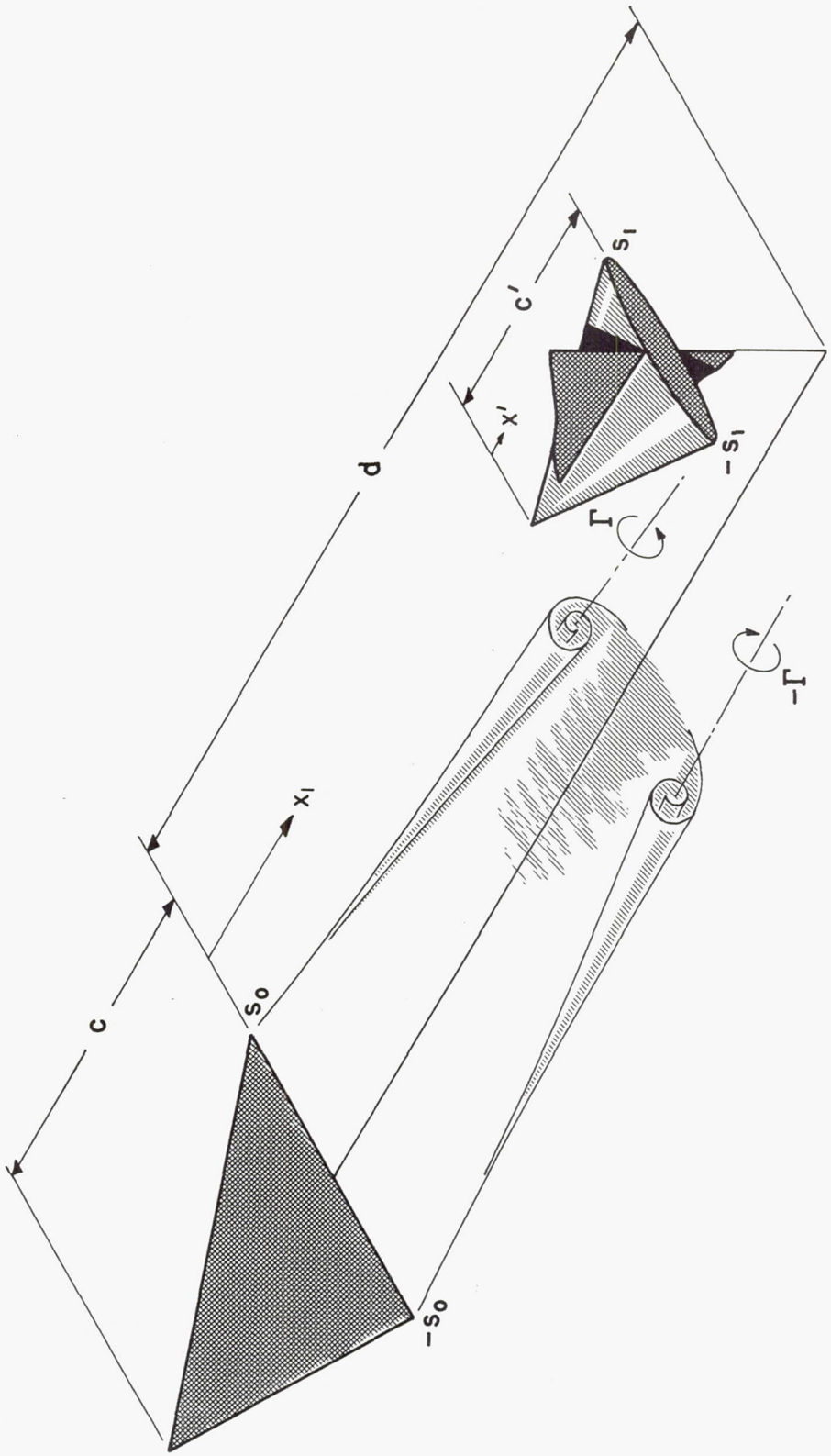
17. Lichtenstein, Jacob H.: Experimental Determination of the Effect of Horizontal-Tail Size, Tail Length, and Vertical Location on Low-Speed Static Longitudinal Stability and Damping in Pitch of a Model Having 45° Sweptback Wing and Tail Surfaces. NACA Rep. 1096, 1952.

18. Goodman, Alex: Effects of Wing Position and Horizontal-Tail Position on the Static Stability Characteristics of Models with Unswept and 45° Sweptback Surfaces with Some Reference to Mutual Interference. NACA TN 2504, 1951.



(a) Coordinate system as fixed in the tail.

Figure 1.- General orientation of wing and tail.



(b) Type of configuration treated for longitudinal stability analysis.

Figure 1.- Concluded.

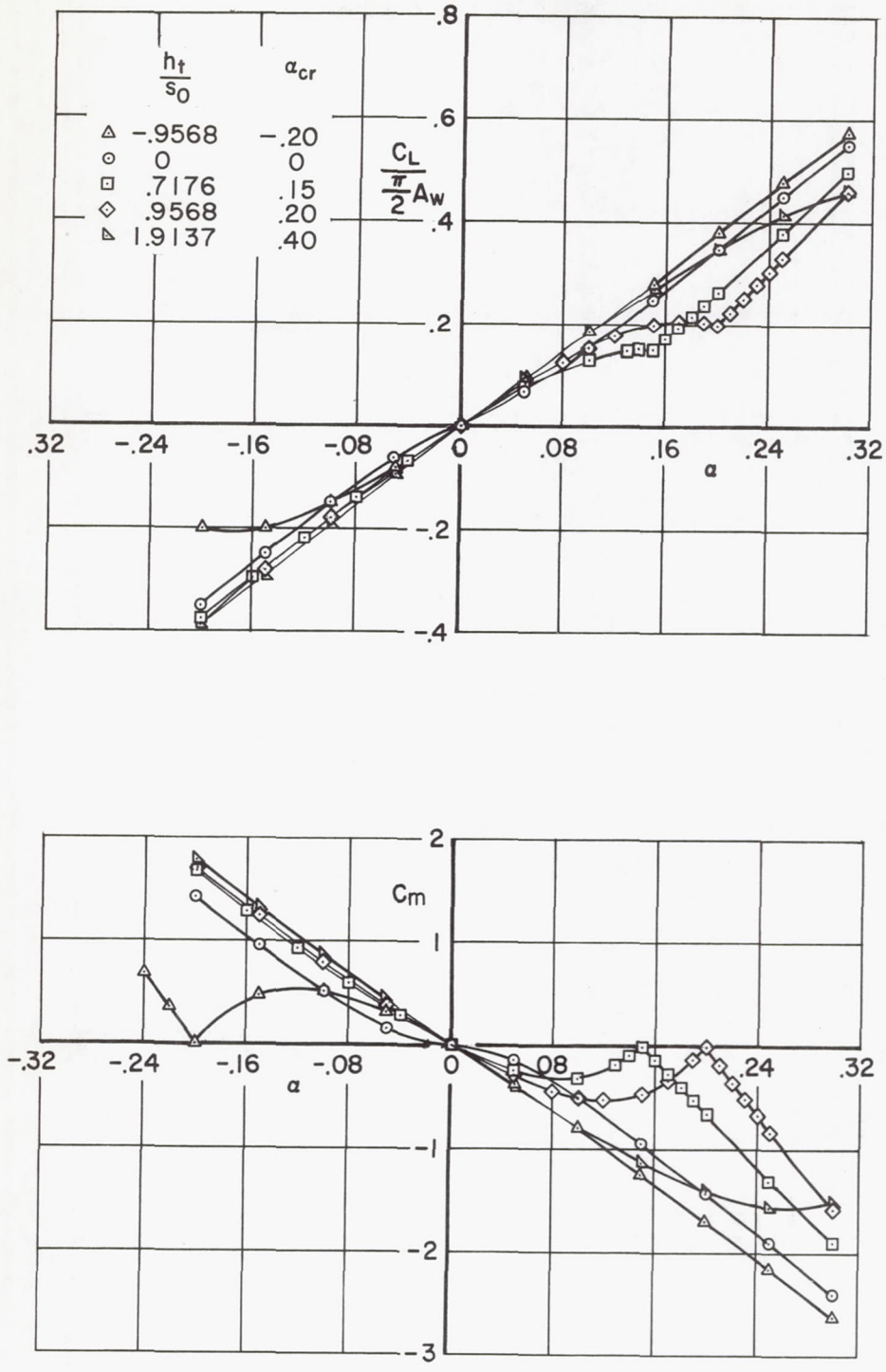


Figure 2.- Effect of horizontal tail height on the variations of lift and pitching moment with angle of attack; plane triangular wing and tail of aspect ratio 2, $d/s_o = 6$, $s_1/s_o = 1$, $i_t = b/s = 0$.

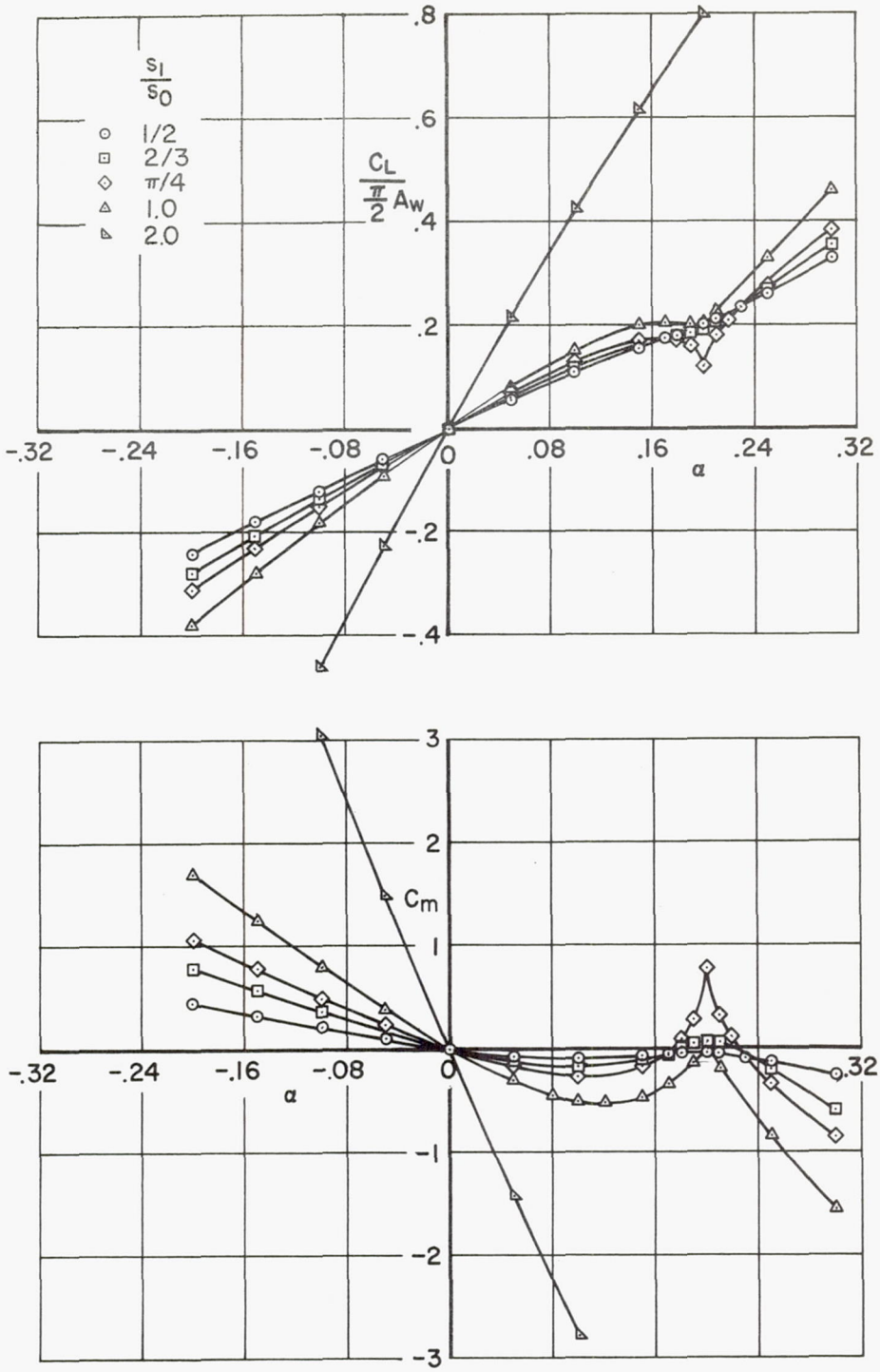
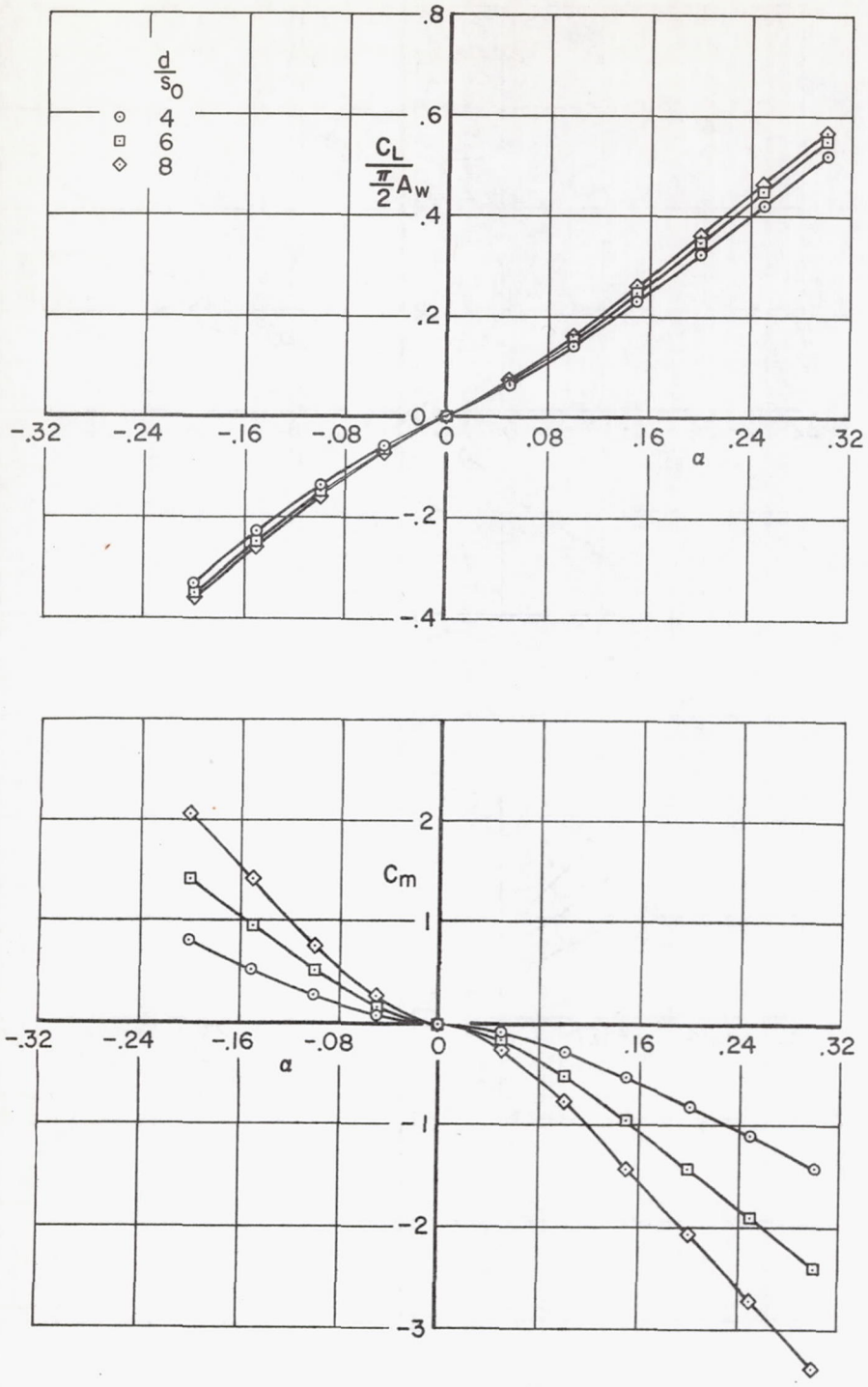
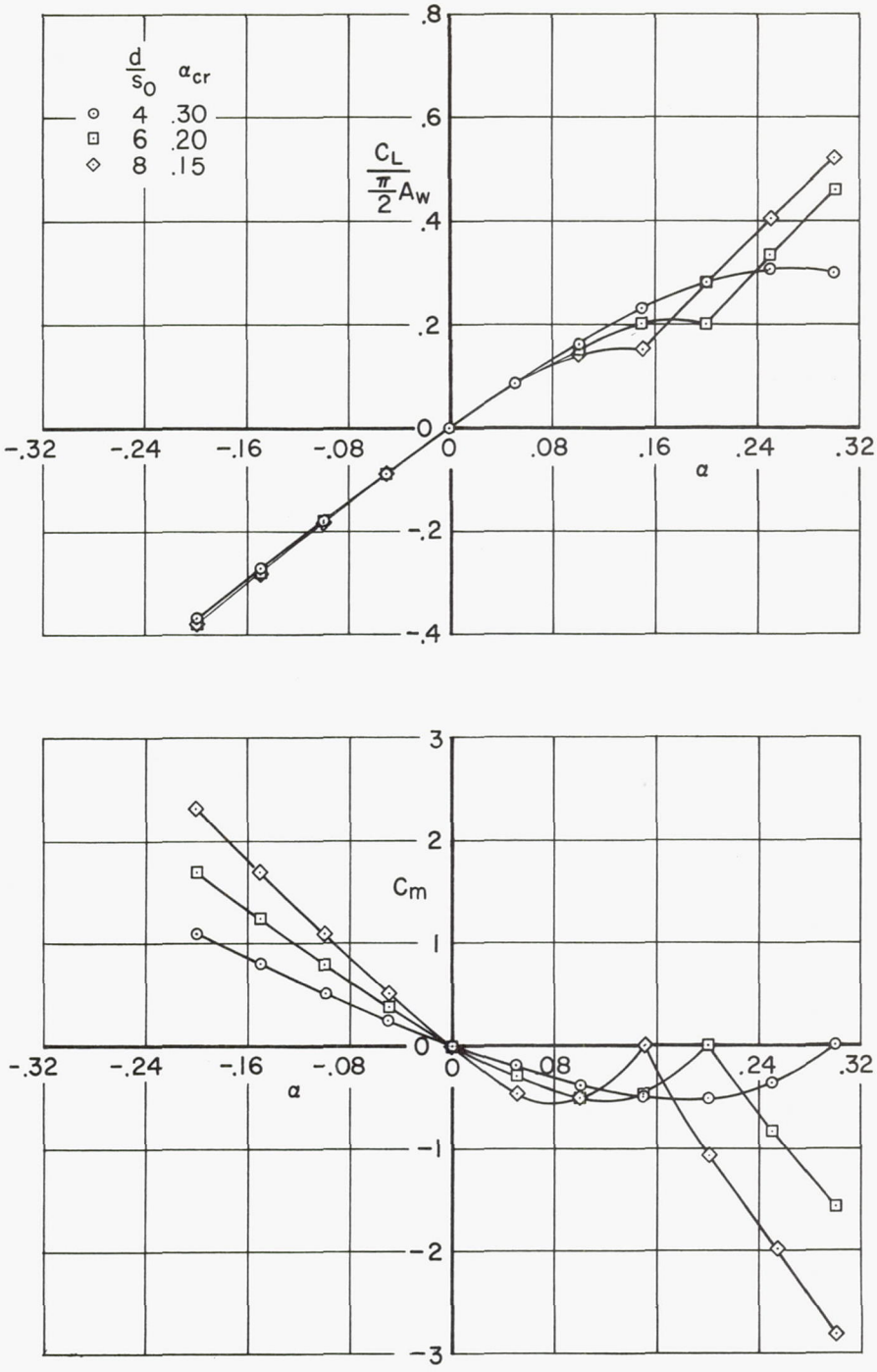


Figure 3.- Effect of tail-span-to-wing-span ratio on the variations of lift and pitching moment with angle of attack; plane triangular wing and tail of aspect ratio 2, $d/s_o = 6$, $h_t/s_o = 0.9568$, $i_t = b/s_o = 0$.



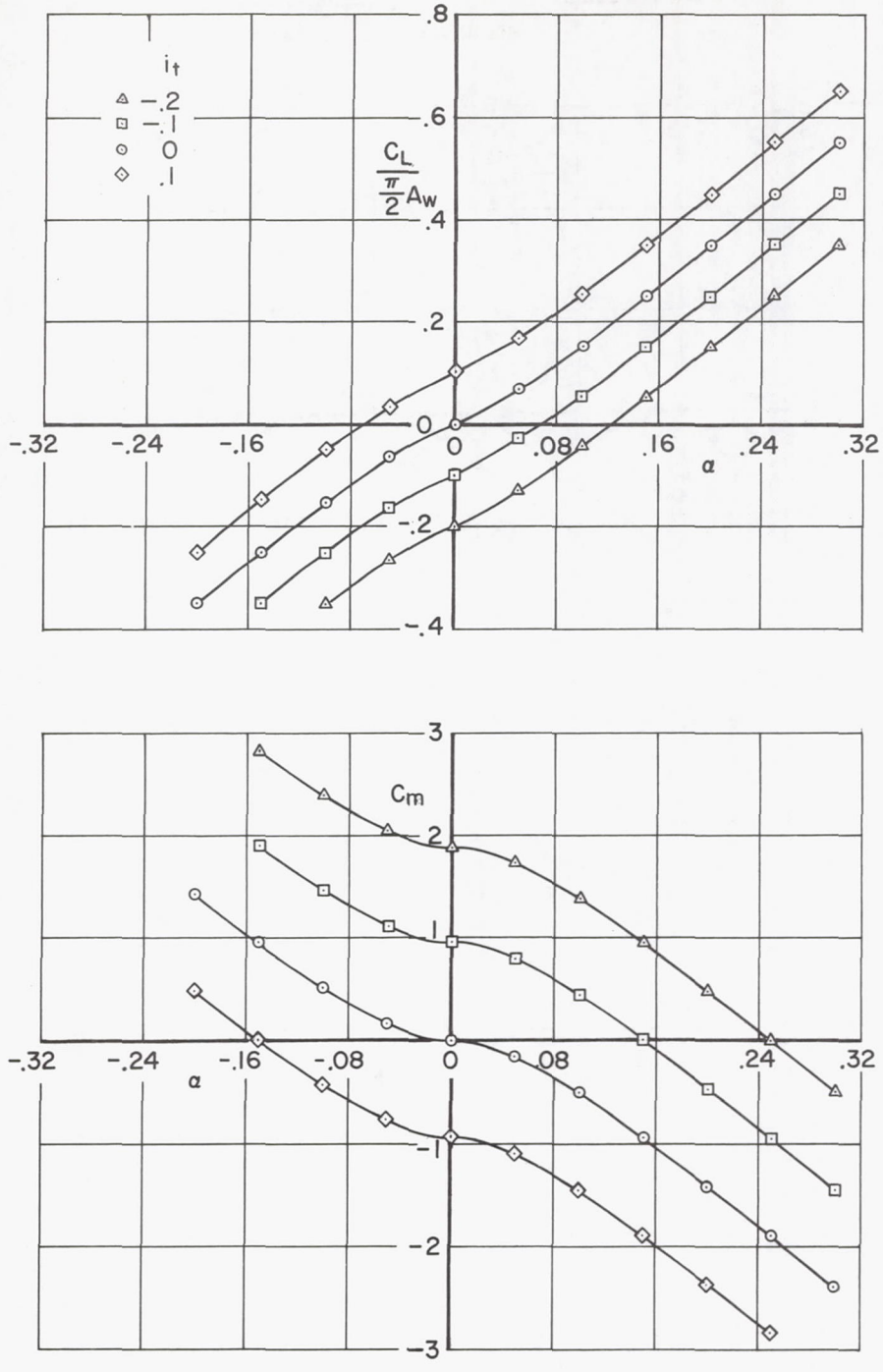
(a) $h_t/s_o = 0$

Figure 4.- Effect of tail length on the variations of lift and pitching moment with angle of attack; plane triangular wing and tail of aspect ratio 2, $s_1/s_o = 1$, $i_t = b/s_o = 0$.



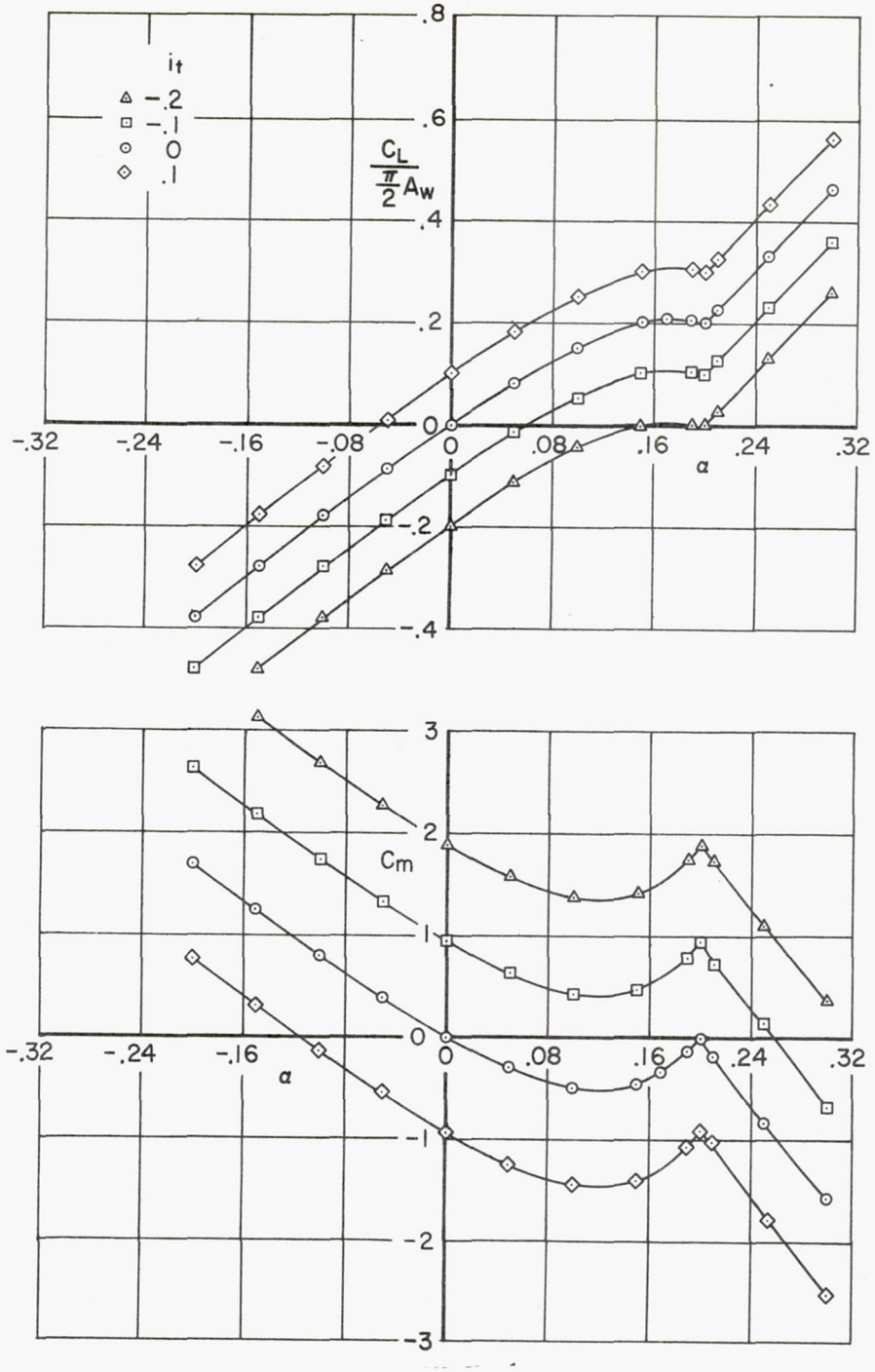
(b) $h_t/s_o = 0.9568$

Figure 4.- Concluded.



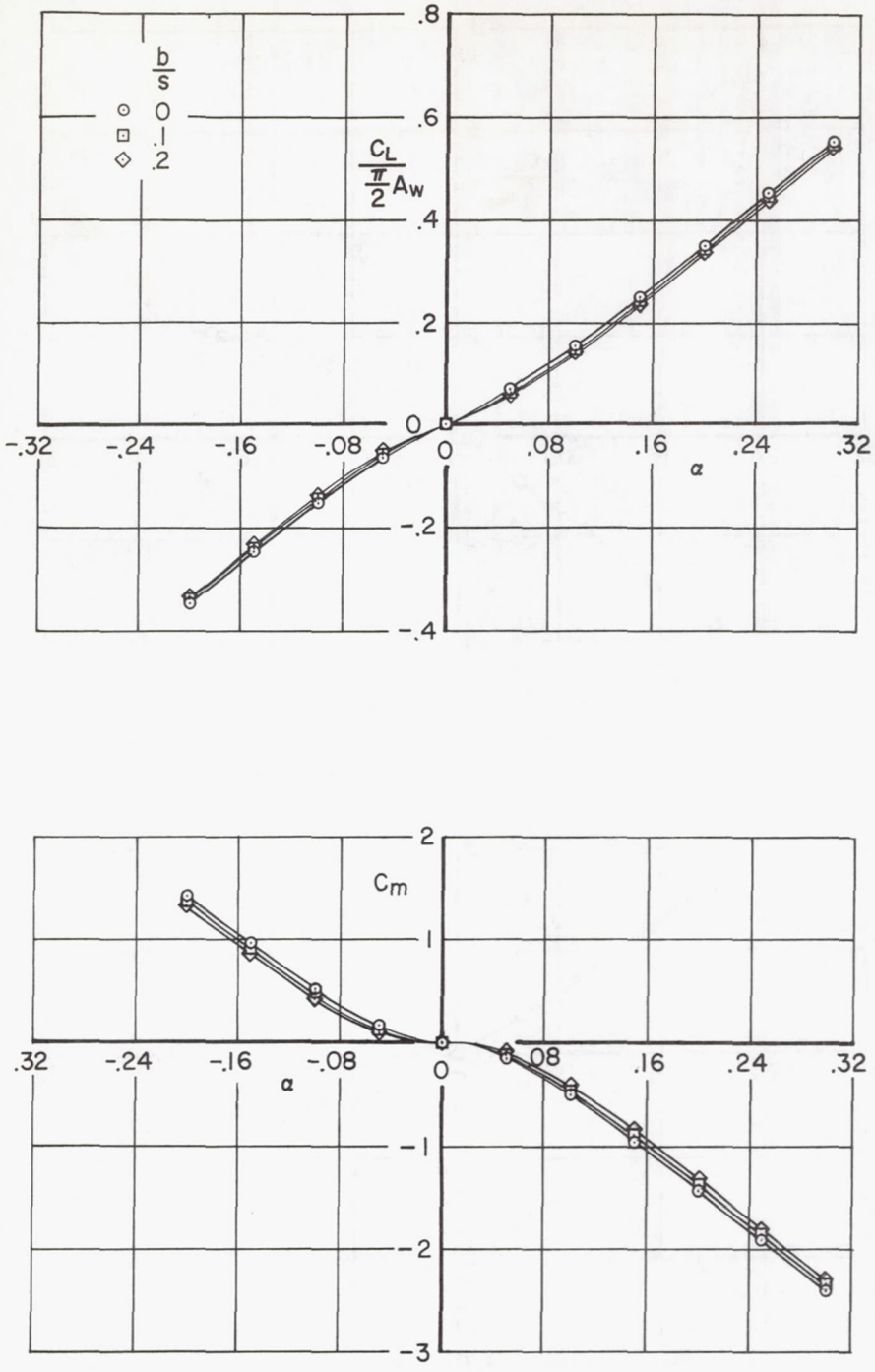
(a) $h_t/s_o = 0$

Figure 5.- Effect of tail incidence on the variations of lift and pitching moment with angle of attack; plane triangular wing and tail of aspect ratio 2, $s_1/s_o = 1$, $b/s_o = 0$, $d/s_o = 6$.



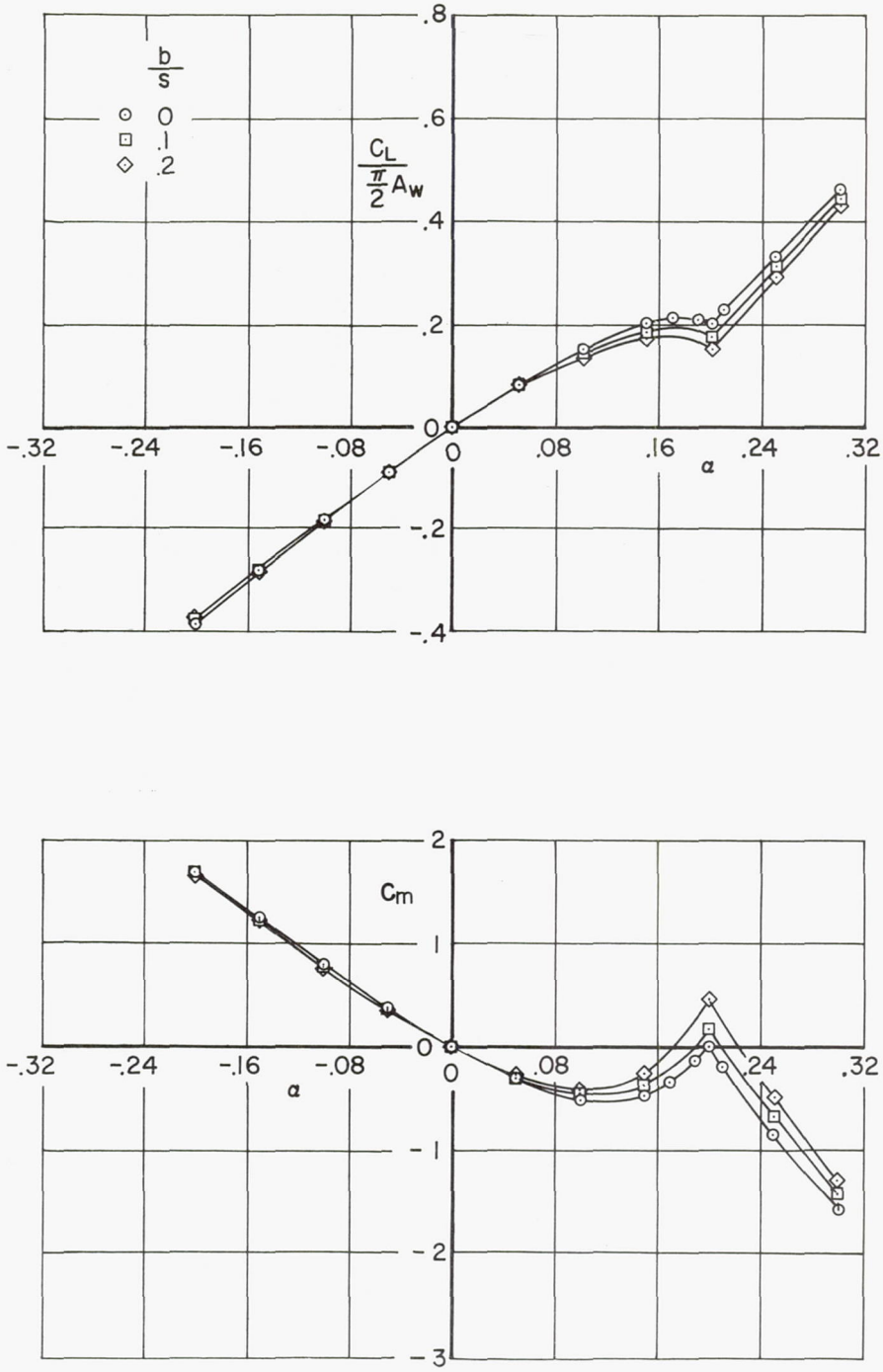
(b) $h_t/s_o = 0.9568$

Figure 5.- Concluded.



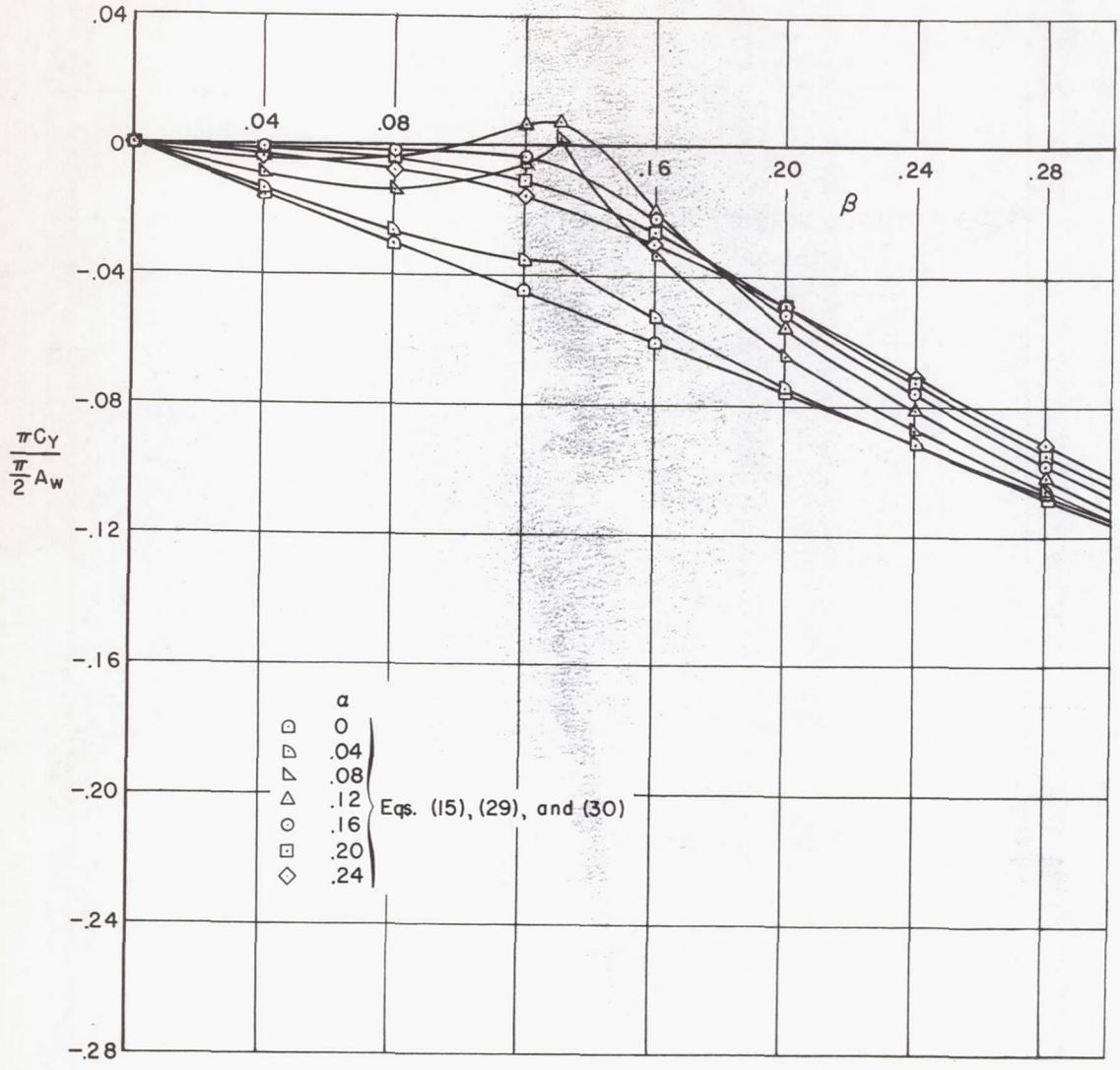
(a) $h_t/s_o = 0$

Figure 6.- Effect of tail thickness on the variations of lift and pitching moment with angle of attack; plane triangular wing and tail of aspect ratio 2, $s_1/s_o = 1$, $i_t = 0$, $d/s_o = 6$.



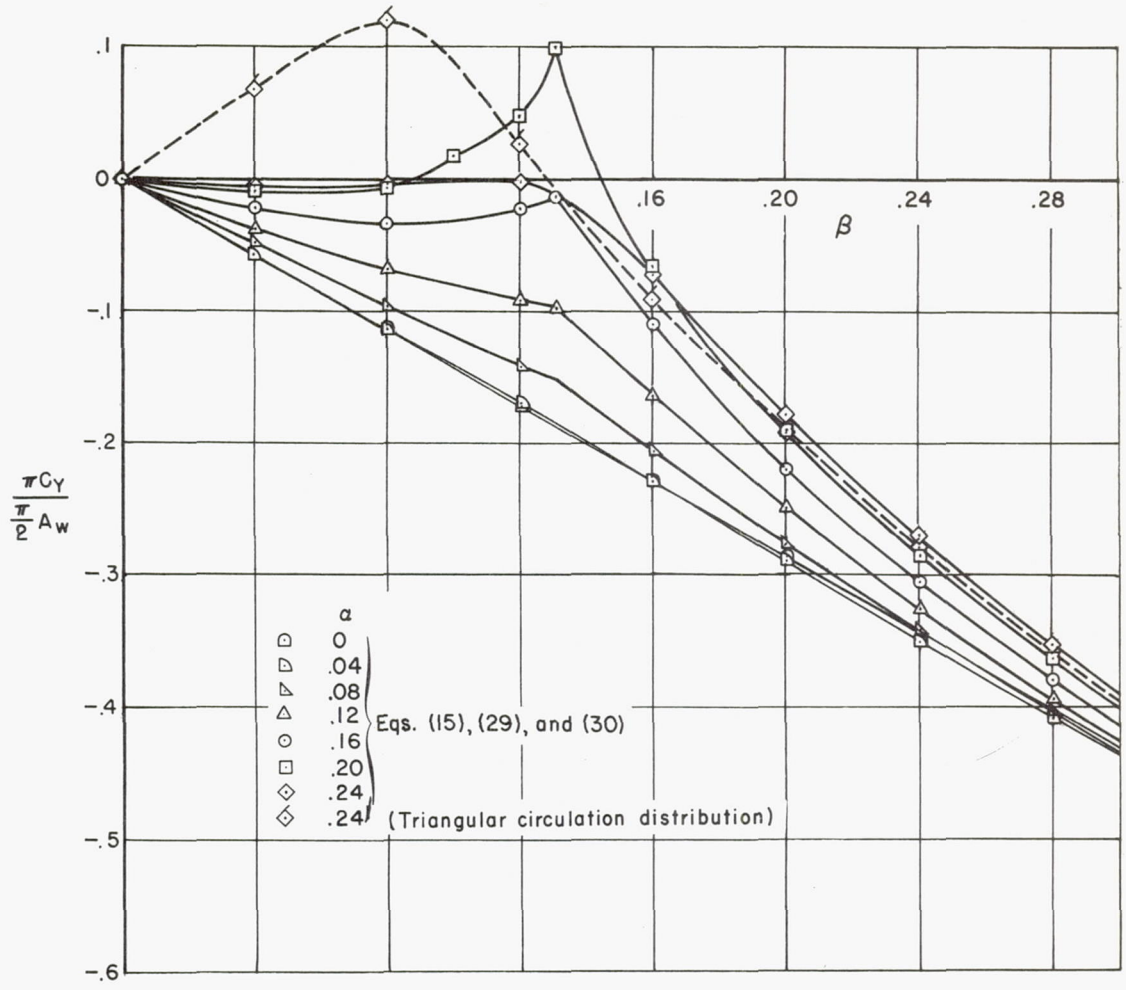
(b) $h_t/s_o = 0.9568$

Figure 6.- Concluded.



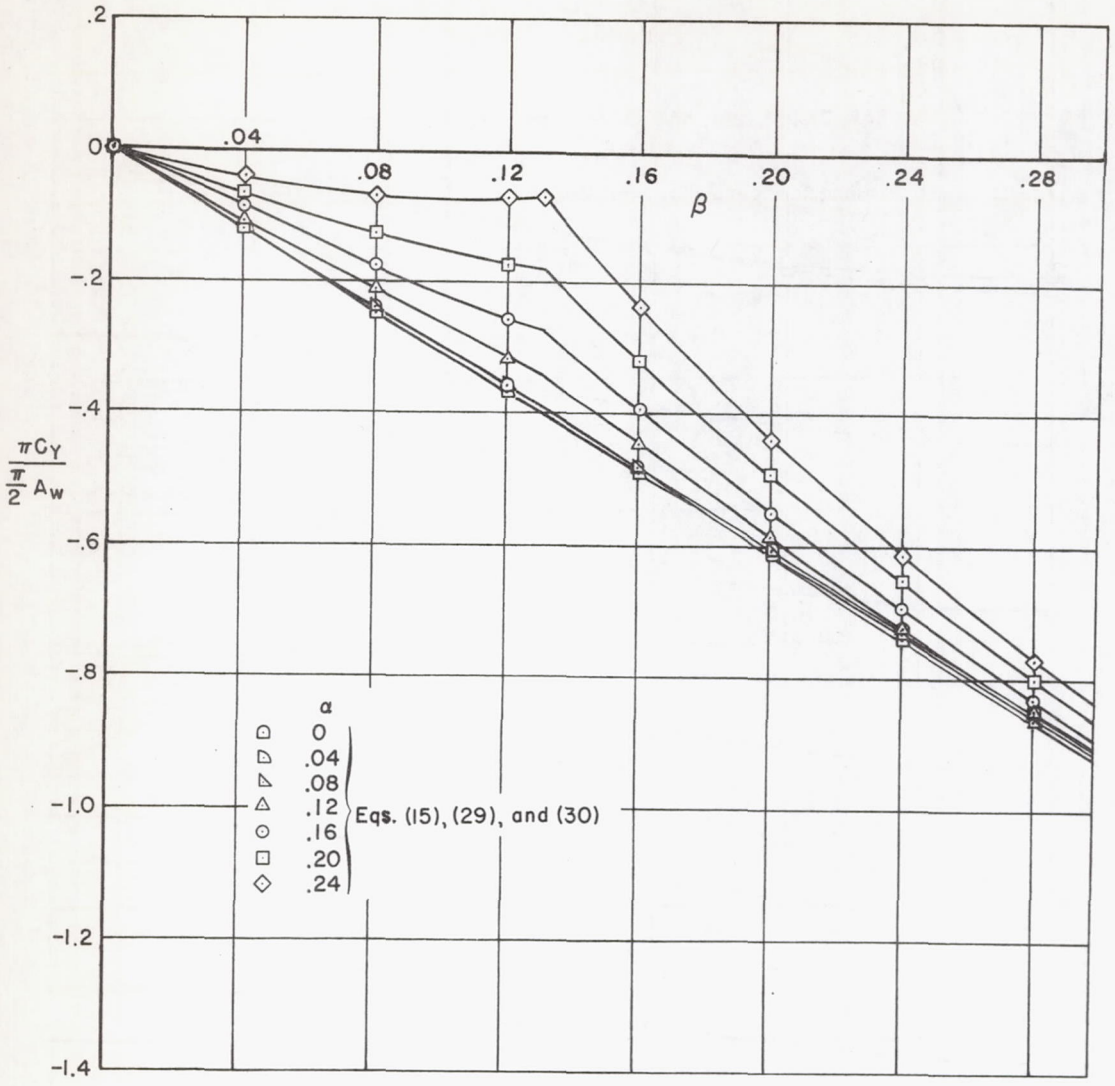
(a) $t_o/s_1 = 0.5$

Figure 7.- Effect of angle of attack on the variation of side force with angle of sideslip; plane wing with horizontal and vertical tail, $s_1/s_o = 1$, $d/s_o = 6$, $h_t/s_o = i_t = 0$.



(b) $t_o/s_1 = 1.0$

Figure 7.- Continued.



(c) $t_o/s_1 = 1.5$

Figure 7.- Concluded.

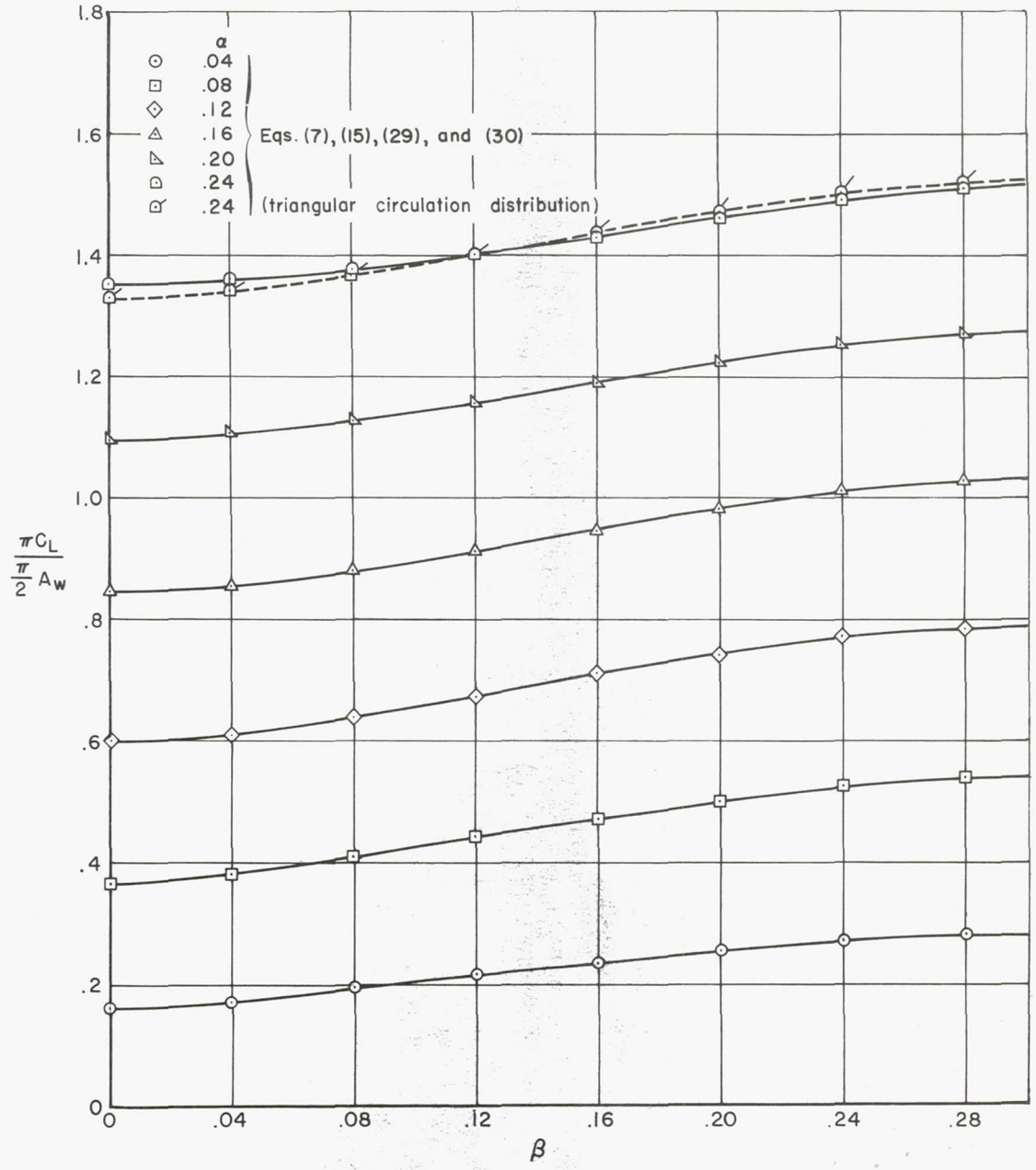


Figure 8.- Effect of angle of attack on the variation of lift coefficient with angle of sideslip for all vertical tail sizes; plane wing with horizontal and vertical tail, $s_1/s_o = 1$, $d/s_o = 6$, $h_t/s_o = i_t = 0$.

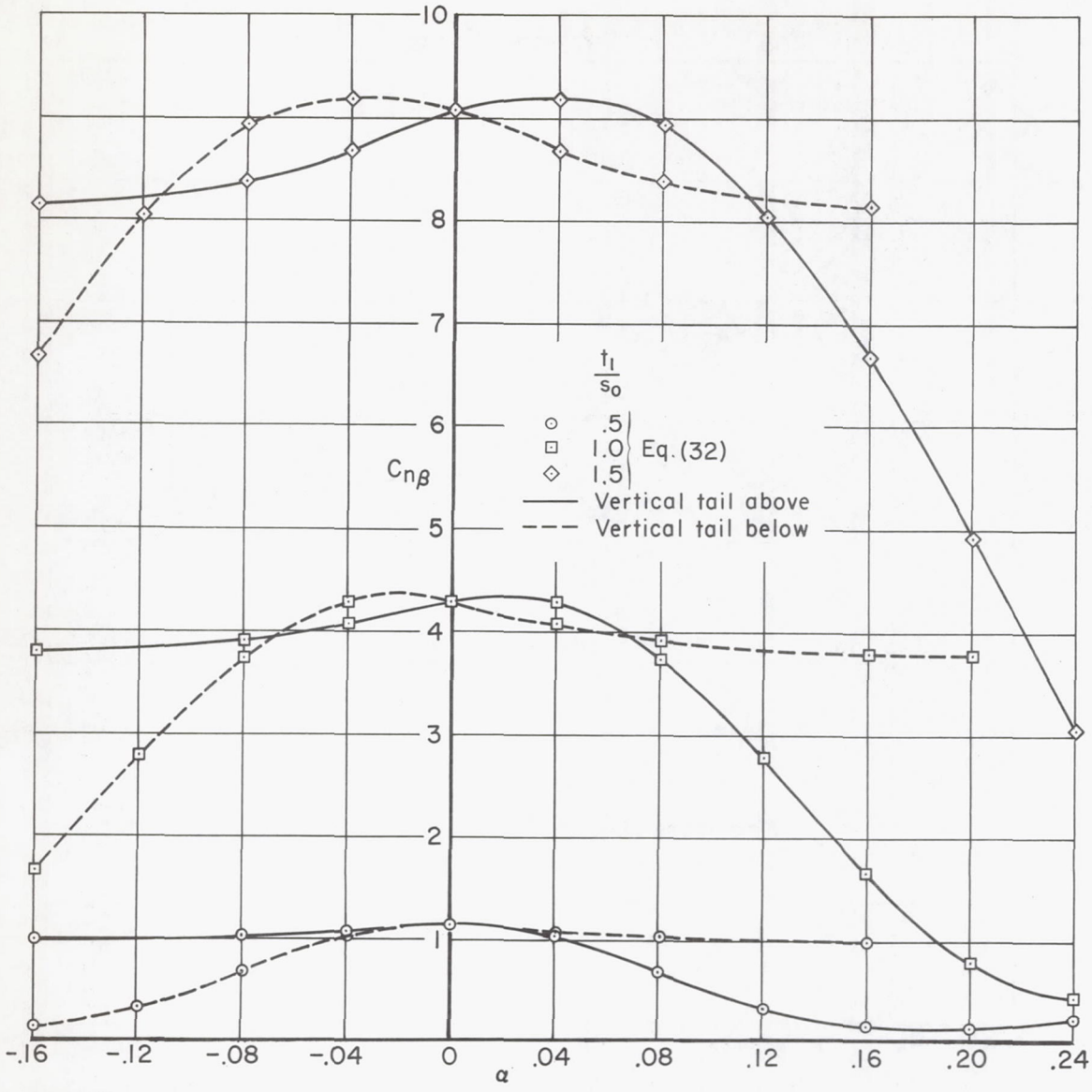


Figure 9.- Effect of vertical-tail size on the variation of yawing moment due to sideslip with angle of attack; plane triangular wing with triangular horizontal and vertical tail, $s_1/s_o = 1$, $d/s_o = 6$, $h_t/s_o = i_t = 0$, $A_w = A_t = 2$.

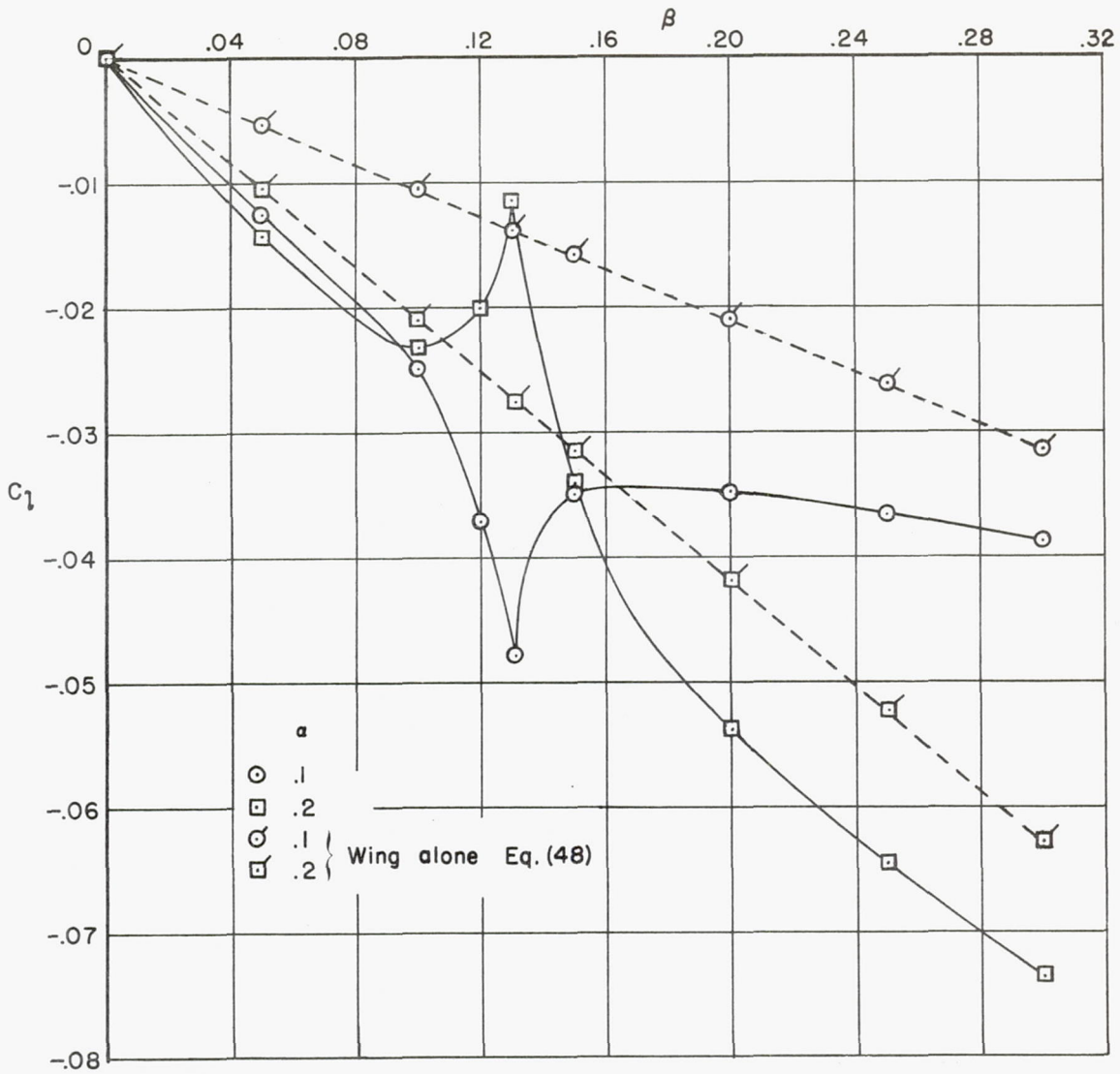


Figure 10.- Effect of angle of attack on the variation of rolling moment with angle of sideslip; plane triangular wing and cruciform in-line tail, $s_1/s_o = 1$, $d/s_o = 6$, $i_t = 0$, $A_w = A_t = 2$.

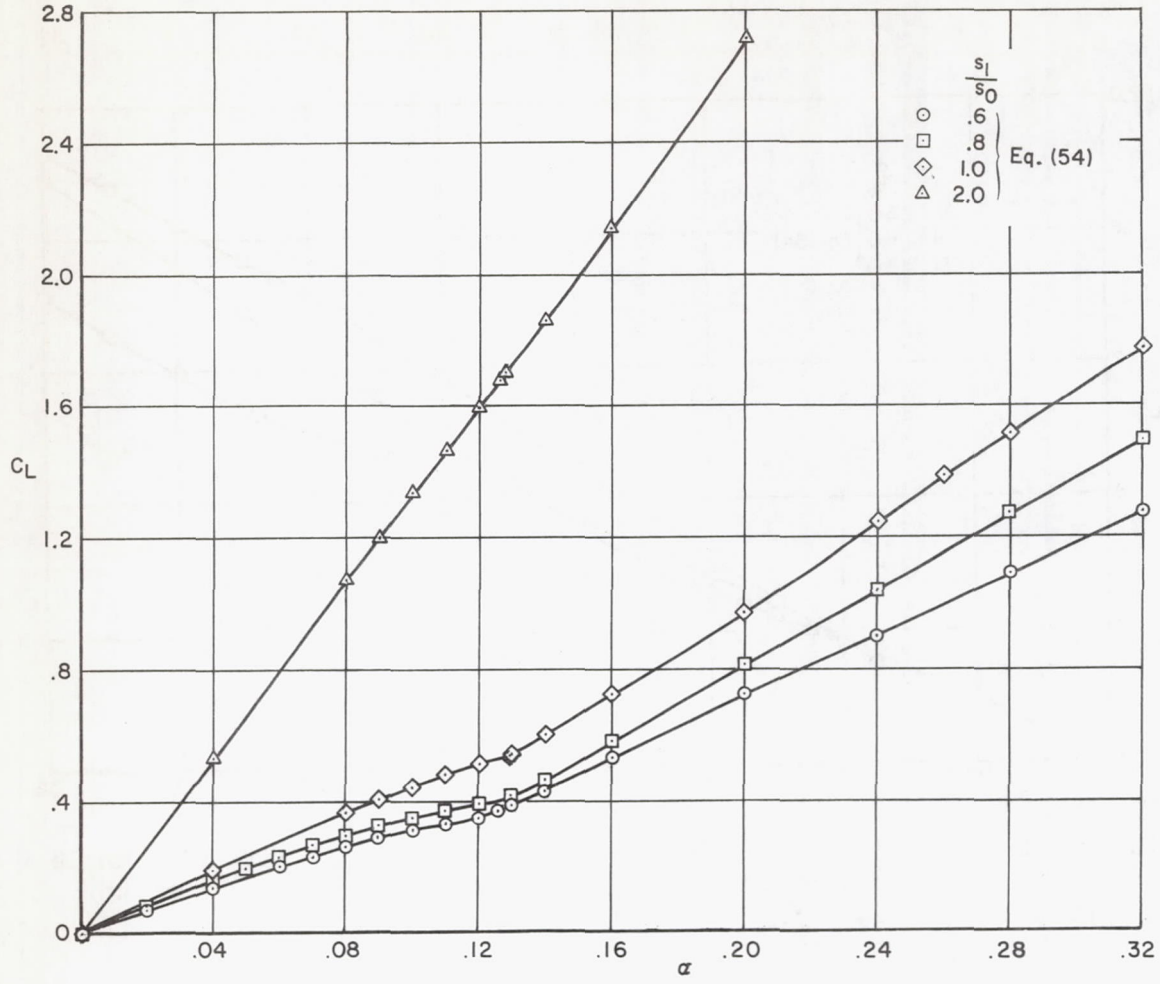


Figure 11.- Effect of tail-span-to-wing-span ratio on the variation of lift with angle of attack; cruciform interdigitated wing-tail combination at 45° bank, $d/s_o = 6$, $h_t/s_o = i_t = 0$, $A_w = A_t = 2$.

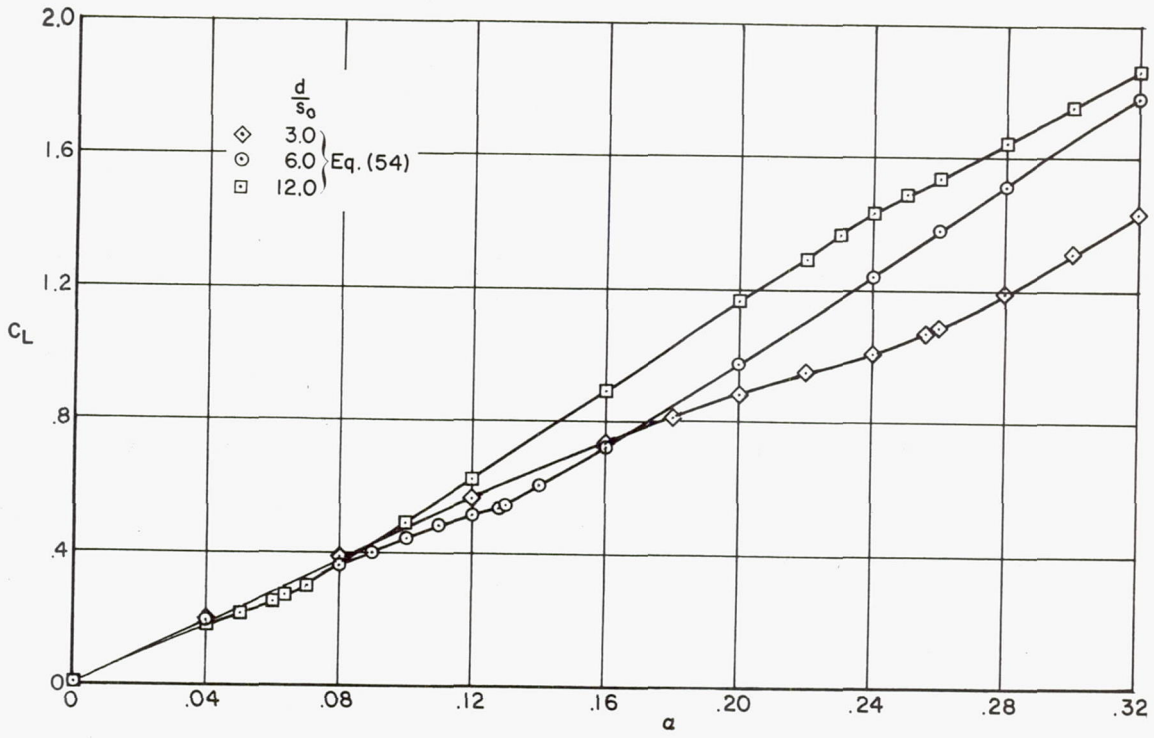


Figure 12.- Effect of tail length on the variation of lift with angle of attack; cruciform interdigitated wing-tail combination at 45° bank, $s_1/s_o = 1$, $h_t/s_o = i_t = 0$, $A_w = A_t = 2$.

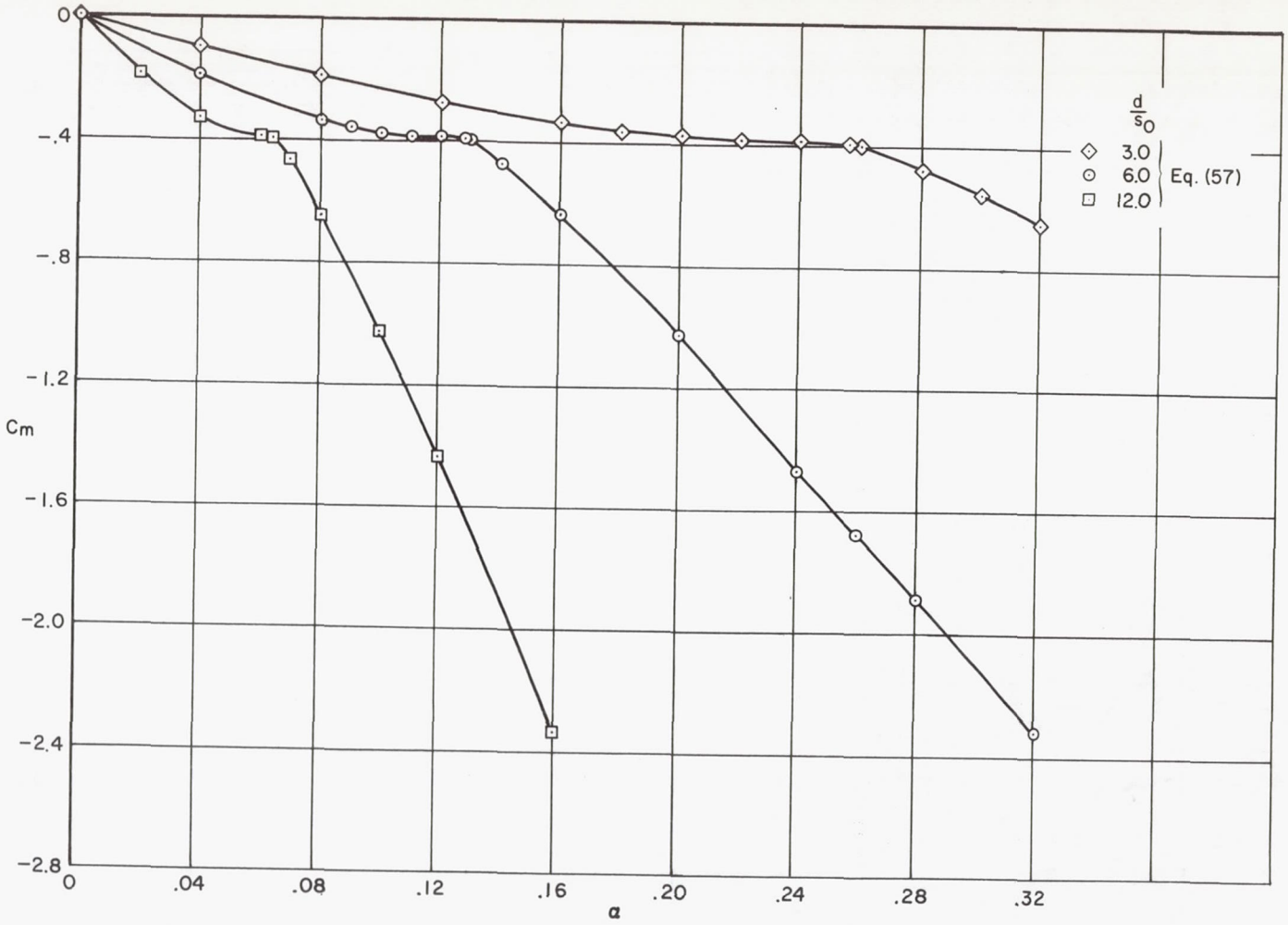


Figure 13.- Effect of tail length on the variation of pitching moment with angle of attack; cruciform interdigitated wing-tail combination at 45° bank, $s_1/s_o = 1$, $h_t/s_o = i_t = 0$, $A_w = A_t = 2$.

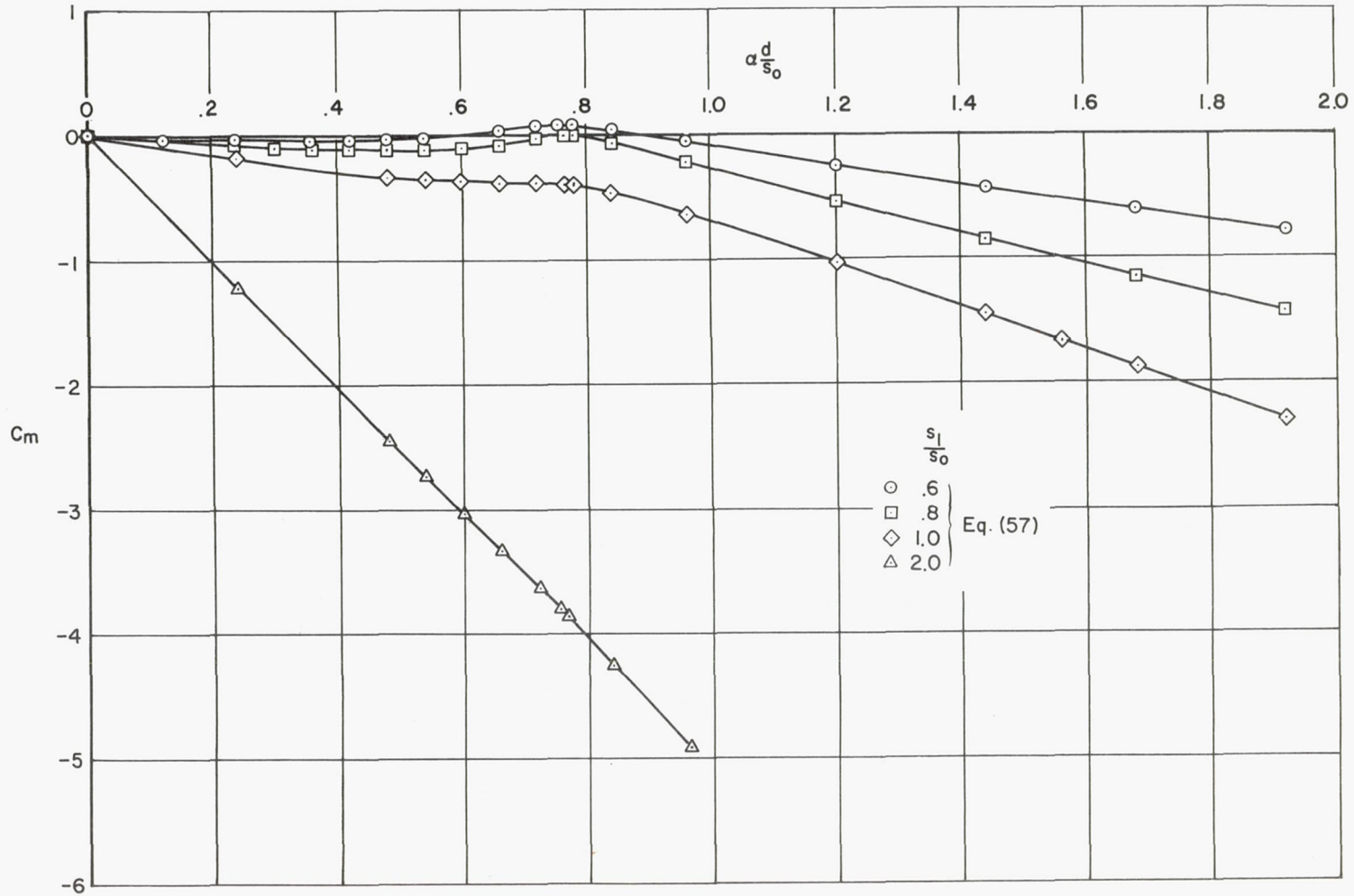


Figure 14.- Effect of tail-span-to-wing-span ratio on the variation of pitching moment with tail length parameter $\alpha d/s_o$; cruciform interdigitated wing-tail combination at 45° bank, $h_t/s_o = i_t = 0$, $A_w = A_t = 2$.

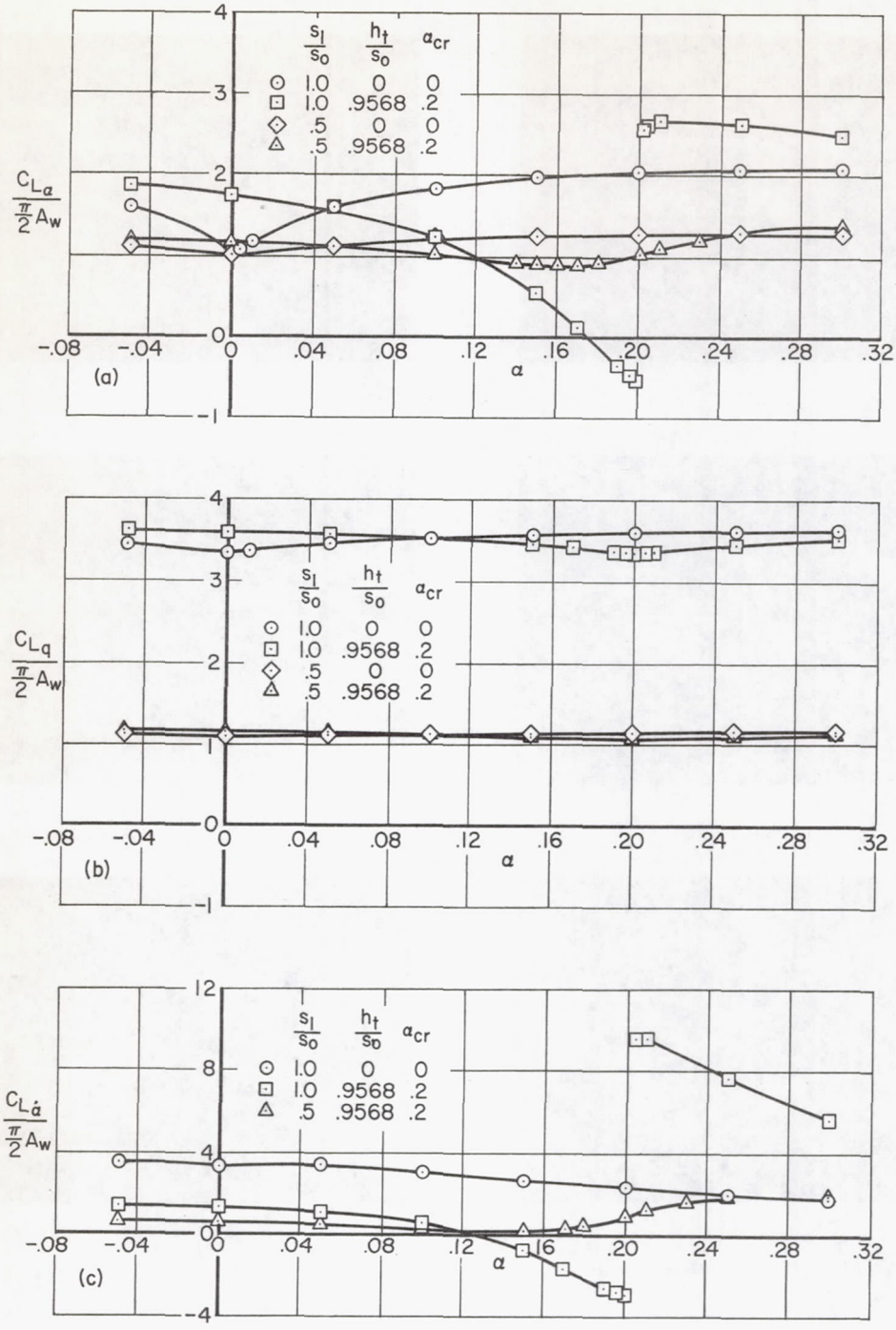
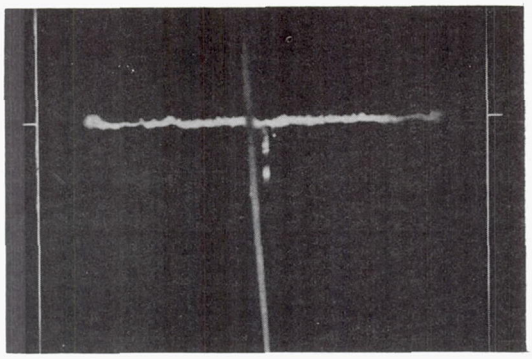
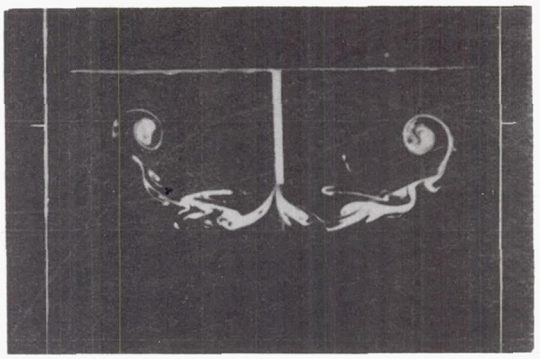


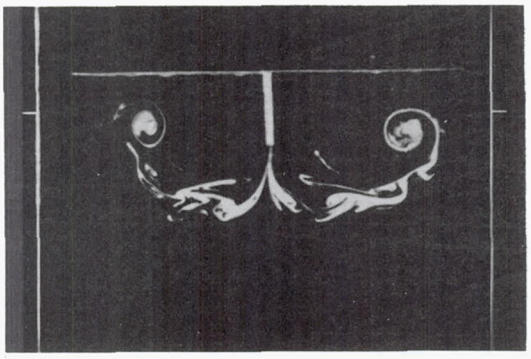
Figure 15.- Effects of horizontal tail height and ratio of tail span to wing span on the variations of the lift derivatives with angle of attack; plane triangular wing and tail of aspect ratio 2, $d/s_o = 6$, $i_t = b/s = 0$.



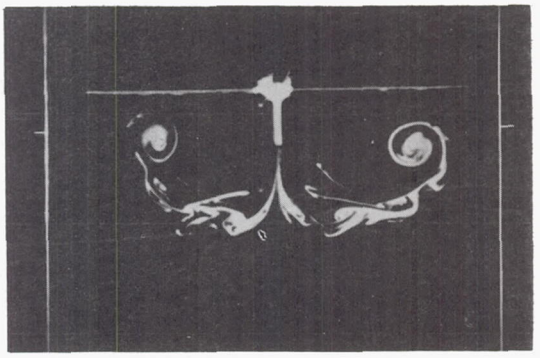
$x_1/s_o = 0$



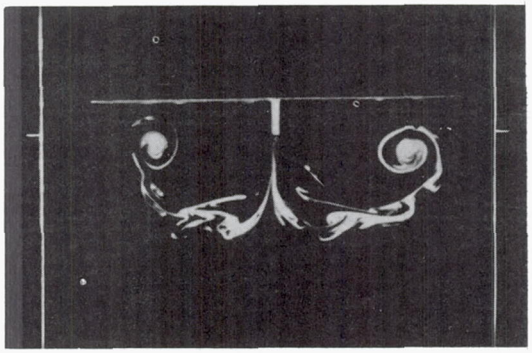
$x_1/s_o = 4.28$



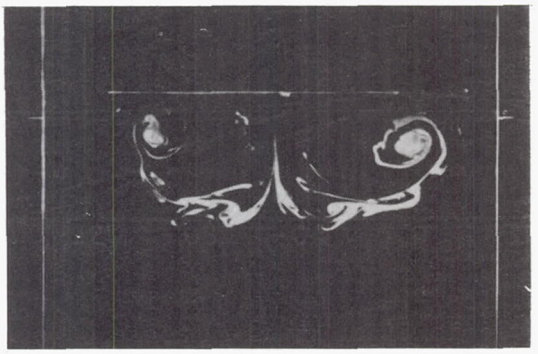
$x_1/s_o = 4.84$



$x_1/s_o = 5.12$



$x_1/s_o = 5.46$

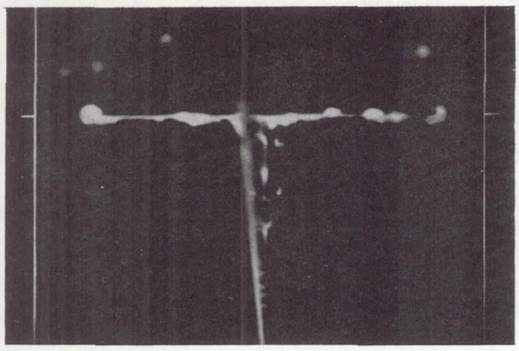


A-20904

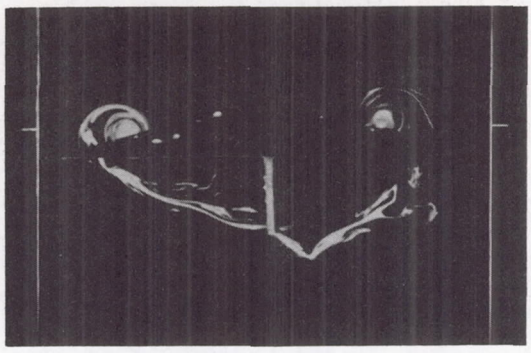
$x_1/s_o = 5.96$

(a) $\alpha = 8^\circ$

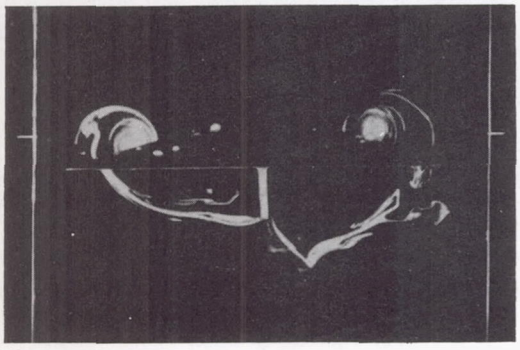
Figure 16.- Photographs of the wing wake in the presence of the tail; identical triangular wing and tail of aspect ratio 2, $d/s_o = 6$, $h_t/s_o = 0.96$, $i_t = 0$.



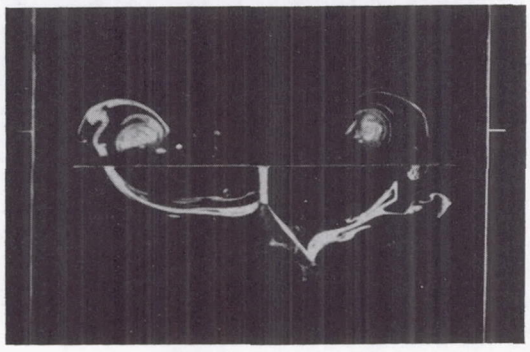
$x_1/s_o = 0$



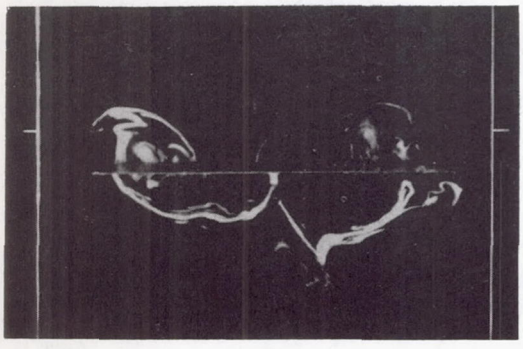
$x_1/s_o = 4.22$



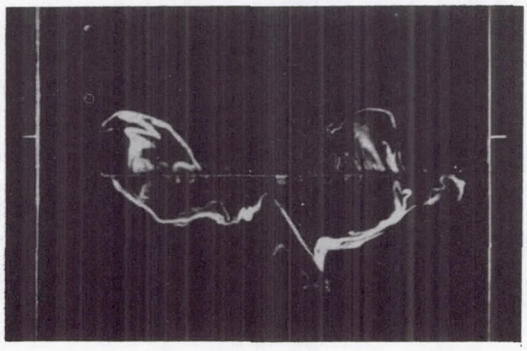
$x_1/s_o = 4.82$



$x_1/s_o = 5.14$



$x_1/s_o = 5.78$

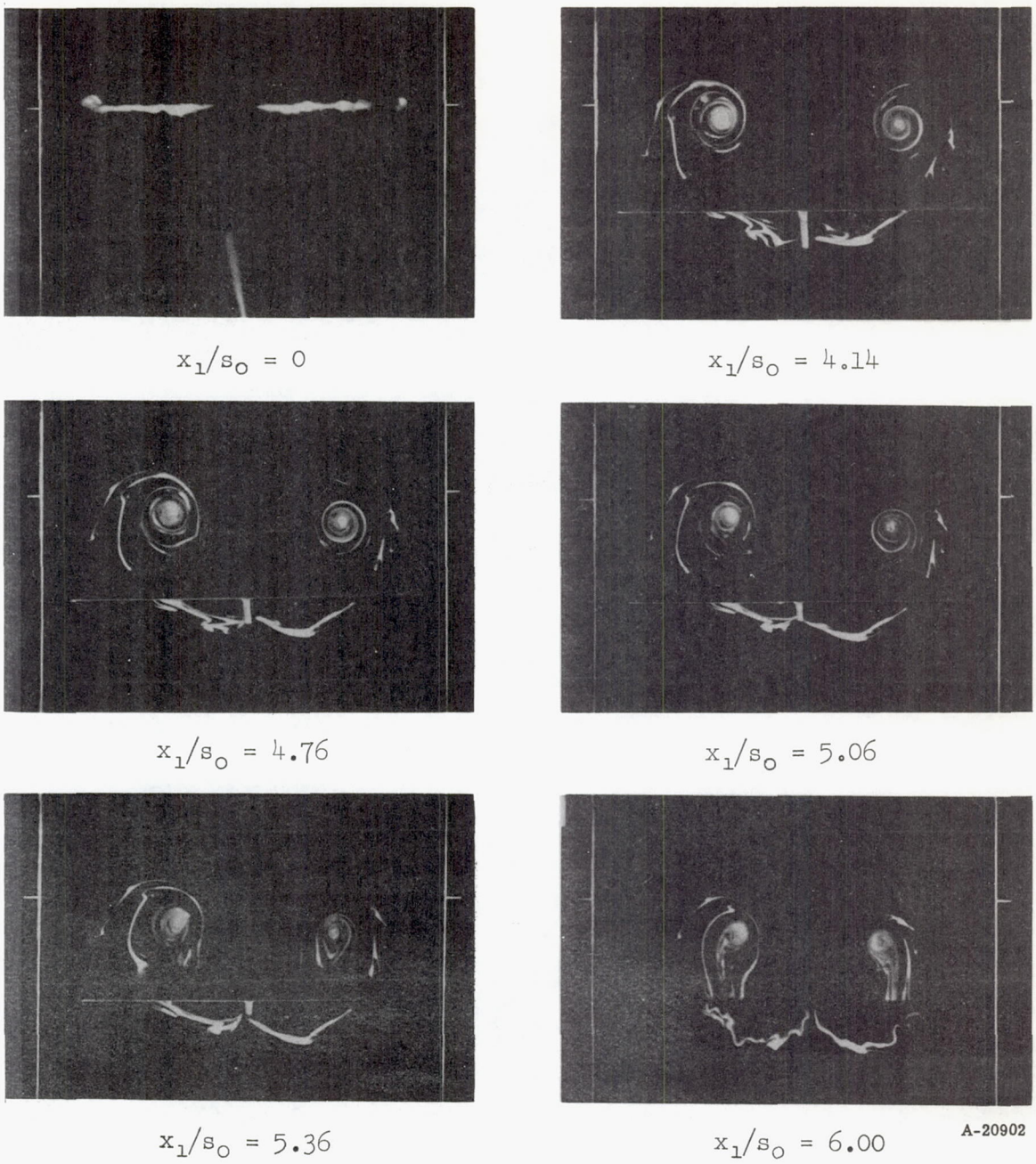


A-20903

$x_1/s_o = 5.98$

(b) $\alpha = 12^\circ$

Figure 16.- Continued.



$x_1/s_o = 0$

$x_1/s_o = 4.14$

$x_1/s_o = 4.76$

$x_1/s_o = 5.06$

$x_1/s_o = 5.36$

$x_1/s_o = 6.00$

A-20902

(c) $\alpha = 16^\circ$

Figure 16.- Concluded.

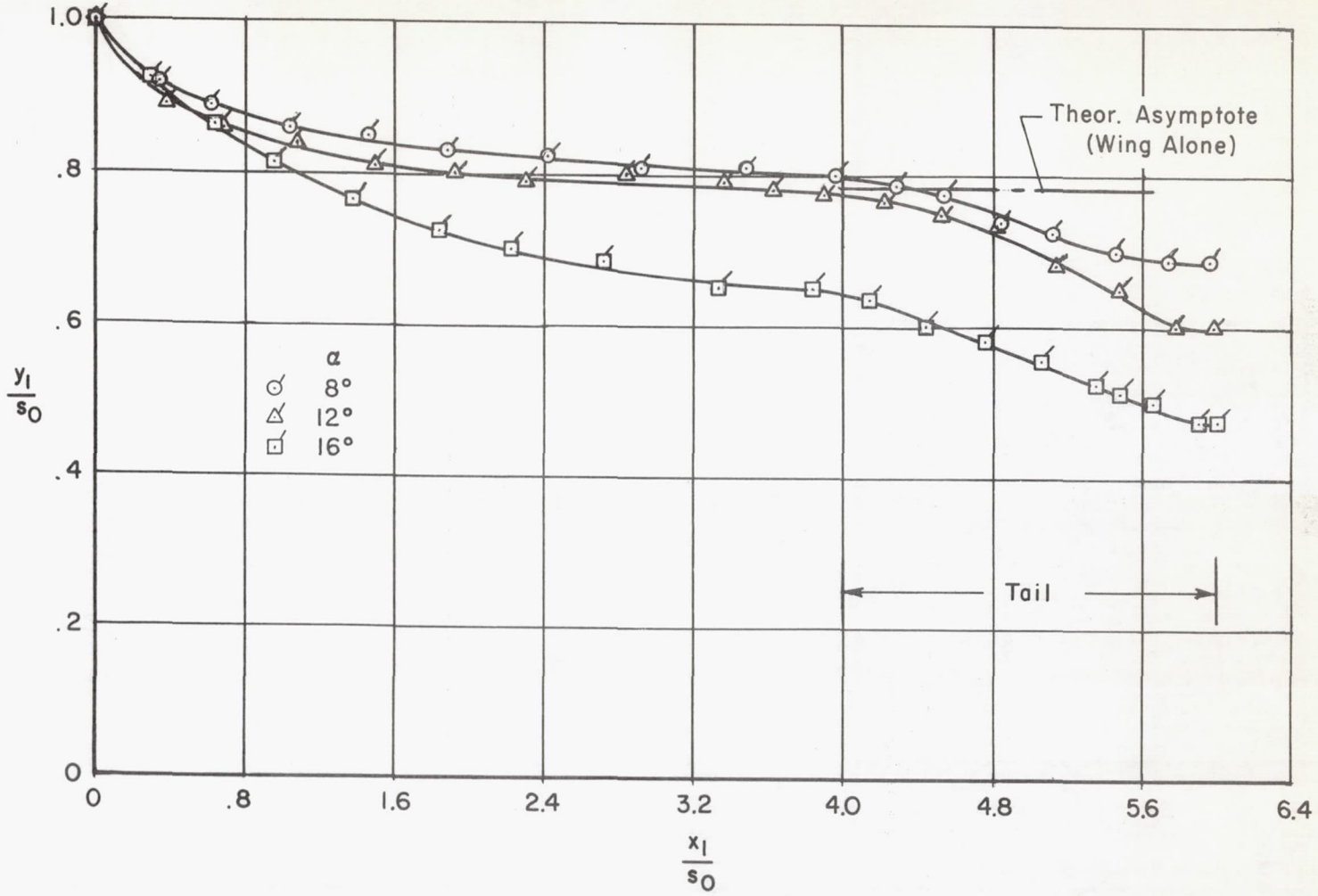


Figure 17.- Water-tank measurements of the influence of the tail on the lateral positions of the vortices shed by the wing; identical triangular wing and tail of aspect ratio 2, $d/s_o = 6$, $h_t/s_o = 0.96$, $i_t = 0$.